UNIVERSITÉ DE SHERBROOKE

Helwan University

**En cotutelle**

# THEORETICAL INVESTIGATION AND NON-LINEAR FINITE ELEMENT ANALYSIS TOWARD DESIGNING REINFORCED CONCRETE FILLED FRP-TUBE COLUMNS

# ÉTUDE THÉORIQUE ET ANALYSE NON-LINIÈRE PAR ÉLÉMENTS FINIS POUR LA CONCEPTION DE COLONNES EN BÉTON ARMÉ CONFINÉES À L'AIDE DE TUBE EN PRF

Thèse de doctorat
Spécialité : génie civil

**Maha Mohamed Hussein Mohamed Abdallah**

A dissertation submitted in partial fulfilment
of the requirements for the degree of
Doctor of Philosophy
(Civil Engineering)

**Jury:**

1. Prof. Radhoune Masmoudi (Directeur de Recherche-Université de Sherbrooke)
2. Prof. Ahmed Moussa (Co-directeur de Recherche- Université de Helwan)
3. Prof. Hamdy Mohamed (Co-directeur de Recherche- Université de Helwan)
4. Prof. Arezki Tagnit-Hamou (Rapporteur-Évaluateur-Université de Sherbrooke)
5. Prof. Khaled E.Galal (Évaluateur--Université de Concordia)

**Sherbrooke (Québec) Canada** **July 2018**

# ABSTRACT

Fibre-reinforced polymer (FRP) composite materials have been extensively used in the field of civil engineering construction, especially in structures subjected to corrosive environments. One of the innovative techniques for using FRP is the FRP tubes which can be used as structurally integrated stay-in-place forms for concrete members as columns, piles, piers and beams.

Extensive research was carried out to understand the behavior of concrete-filled FRP tube (CFFT) columns under axial loading, but comparatively limited research was conducted on the reinforced CFFT columns under eccentric loading. This thesis aims to provide experimental work as well as extensive theoretical analysis and design recommendations of circular CFFT columns reinforced with steel bars or carbon fibre reinforced polymer (CFRP) bars. CFFT columns were tested under monotonic loading with different levels of eccentricity. Test variables included the eccentricity to diameter ratio (e/D) and reinforcement type (CFRP bars vs steel). All specimens measured 152 mm in diameter and 912 mm height. The tubes used is basically filament wound glass fibre reinforced polymer tube (GFRP) with a core diameter of 152 mm and a wall thickness of 2.65 mm (6 layers). The fibre orientation of the tube was mainly in the hoop direction (± 60 degree with respect to the longitudinal axis). Six reinforcing bars (steel or CFRP) were used and distributed uniformly in each specimen. Test results indicate that specimens with CFRP reinforcement (CFRP-CFFT) behaved very similar to their steel counterparts with nearly the same nominal axial forces. Failure of CFFT columns was dominant by overall instability of the columns along with the combination of tensile rupture of FRP tube and CFRP bars or steel yielding. Experimental strain results revealed that the CFRP bars developed high strains on the compression and tension sides, thus CFRP bars contribution was considered effective in resisting tensile and compressive stresses. In addition, the maximum tensile strain reached in the GFRP tube was considered low when compared to the GFRP hoop strain, thus, it was concluded that the confinement induced by the GFRP tube become less significant in the case of eccentrically loaded column. Experimental axial-moment interaction diagrams were presented to indicate the failure envelope of steel and CFRP reinforced CFFT columns. Moreover, a theoretical model was developed to indicate the axial-moment capacities of steel and CFRP reinforced CFFT columns using plane sectional analysis

and compared to the experimental results counterparts. Theoretical sectional analysis based on layer by layer approach was developed to predict the moment-curvature response for steel and CFRP- reinforced CFFT columns. These results were compared to the experimental moment-curvature curves and it was clear that regardless of the type of reinforcement and value of eccentricity, all specimens exhibit non-linear moment curvature behavior.

An extensive study was conducted on the effective flexural stiffness of CFFT columns, on the basis of experimental parametric study and theoretical simulation. Proposed equations were developed and validated against the experimental results to represent the stiffness of steel and CFRP- CFFT circular columns at service and ultimate loads.

Moreover, a theoretical investigation was conducted to propose a more precise formula for the critical slenderness limit to control the buckling mode of failure of FRP-reinforced CFFT columns. It was found that the critical slenderness limit of 14 could be used as a safe value for practical design purposes. The theoretical analysis in this research was carried out using excel.

Finally, a nonlinear finite element model using ABAQUS software was presented based on Lam and Teng confined concrete model considering material and geometric nonlinearities of CFFT columns. This model aims to provide insight on the structure behavior and failure mechanism of CFFT columns.

**Keywords:** Concrete, FRP bars, FRP tubes, columns, eccentricity, failure, sectional analysis, curvature, stiffness, buckling, finite element analysis.

# RÉSUMÉ

Les matériaux composites en polymères renforcés de fibres (PRF) ont été utilisés largement dans le domaine de la construction en génie civil, particulièrement pour les structures exposées à un environnement corrosif. L'utilisation des tubes en polymères renforcés de fibres (PRF) est une technique innovante pour les éléments de structures en béton armé tels que les colonnes, les piliers et les poutres, où les tubes en PRF sont utilisés comme coffrage permanent.

Des recherches précédentes ont été effectuées pour comprendre le comportement des colonnes (CFFT) sous chargement axial mais il existe très peu de données concernant le comportement des colonnes en béton armé et renforcées de tubes en PRF sous chargement excentrique.

Cette thèse présente des données expérimentales, une analyse théorique approfondie et des recommandations de conception pour colonnes cylindriques CFFT armées de barres d'acier ou de barres en polymères renforcés de fibres de carbone (CFRP). Les colonnes CFFT ont été testées sous un chargement monotone avec différents niveaux d'excentricité. Le rapport d'excentricité (e / D), et le type d'armature longitudinale (barre CFRP versus barre en acier) sont considérés comme des variables pour tous les essais effectués. Le diamètre et la hauteur de chaque spécimen sont égaux à 152mm, 912mm respectivement. L'angle d'orientation des fibres du tube a été principalement dans la direction circonférentielle (± 60 degrés par rapport à l'axe longitudinal). Six barres d'armature (acier ou CFRP) ont été utilisées et sont réparties uniformément dans chaque échantillon.

Les résultats de cette étude ont révélé que les échantillons armées avec des barres en PRFC se comportent de manière très similaire aux échantillons armés de barres en acier et atteignent, à toute fin pratique, les mêmes résistances axiales. Le mode de rupture des échantillons de CFFT a été dominé par l'instabilité globale des colonnes ainsi que par la combinaison de la rupture en traction du tube en PRF et des barres en PRFC ou en acier.

Les résultats expérimentaux de la déformation ont montré que les barres de PRFC développent des déformations élevées sur les côtés de compression (Valeur maximale en compression -5000 με) et de traction (Valeur maximale en traction 10,400 με), ainsi les barres PRFC résistent mieux aux contraintes de la traction et de la compression.

En outre, la contrainte de traction longitudinale maximale enregistrée dans le tube en PRF est considérée comme étant une contrainte faible par rapport à celle enregistrée dans la direction circonférentielle du tube en PRF. D'après les résultats expérimentaux enregistrés, le confinement induit par le tube en PRF est moins important dans le cas d'une colonne sous charge excentrée. Des diagrammes expérimentaux d'interaction charge axiale-moment ont été présentés pour déterminer l'enveloppe de rupture des échantillons CFFT armées de barres en acier ou de barres en PRFC.

De plus, une analyse théorique a été développée pour calculer les résistances des colonnes CFFT soumises à un chargement excentrique. Une comparaison avec les résultats expérimentaux a été effectuée. Aussi, une analyse théorique basée sur l'approche couche par couche a été développée pour prédire la réponse moment versus courbure des colonnes CFFT armées de barres en acier ou de barres en PRFC. Ces résultats ont été comparés aux résultats expérimentaux des courbes de moment-courbure. Il a été conclu que quelques soient le type d'armature (acier versus PRFC) pour les colonnes CFFT et la valeur de l'excentricité, le comportement moment-courbure de tous les échantillons est non linéaire.

Par ailleurs, une étude approfondie a été effectuée sur la rigidité en flexion (*EI*) effective des colonnes CFFT. Cette étude est basée sur une étude paramétrique expérimentale et une simulation théorique. Les équations proposées ont été développées et validées par rapport aux résultats expérimentaux afin de représenter la rigidité des colonnes CFFT armées de barres en acier ou de barres en FRPC. Ces équations sont établies pour deux états-limites : les états-limites de service et les états-limites ultimes.

Aussi, une formule précise pour la prédiction du taux d'élancement pour contrôler le mode de rupture par flambement pour les colonnes CFFT armées de barres en PRFC a été proposée. Il a été établi qu'un taux d'élancement égal à 14 présente une valeur sécuritaire pour la conception de ces colonnes CFFT en béton armé.

Enfin, un modèle non-linéaire par éléments finis utilisant le logiciel ABAQUS a été développé et présenté sur la base d'un modèle de béton confiné « Lam et Teng» prenant en considération la non- linéarité matérielle et géométrique des colonnes CFFT. Ce modèle permet de fournir un aperçu sur le comportement de la structure et du mécanisme de rupture des colonnes CFFT.

**Mots clés:** Béton, barres en PRF, tubes en PRF, colonnes, excentricité, moment-courbure, rupture, analyse par section, bloc de contrainte, courbure, rigidité, flambement, analyse par éléments finis.

# BIBLIOGRAPHY

During this research work, the candidate has participated in the following publications;

## *Journal Papers*


- **Abdallah, M.H.**, Mohamed, H.M., Masmoudi, R., and Moussa, A "Analytical Modeling of Moment-Curvature Behavior of Steel and CFRP RC Circular Columns Confined with GFRP Tubes . " *Journal of composite Structures*, Elsevier, 189 (2018), 473-487.
- **Abdallah, M.H**., Mohamed, H.M., Masmoudi, R., and Moussa, A "Experimental and Theoretical Development of Effective Flexural Stiffness for Concrete-Filled FRP Tube Columns*" Journal of Engineering Structures,* Elsevier. (Submitted in Jan. 2018, Under review)

- **Abdallah, M.H**., Mohamed, H.M. and Masmoudi, R "Experimental Assessment and Theoretical Evaluation of Axial Behavior of Short and Slender CFFT Columns Reinforced with Steel and CFRP Bars" *Journal of Construction and Building Materials*, 181 (2018) 535–550.

- **Abdallah, M.H.**, Shazly,M., Mohamed, H.M., Masmoudi, R., and Moussa, A "Nonlinear finite element analysis of short and long reinforced concrete columns confined with GFRP tubes . " *Journal of Reinforced Plastics and Composites*, 13(2017), 972 – 987.


## *Refereed Conference Publications*


- **Abdallah, M.H.**, Shazly, M., Mohamed, H.M., Moussa, A., and Masmoudi, R. [2016] "Numerical Analysis of Concrete-Filled Fiber Reinforced Polymer Tube Columns." *The ninth Alexandria international conference on Structural and Geotechnical Engineering*, Alexandria, Egypt, December 19-21, pp.796-803
- Mohamed, H.M., **Abdallah, M.H.**, and Masmoudi, R. [2016] "Experimental Behavior of Steel and Carbon FRP-Confined Concrete Columns under Eccentric Loads." *The ninth Alexandria international conference on Structural and Geotechnical Engineering*, Alexandria, Egypt, December 19-21, pp.804-811
- **Abdallah, M.H.**, Mohamed, H.M., Masmoudi,R., and Moussa, A "Moment-Curvature Characteristics for Steel and CFRP Reinforced CFFT columns: Experimental and Theoretical Study" [Submitted Dec. 2017], *9th International Conference Fibre-Reinforced Polymer (FRP) Composites in Civil Engineering* (CICE 2018) ,Paris, France on 17-19 July 2018.
- **Abdallah, M.H.**, Mohamed, H.M., Masmoudi, R., and Moussa, A" Non-Linear Effective Flexural Stiffness for Slender Steel CFFT Columns" [Submitted Dec.2017],

*10th International Conference on Short and Medium Span Bridges, Quebec City*, Quebec, Canada, July 31 – August 3, 2018.

- Masmoudi, R., Mohamed, H.M., **Abdallah , M.H.** " Behavior of Concentric and Eccentric CFFT Columns" *1st International Conference on Vulnerability and Rehabilitation of Structures, Algiers, Algeria, May 7-8, 2018.*

# Dedication

*To my father's soul, he is the reason for who I am today and who I will be in the future.*

# ACKNOWLEDGEMENT

All praise be to almighty ALLAH.

Words cannot express the author sincere gratitude and appreciation to her supervisor Professor Radhouane Masmoudi (University Sherbrooke) and her co-supervisors Professor Ahmed Moussa and Professor Hamdy Mohamed (Helwan University-Egypt) for their guidance, support, inspiration and encouragement throughout this research program.

Sincere words of thanks must also go to Professor Arezki Tagnit-Hamou and Professor Khaled E. Galal for their valuable suggestions and critical comments that helped in advancing the research.

The author wishes to thank Dr Mostafa Shazly (Director of Center of Advanced Materials, The British University in Egypt) for his guidance and support during the finite element phase of this research program.

The author also expresses his thanks and deep appreciation to her mother, brother and sisters for their endless love and support.

Finally, the author wishes to extend her deep love and appreciation to her husband Yasser and her son Younes for their continuous devotion, kindness and support in every step throughout this research.

# CONTENTS

# List of Figures

# List of Tables

# CHAPTER 1

# INTRODUCTION

## 1.1 General Background

Corrosion of steel reinforcement causes continual degradation to infrastructures worldwide, which has challenged engineers involved in designing and improving reinforced concrete structures. Fibre reinforced polymers composite materials have proven to be a solution for the corrosion problem due to its high corrosion resistance where FRP reinforcement have been introduced to concrete structures in the form of bars, tubes and grids in a wide variety of forms, types and characterizations. Recently, the use of fibre reinforced polymers (FRP) tubes, as structurally integrated stay in place forms for concrete members, such as beams and columns has emerged as an innovative solution to the corrosion problem and has saved millions of dollars spent yearly in reparation of concrete structures. The FRP tube is used mainly in structures subjected to harsh corrosive environment as an alternative to conventional reinforced concrete and steel components especially in tidal areas for marine piles and zones where de-icing is used. The FRP composite tube act as a stay in place formwork to contain fresh concrete which saves the cost of formwork used in precast and cast in-place industries and provide a light weight protective jacket. Different parameters including fibre orientation, fibre thickness, type of fibres and number of fibres layers in the FRP tube should be thoroughly investigated to ensure the optimum design for each individual application. This research investigated these different parameters through different parametric studies.

Generally, the use of FRP tubes as an external confinement for concrete structures is rapidly increasing. Nevertheless, its use as an external confinement in concrete columns reinforced with carbon FRP bars (CFRP) has not been thoroughly investigated. Most of the design provisions incorporated in codes and design guides are based on the design formulas of

members reinforced with conventional steel considering some modifications to account for the substantial differences between FRP and steel reinforcement.

Many researchers have investigated the behavior of concrete-filled fibre reinforced polymers (FRP) tube CFFT columns reinforced with conventional steel and FRP bars under concentric loads. On the other hand, the behavior of CFFT columns reinforced with FRP bars under eccentric load has not yet well investigated. This creates a research gaps in need of valuable investigations to introduce appropriate provisions in guidelines and codes for the design issues of FRP reinforced CFFTs columns under concentric and eccentric loads

## 1.2 Research Objectives

This research originally discussed the behavior of reinforced circular full-scale CFFT columns under concentric and eccentric compression. The main longitudinal reinforcement used was steel and CFRP bars. The efficiency of the CFRP bars as an alternative reinforcement was compared to steel, in addition to the efficiency of the GFRP tube as an external confinement. The interaction diagrams and moment-curvature curves were developed theoretically for all specimens and compared to the experimental results. The research also discussed the issue of compression contribution of CFRP bars and recommendations were presented. Moreover, the research proposed new design equations for the effective flexural stiffness of CFFT columns. Finally, using finite element modelling to provide insights of the structural behavior of the CFFT columns.

The main objectives of this research could be summarized as follow;

1. Investigating the behavior and failure mechanism of reinforced CFFT columns subjected to eccentric loading and comparing it to the behavior of their counterparts subjected to concentric loading.
2. Studying the effect of reinforcement type (Steel or CFRP bars) and eccentricity to diameter ratio (e/D) on the behavior of CFFT columns.
3. Developing complete interaction diagrams for steel and CFRP reinforced CFFT columns experimentally and theoretically.

4. Studying the moment-curvature behavior of reinforced CFFT columns.
5. Developing new expressions for the effective flexural stiffness of CFFT columns based on experimental and theoretical simulations.
6. Understanding the instability buckling behavior of FRP reinforced CFFT columns and developing a new slenderness limit equation for design purposes.
7. Providing insight to the behavior of CFFT columns using finite element analysis.

A general objective could be assigned for this research as the possibility of using CFRP bars in CFFT columns under concentric and eccentric compression loadings and providing design provisions and recommendations for codes and guidelines.

## 1.3 Methodology

To achieve the above-described objectives, a research plan including experimental program and theoretical studies were conducted. The experimental program included testing of full-scale circular CFFT columns reinforced with carbon FRP as well as steel reinforcement. The results were discussed in terms of general behavior, effect of test parameters, interaction diagrams and moment-curvature behavior. On the other side, theoretical studies were prepared to analytically develop the interaction diagrams of the tested specimens along with parametrical investigation. The effective flexural stiffness for the CFFT columns was investigated. The slenderness limit for designing FRP reinforced CFFT columns to avoid column instability was studied. The following flow chart summarized the methodology prepared for this work.

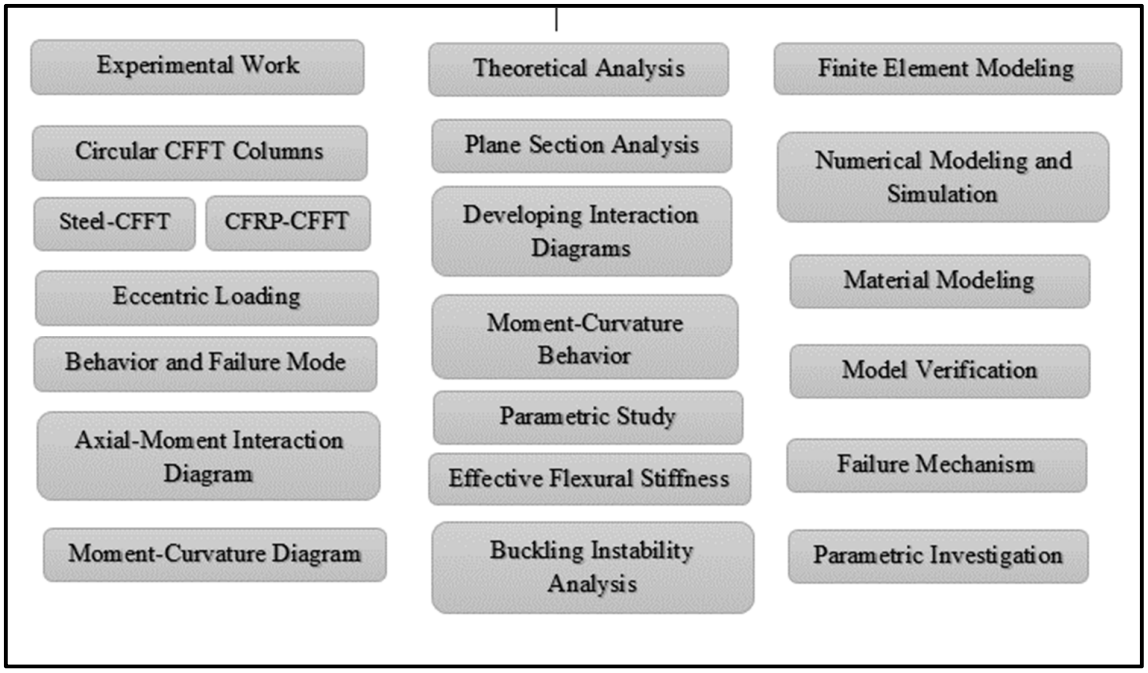


**Figure 1-1**– Flow chart of the research program

## 1.4 Thesis organization

The thesis first begins commonly with a short literature review in **Chapter 2**.

**Chapter 3** (1st article) presents the results of an experimental investigation on the eccentric behavior of circular (steel or CFRP) reinforced CFFT columns. The axial force–moment interaction diagrams were predicted based on the principles of strain compatibility and internal force equilibrium and layer by layer approaches. The moment-curvature behavior was presented and discussed for all specimens. Furthermore, a comprehensive parametric investigation was performed to generate numerous moment-curvature diagrams.

**Chapter 4** (2nd article) presents new developed equations of Effective Flexural stiffness of reinforced and unreinforced CFFT columns based on experimental parametric study and theoretical simulation. Developed equations were compared with experimental effective stiffness at service and ultimate loads.

**Chapter 5** (3rd article) presents a theoretical study for the buckling instability analysis of FRP reinforced CFFT columns. A new equation was suggested for the critical slenderness ratio of CFFT columns for safe design values. A parametric study was conducted to accounts for the effect of different parameters on the buckling behavior of FRP reinforced CFFT columns

**Chapter 6** (4th article) presents a nonlinear finite element analysis using ABAQUS software to understand failure mechanism of CFFT columns and provide deep explanation for experimental observations where test measurements are impossible. This model accounts for cracking and plasticity of concrete and include the effect of material and geometric nonlinearities. A parametric study was conducted to examine the effect of different key parameters on the ultimate capacity and failure mode of CFFTs, namely, number of FRP layers, fiber orientation and reinforcement ratio.

The last Chapter of the thesis, **Chapter 7**, presents some detailed conclusions of the results obtained from the experiments and analyses with respect to observations and highlights discussed throughout the thesis in addition to recommendations for future work.

# CHAPTER 2

# LITERATURE REVIEW

## 2.1 Background on Materials

### 2.1.1 FRP COMPOSITE MATERIALS

Fibre Reinforced Polymers have been extensively used over the past two decades in the construction industry, this refers to its several significant advantages which could be summarized as follows:

- Light weight which results in speed and ease of installation
- High strength to weight ratios
- Outstanding durability in severe environments (Marine conditions, de-icing salts, Chemical products and Moisture)
- High energy absorption
- Its design adaptability as it can be fabricated in wide range of shapes and sizes including bars, tubes, sheets and plates.

Although FRP has been used for rehabilitation and strengthening of existing structures and buildings its use in new construction is becoming more prevalent. FRP composite materials have been used as internal and external reinforcement for concrete structures. FRP bars have been used as internal reinforcement for concrete slabs, barrier walls, bridge decks, and other reinforced pavements corrosive environments (Al-Sayed et al., 2000). In addition FRP composites have been used as an external confinement for strengthening and rehabilitation of structures in terms of sheets, wraps and tubes. One of the most promising confinement techniques that has been used extensively in the recent years is the FRP

composite tube. The FRP tube is used mainly in structures subjected to harsh corrosive environment as an alternative to conventional reinforced concrete and steel components especially in tidal areas for marine piles and zones where de-icing is used, in these areas the conventional materials as steel, timber and reinforced concrete become subjects to rotten, corrosion and disintegration. The FRP composite tube provide a light weight protective jacket and stay in place formwork to contain fresh concrete which saves the cost of formwork used in precast and cast in-place industries. Different parameters are provided by this system to achieve optimum design for each individual application including, fibre orientation, concrete wall thickness, type of fibres and number of fibres layers in the composite shells.

FRP tubes may be manufactured using different techniques including, manual layup, autoclave molding, filament winding, pultrusion and resin transfer molding, though filament winding and plutrusion are considered the most common techniques in forming hollow tubular sections. According to (Ozbakkaloglu & Vincent 2014) , FRP tubes manufactured automatically by using a filament winding technique provide greater strength and strain enhancement for CFFTs compared with tubes manufactured manually using a wet layup process.

## 2.2 Behavior of CFFTs

### 2.2.1 Axial Behavior of CFFT

- **Saafi et al. (1999)**

Saafi et al. (1999) conducted experimental and analytical studies of the performance of concrete columns confined with carbon and glass FRP composite tubes. Concrete filled FRP tubes are instrumented and tested under uniaxial compressive load. Test variables include type of fibre, thickness of tube, and concrete compressive strength.

To test the performance of concrete confined with FRP tubes, 30 concrete cylinders (18 concrete-filled FRP tubes and 12 plain concrete) were tested under compression. All specimens consisted of short columns with a length-to-diameter ratio of 2.85. Each

specimen measured 152.4 mm in diameter and 435 mm in length. The FRP tubes used in this study were made of glass-fibre and carbon-fibre filament winding-reinforced polymers—all consisting of 60 percent fibre and 40 percent polyester resin. The fibres oriented in the circumferential direction of the cylinders. Three tube thicknesses of each fibre type were used. The thicknesses of the glass tubes were 0.8, 1.6, and 2.4 mm, and the carbon tubes were 0.11, 0.23, and 0.55 mm.

It was concluded that:

1. The FRP tube composites are an effective means of confinement. They significantly increase both the strength and ductility of concrete. The rate of increase is dependent upon the tube thickness and the mechanical properties of the composite tube and the unconfined concrete.

2. The stress-strain response of FRP tube-confined concrete is bilinear in both the axial and lateral direction. The first slope of the response depends on the concrete core, while the stiffness of the FRP tube controls the second slope. The bent point between the two slopes takes place at stress levels slightly higher than the unconfined strength of the concrete core.

3. The proposed equations to estimate the ultimate stresses and failure strains produce satisfactory predictions as compared to current design equations available in the literature. The effect the lateral strain is considered in the proposed equations.

4. The predicted stress-strain response in both axial and lateral directions of concrete-filled FRP tubes compares satisfactorily with the experimental values. However, the model underestimates the results of concrete columns confined with FRP composite sheets.

- **Mohamed and Masmoudi (2010)**

Mohamed and Masmoudi (2010) investigated the behaviors of small and medium internally reinforced CFFT columns with different slenderness ratios under concentric axial loading and two types of concrete were presented. The experimental results for 20 unconfined cylinders,

eight CFFT cylinders, eight CFFT columns and one control specimen were investigated. The slenderness ratios ranged between 2, 4, 6 and 8 were examined in the present study. The findings of this research can be summarized as follows:

1. The longitudinal steel bars provide significant dowel action, which delays the dilation of concrete core inside CFFT, thereby improving the ductility of CFFT columns.
2. The ultimate strength of the CFFT is mainly dependent on the stiffness of the GFRP tubes, and it is more effective for normal than medium strength concrete.
3. The failure modes for CFFT are affected by the slenderness ratio.
4. Increasing the slenderness ratio (H/D) of the reinforced CFFT specimens more than six reduce significantly the ultimate load capacity due to the buckling phenomenon.
5. The average ultimate rupture strain of the GFRP tubes is close to the rupture strain obtained from split-disk test.

- **Ozbakkaloglu and Vincent (2014)**

Ozbakkaloglu and Vincent (2014) conducted an experimental study on the axial compressive behavior of 83 monotonically-loaded circular CFFTs. The effects of fiber type, concrete strength, specimen size, and manufacturing method on the compressive behavior of CFFTs were investigated. The CFFTs were manufactured with carbon FRP (CFRP), high-modulus CFRP (HMCFRP), or aramid FRP (AFRP) tubes, and their average unconfined concrete strengths ranged between 34–110 MPa. The diameters of the test specimens ranged from 75–300 mm with all specimens maintaining a 2∶1 height-to-diameter ratio. The effect of the CFFT manufacturing method was investigated through AFRP specimens that were manufactured through either an automated filament winding or manual wet layup technique. The following points were concluded:

1. The specimen size does not have a significant effect on the compressive behavior of CFFTs and a strong correlation exists between the ultimate tensile strain ($\varepsilon_{fu}$) of the fibers and the ultimate axial strain ($\varepsilon_{cu}$) of the CFFTs.
2. Adequately confined high-strength CFFTs can exhibit highly ductile behavior. However, the behavior of these CFFTs is highly sensitive to the level of confinement,

and lightly confined HSCFFTs may not be able to maintain their load-carrying capacity after their initial peak strengths are attained.

3. For a given nominal confinement ratio ($f_{lu}/f'_{co}$) an increase in concrete compressive strength ($f'_{co}$) and associated brittleness leads to an overall decrease in the strength enhancement ratio ($f'_{cc}/f'_{co}$), the strain enhancement ratio ($\varepsilon_{cu}/\varepsilon_{co}$) and the strain reduction factor ($K_\varepsilon$).
4. FRP tubes manufactured automatically by using a filament winding technique provide greater strength and strain enhancement ($f'_{cc}/f'_{co}$ and $\varepsilon_{cu}/\varepsilon_{co}$) for CFFTs compared with tubes manufactured manually using a wet layup process.

### 2.2.2 Flexure Behavior of CFFT

Generally the circular CFFT columns experience better performance than the conventional RC columns in terms of flexure strength and ductility, CFFT columns can exhibit superior additional flexural capacities in the post-yielding stage. This was attributed mainly to the FRP tube contributed in the flexural reinforcement and it forced the concrete core to withstand higher strains.

- **Fam and Rizkalla (2002)**

  Fam and Rizkalla (2002) proposed an analytical model proposed to predict the behavior of concrete-filled rectangular fiber reinforced polymer tubes (CFRFT) subjected to bending, axial compression loading or combined loading. The model accounts for different laminate structures of the flange and the web of the FRP tube through the Classical Lamination Theory (CLT). The gradual reduction of stiffness resulting from the progressive failure of different FRP layers oriented at various angles is accounted for through the Ultimate Laminate Failure (ULF) approach. The model adopts the

cracked section analysis using layer-by-layer approach and accounts for both totally filled tubes and tubes with inner voids.

The following conclusions were drawn:

1. Conventional RC sections of the same moment capacity as CFRFT have higher axial compressive strength, while RC sections with the same axial strength as CFRFT have substantially lower flexural strength.
2. RC sections with similar flexural strength, reinforcement ratio, or reinforcement index to CFRFT are significantly stiffer, but have very low ductility. RC sections with reinforcement ratio based on equivalent axial stiffness (EA) of reinforcement, are quite ductile but substantially lower in flexural capacity than CFRFT.
3. A small fraction of carbon fibers placed longitudinally in the FRP flange of the tube (hybrid laminate), could result in significant gain in flexural strength and stiffness.
4. In CFRFT flexural members, the void size can be optimized for maximum strength-to self-weight ratio.
5. Increasing the wall thickness for a given laminate or increasing the percentage of fibers in the axial direction of the laminate results in increasing the flexural strength and stiffness of CFRFTs. However, failure mode could change from tension to compression. Concrete strength, on the other hand has marginal effect on the flexural response of the CFRFTs.
6. The balanced reinforcement ratio of CFRFT under pure bending depends on the laminate structure. It reduces gradually with increasing axial stiffness of the laminate of the tube.
7. Variation of flexural strength with reinforcement ratio in CFRFT is quite different from singly reinforced RC sections but very similar to that of doubly reinforced RC section.

8. There is insignificant confinement effect on enhancing the strength of CFRFT. Unlike circular members, the unconfined concrete stress-strain curve used in the model predicts well the behavior of CFRFTs under combined bending and axial loading.

9. Increasing the wall thickness or percentage of fibers in axial direction of the tube, results in large gain in flexural strength. In thin tubes, increasing the percentage of fibers in axial direction has insignificant effect on axial strength.

- **FAM et al. (2003)**

Fam et al. (2003) conducted an experimental program and proposed an analytical model for 10 concrete filled GFRP circular tubes under concentric and eccentric axial loads using column specimens as well as under pure bending using beam specimens for the given specimens. Two different laminate structures were used for the GFRP tubes, Axial load/bending moment interaction curves are presented. It has been concluded that:

1. Interaction curves of concrete-filled FRP tubes of moderate diameter-to-thickness ratios are similar to that of reinforced concrete members. As axial load increases, the moment capacity also increases and failure is governed by rupture of the FRP tube at the tension face. A balanced point is reached, beyond which the moment capacity is reduced by increasing the axial load and failure is governed by crushing of the FRP tube in the compression side;

2. The variable confinement model of concrete provides the best prediction of interaction curves. The full confinement model also provides reasonable prediction, however, for tubes with adequate confinement stiffness (as Type I); it overestimates bending capacity at low axial loads;

3. The unconfined concrete model significantly underestimates the interaction diagrams for concrete-filled FRP tubes with adequate confinement stiffness.

The unconfined model with extended strain softening, however, predicts the pure bending strength very well;

4. For a given laminate structure, increasing the wall thickness of the tube increases the axial and bending strengths as evident from the increased size of interaction diagram. The curve could, however, change from the typical shape with the balanced point being the maximum moment (for small thickness tubes) to a shape with the pure bending strength being the maximum moment, and the full curve is governed by compression failure (for large-thickness tubes, particularly for tubes with higher axial stiffness);
5. For both concrete-filled thin and thick tubes, increasing the ratio of fibers in the axial direction significantly increases the flexural strength;
6. Increasing the ratio of fibers in the hoop direction would increase the axial strength of concrete-filled thin tubes only;
7. The axial strength of concrete-filled thick tubes tends to increase by increasing the amount of fibers in the axial direction rather than in the hoop direction. In thick tubes, the contribution from axial stiffness of the tube is more significant than the gain from confinement of concrete;
8. For small-thickness tubes, changing the proportion of fibers in the axial and hoop directions results in a family of interaction curves, intersecting at certain points, which provide an optimum laminate structure for a particular eccentricity for a given wall thickness. For relatively thick tubes, the interaction curves do not intersect and the optimum laminate seems to be the one with maximum axial stiffness and minimum hoop stiffness, regardless of the eccentricity; and

- **Fam and Rizkallah (2005)**

Fam and Rizkalla (2005) conducted an experimental study on three beams and five short columns, consisting of glass fiber reinforced polymer concrete-filled rectangular filament-wound tubes (CFRFTs). The tubes included fibers oriented at ±45° and 90° with respect to the

longitudinal axis. Additional longitudinal fibers [0°] were provided in flanges for flexural rigidity. Beams included totally filled tubes and a tube partially filled with concrete, which had a central hole for reducing deadweight. The effect of reinforcement ratio was examined by using tubes of two different sizes. Flexural behavior of CFRFT was compared to concrete-filled rectangular steel tubes (CFRSTs) of similar reinforcement ratios. Short columns were tested under eccentricity ratios *(e/h)* of 0, 0.09, 0.18, and 0.24, where h is the section depth. Transverse strains were measured around the perimeter of concentrically loaded column to evaluate confinement effect. It was concluded that:

1. CFRFT provide feasible and easy ways to construct structural members for beam and column applications. The FRP tube provides permanent formwork and is the sole reinforcement or concrete in the axial and transverse directions. Unlike steel tubes, strength and stiffness of FRP tubes can be controlled independently in the flanges and webs and also in both directions.

2. The laminate stress–strain behavior of FRP tubes could be quite nonlinear. Laminates with fibers oriented at ±45° show significant nonlinearity under tension and compression. Nonlinearity could also result from progressive failure of layers oriented at various directions.

3. The load–deflection behavior of CFRFT beams is slightly nonlinear due to the nonlinearity of both FRP tube and concrete. The beam with inner hole had an overall strength-to weight ratio, 77% higher than the totally filled beam. Further study is needed to optimize the size and shape of the concrete flange in partially filled beams to avoid premature compression failure.

4. Totally filled CFRFT beam failed by rupture of FRP in the tension side while the beam with a hole failed by inward buckling and fracture of the concrete compressive flange. In both beams outward buckling of the FRP compressive flange was observed.

5. CFRFT beams with $[90/\pm45_2/0_2/90]_s$ GFRP flanges, which have width-to-thickness (b/t) ratios up to 19 fail in tension before local buckling of the flange.

Similar beams, but with b/t=30, fail by local buckling at an axial strain of only 25% of the ultimate compressive strain of the flange.

6. The compression zone depth in CFRFT beams is stable after cracking at 20–30% of the section depth, throughout the loading history. Linear strain distribution is also observed.

7. The flexural strength of CFRFT is comparable to that of CFRSTs of similar reinforcement ratio. Their load–deflection behavior, however, is quite different. The CFRSTs are initially stiffer due to the higher Young's modulus of steel, compared to GFRP. Once the steel yields, plastic behavior is observed, whereas CFRFTs do not show plasticity.

8. Short CFRFT columns loaded over the entire cross section could fail in a brittle manner by fracture of the FRP tube at the round corner, due to a high level of biaxial stresses.

9. The round corners of CFRFT columns provide limited confinement. The flat sides of the FRP tube bends outwards and causes the column to bulge and the concrete core to lose restraint. Consequently, the confinement effect is further reduced.

- **Hadi et al. (2016b)**

Hadi et al. (2016b) investigated the axial and flexural behavior of concrete filled Glass FRP (GFRP) tube columns with and without GFRP bar. The experimental program included four steel RC specimens (REF), four GFRP-CFFT specimens (GT), and four GFRP bar–reinforced GFRP-CFFT (GTGR) specimens with an outer diameter of 205–206 mm and a height of 800–812 mm. The specimens were tested under concentric and 25- and 50-mm eccentric axial loads and four-point load. The experimental results showed that GFRP bar–reinforced GFRP-CFFT specimens sustained higher peak axial loads, axial and lateral deformations at peak axial load, and flexural loads than GFRP-CFFT specimens without reinforcing GFRP bars and steel RC specimens. Axial load and bending moment (P-M) interactions of GFRP-CFFT specimens with and without reinforcing GFRP bars and steel RC specimens were analytically modeled. The following conclusions were drawn;

1. The experimental P-M interaction of the GTGR group was larger than the P-M interactions of the GT and REF group as the GTGR group resisted higher axial and flexural loads and lateral deformations at peak axial loads than the GT and REF groups. The confinement effectiveness of GFRP tube was reduced with the increase in the applied load eccentricity.
2. For the GT and GTGR groups, the analytical axial loads and bending moments calculated by using Samaan et al.'s (1998) and Lam and Teng's (2003) stress-strain models underestimated the experimental axial loads and bending moments, resulting in conservative estimates. Also, the layer-by-layer numerical integration method adopted in this study can be used to accurately compute the axial loads and bending moments of the GT, GTGR and REF groups.

## 2.3 Field Applications of CFFT

Concrete Filled FRP Tube (CFFT) are used in many field applications as piles, finder piles, piers and bridge deck and girders.

- **Fam et al. (2003a)**

Fam et al. (2003a) presented a detailed review of applications of CFFT in marine piles where they discussed the different types of marine piles as follows:

(a) Fender Piling: In front of marine structures, piles are used extensively as vertical fenders, as shown in Figure 2-1.a. The fender piles act as a buffer to absorb and dissipate the impact energy of the ship during berthing and prevent vessels from going underneath the pier.

(b) Dauphins: Dauphins are groups of piles, as shown in Figure 2-1.b placed near piers and wharves to guide vessels into their moorings, to keep them away from structures or to serve as mooring points.

(c) Light Structural piling: The piles can be used to support the loads of light-duty piers and wharves. In this application, bracing between piles is normally used to increase the strength and stiffness of the foundation of the structure as shown in Figure 2-1.c.

(d) Bridge Pier Protection: Piles and dauphins can also be used to create protective structures for bridge piers and to guide vessels into the channel and away from bridge supports as shown in Figure 2-1.d.

They conducted an experimental program over a period of six years to evaluate the structural performance of the CFFT composite piles. During this period, test results and recommendations were continuously fed to the industry, including the design engineers and contractors in charge of the field projects stated above. Full scale tests have been conducted on the most commonly used size of the composite pile (the 323 mm diameter pile), including axial compression short column tests, bending tests using beam specimens and combined bending and axial compression tests using eccentrically loaded columns tested at various eccentricities to establish the axial load - bending moment interaction curves of the pile, and they discussed the following points:

1. Concrete-filled FRP tubes (CFFT) have indeed gained large potential for marine pile applications. The system is becoming more popular as it provides several advantages over conventional piles. Non-corrosive characteristics, elimination of internal steel reinforcement and utilizing the FRP tube as reinforcement and permanent formwork are the most unique features.

2. Eight different field projects have been successfully completed using the CFFT composite piles along the east and west coasts of the United States. The piles were utilized in a verity of configurations including fendering, dauphins, support of light structures and bridge pier protection.

3. The composite piles in the field projects have been in service for several years and some went through severe hurricanes. To date, based on regular inspections, the piles are performing very well.

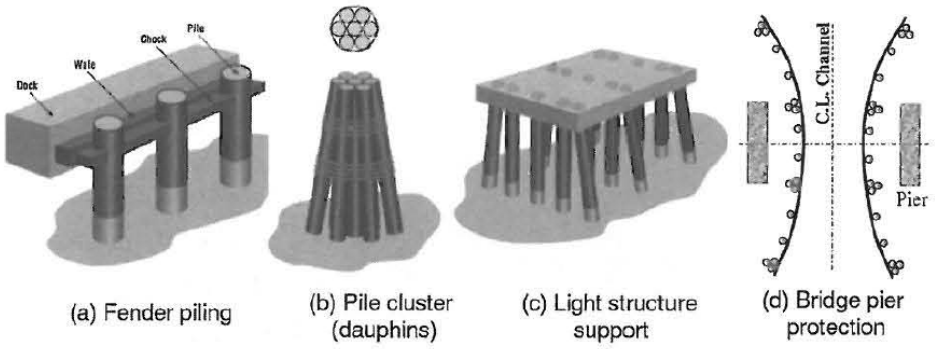


**Figure 2-1-**Different applications of CFFT composite marine piles (Fam et al., 2003a)

## 2.4 Behavior of RC Columns Reinforced with FRP Bars

### 2.4.1 Columns Behavior under Concentric Loading

- **Lotfy ehab. (2010)**

Lotfy (2010) conducted an experimental investigation of the axial behavior of small scale square reinforced concrete columns with fibre reinforced polymer (FRP) bars, a series of 8 columns were tested in a vertical position and under compressive axial static loading. All columns had the same dimensions 250*250mm and 1250mm height, main reinforcement 4#12mm, 6#12mm, and 8#12mm, the transverse reinforcement was ø6@120mm closed stirrups along column. The major parameters included in this research were the main reinforcement ratios, the main reinforcement types, the transverse reinforcement ratios in the column, and the characteristic strength of concrete.

It was concluded that:

1. Tested column with steel reinforcement has ductility more than column with GFRP reinforcement, where ultimate load, ultimate strain and initial cracking loads of column

with steel reinforcement increase with 118, 117 and 117% respectively of column with GFRP reinforcement.

2. Increasing of main reinforcement ratios with GFRP bars increase the ductility of cross section, so it has a significant effect on the initial cracking loads, ultimate strain, and ultimate loads that the columns resist.
3. Increasing of GFRP reinforcement ratios from 0.723 to 1.08% has a noticeable significant effect on the all behavior of tested columns more than the increase of reinforcement ratios from 1.08 to 1.45%.
4. Increasing of transverse reinforcement ratio leads to increase the toughness and ductility of tested columns with GFRP bars, where the increase of transverse reinforcement ratios confines the columns so it is lead to increasing the ultimate loads which the columns resisted, hence increasing ultimate strain, and initial cracking loads. And the column with GFRP bars has toughness and ductility more than column with steel bars and normal transverse reinforcement distribution.
5. Increasing of characteristic strength of concrete has significant effect on the behavior of tested columns where increase toughness and ductility of tested columns.

- **De luca et al. (2011)**

Luca et al. (2011) conducted an experimental program on full-scale GFRP reinforced concrete (RC) columns under pure axial load using specimens with a 24 x 24 in. (0.61 x 0.61 m) square cross section. The study was conducted to investigate whether the compressive behavior of longitudinal GFRP bars impacts the column performance, and to understand the contribution of GFRP ties to the confinement of the concrete core, and to prevent instability of the longitudinal reinforcement. The following conclusions were drawn:

1. The behavior of RC columns internally reinforced with GFRP bars is very similar to that of conventional steel

RC columns if the longitudinal reinforcement ratio is equal to 1.0%. No appreciable difference was observed in terms of peak capacity. Failure of the steel RC specimen happened due to buckling of the longitudinal reinforcement when still in the elastic range, whereas the GFRP RC specimens failed due to the crushing of the concrete core at axial strains higher than those measured in the steel RC counterpart.

2. The use of longitudinal GFRP bars is not detrimental to the performance of RC columns. The contribution of the GFRP bars to the column capacity, however, was less than 5% of the peak load, which is significantly lower than that of approximately 12% of the steel bars in the steel RC counterpart. It is concluded that the contribution of the GFRP bars may be ignored when evaluating the nominal capacity of an axially loaded RC column.
3. The difference in the GFRP bar manufacturers does not affect the performance when bars are of comparable quality.

- **Tobbi et al. (2012)**

Tobbi et al. (2012) conducted an experimental study on eight RC square columns 50 x 350 x 1400 mm (13.78 x 13.78 x 55.1 in.) to study their behavior under axial loads and to estimate the effect of FRP bars as longitudinal and lateral reinforcement on the strength and strain capacities of the concrete column. The eight columns were classified as follows, one made of plain concrete with no reinforcement, two steel RC columns reinforced by 8M15 bars, three GFRP columns reinforced by 8 #19 bars and two GFRP columns reinforced by 12 #16. All of the RC columns had similar areas of longitudinal reinforcement, comprising 1.9% of the gross section area Ag. The effect of different parameters were studied such as concrete cover, tie configuration and tie spacing. Figure 2-2 (a) and (b) show testing details and GFRP bar failure modes respectively.

The following conclusions were conducted:

1. The early spalling of the concrete cover resulted in a loss of axial capacity before any lateral confinement came into effect. After the concrete cover had completely spalled off, important gains in strength, ductility, and toughness were recorded for the concrete cores of well-confined specimens.
2. Studying tie configuration and spacing clarified the effectiveness of GFRP as transverse reinforcement in increasing strength, toughness, and ductility of the confined concrete core. Further research is needed to study limitations of tie spacing.
3. The strength reduction factor of 0.85 (the case for steel) can be adopted for GFRP-reinforced columns.
4. Setting the FRP compressive strength at 35% of the FRP maximum tensile strength yielded a reasonable estimate of ultimate capacity compared to the experimental results. More experimental evidence is needed, however, to more accurately define FRP compressive strength.
5. The GFRP bars used contributed 10% of column capacity, which is close enough to steel's contribution (12%).

This proves that GFRP bars could be used in compression members provided there was adequate confinement to eliminate bar buckling.

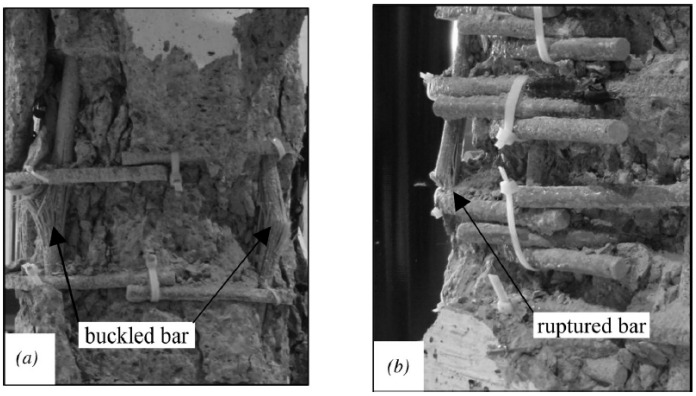


**Figure 2-2-**GFRP bar Failure (Tobbi et al., 2012)

The same authors conducted another experimental program (Tobbi et al. 2014) to study concrete columns reinforced longitudinally with glass FRP (GFRP), carbon FRP (CFRP), and steel bars and GFRP and CFRP transverse reinforcement subjected to concentric loading. Twenty concrete columns were tested measuring 350 x 350 x 1400 mm (13.8 x 13.8 x 55.1 in.) subjected to concentric compressive loading. One column was kept un-reinforced (plain concrete) while the remaining 19 were internally reinforced with FRP and steel according to different parameters.

All used transverse reinforcements were GFRP or CFRP, while the longitudinal reinforcement was GFRP, CFRP, or steel bars.

Different parameters were studied including the shape of transverse reinforcement, longitudinal reinforcement ratio, longitudinal reinforcement material (GFRP, CFRP, or steel), FRP-transverse reinforcement material (GFRP or CFRP), the diameter of the transverse reinforcement (No. 9.5 and 12.7 mm [No. 3 and No. 4]), transverse reinforcement spacing, and confining volumetric stiffness. Figure 2-3 shows Failure mode of columns reinforced longitudinally and transversely with FRP. Finally the following points were concluded:

1. The confinement efficiency of closed FRP transverse reinforcements cut from continuous square spiral is higher than C-shaped type transverse reinforcements.
2. The ultimate axial strain of columns reinforced longitudinally with FRP is almost 30% lower than those reinforced with the same volume of steel.

3. The ultimate axial compressive strain for columns reinforced longitudinally and transversally with FRP can reach a value on the same order of magnitude as the FRP ultimate tensile strain of the longitudinal bars under good confinement conditions.

4. The contribution of FRP longitudinal reinforcement in concrete columns subjected to axial concentric loading should not be neglected. A proposed equation based on elastic theory yields good predictions compared with laboratory test data.

5. FRP transverse reinforcement configuration and spacing are the most important parameters (compared with confinement provided by concrete cover) affecting confining efficiency in internally reinforced concrete columns under axial loading.

6. In the case of large spacing with low volumetric ratio, CFRP transverse reinforcement performed significantly better than GFRP. Increasing the volumetric ratio while reducing spacing will eliminate the effect of material stiffness. In such cases, the GFRP transverse reinforcements are more cost effective.

7. Columns internally reinforced with a combination of steel longitudinal bars and FRP transverse reinforcements exhibit good gains in terms of compressive strength and ultimate axial strain. Nonetheless, the use of FRP transverse reinforcement should still improve corrosion resistance of a column by adding an extra 10 mm (0.4 in.) of cover to the steel.

8. The presented study showed the applicability of exclusively reinforcing the columns with FRP and subjected to on centric load. Further research elaboration is necessary to investigate the behavior of FRP reinforced columns loaded laterally or subjected to load combination (axially and laterally).

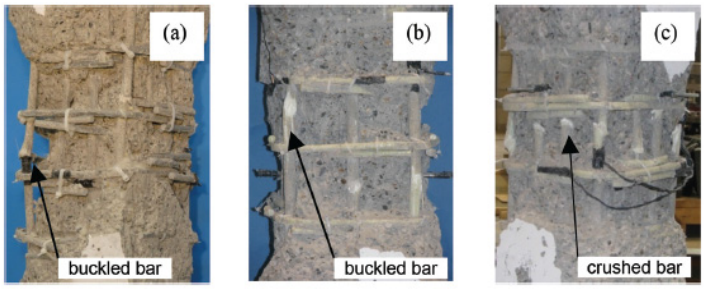


**Figure 2-3-**Failure mode of columns reinforced longitudinally and transversely with FRP (Tobbi et al, 2014)

- **Afifi et al. (2014)**

Afifi et al. (2014) conducted an experimental study to evaluate the performance Evaluation of Concrete Columns Reinforced Longitudinally with FRP Bars and Confined with FRP Hoops and Spirals under Axial Load. 14 full scale specimens were tested under pure axial load, including 12 RC columns reinforced with longitudinal GFRP or CFRP bars and confined with GFRP or CFRP spirals or circular hoops. Plain and steel RC columns were introduced as reference specimens. Two different modes of failure were observed in the 14 columns tested in this study. The GFRP and steel RC specimens failed in a ductile manner with the gradual spalling of the concrete cover, followed by buckling of the longitudinal bars and then rupture of the spirals or hoops. The CFRP columns failed in a rather sudden and brittle manner, closely similar to the failure of the plain specimen as shown in Figure 2-4 and Figure 2-5

The following conclusions can be drawn:

1. The GFRP and CFRP RC columns behaved similarly to the steel RC columns and exhibited linear load-strain behavior in the ascending part up to 85% of their peak loads;
2. The experimental evidence of the current study indicated that the use of FRP spirals and hoops as lateral reinforcement, in accordance with CSA S806-12 (CSA 2012) limitations, effectively confined the concrete core in the post peak stages;
3. FRP circular hoops were found to be as efficient in confining concrete as spirals; the GFRP and CFRP RC columns with spirals attained 1.3% and 2.2%, respectively, higher

strength than their counterpart specimens confined with hoops, with an insignificant increase in ductility and confinement efficiency;

4. The GFRP and CFRP bars developed up to 0.4% and 0.7% compressive strain, confirming that the FRP bars were effective in resisting compression until after crushing of the concrete;

5. The GFRP and CFRP RC columns failed in a brittle and explosive manner when confined with less than a 1.5% volumetric ratio; failure of the well-confined GFRP RC columns was attributed to crushing of the concrete core and rupture of the GFRP spirals;

6. The test results indicated that using a splice length equal to 20 times the diameter of the hoops was sufficient to avoid pullout or slippage failure with the GFRP and CFRP hoops; more experimental evidence and future works are needed, however, to more accurately define the splice length;

7. The design equation was modified to predict the nominal capacity of the GFRP and CFRP RC columns; limiting the compressive strain of the CFRP and GFRP bars to 0.002 provided accurate predictions of the nominal capacity of the tested RC columns;


**Figure 2-4-**Overview of the GFRP RC column specimens after failure (Afifi et al., 2014)


**Figure 2-5-**Overview of the CFRP RC column specimens after failure (Afifi et al.,2014)

## 2.4.2 Columns Behavior under Eccentric Loading

- **Tikka et al. (2010)**

Tikka et al. (2010) conducted an experimental program on 8 slender columns with 1800 mm length and square 150 x 150 mm cross section reinforced with GFRP longitudinal bars and laterally hooped using a carbon fiber spiral wrap to investigate the behavior of the slender concrete beam-columns under eccentric loads. Figure 2-6 showed GFRP reinforcement cage with carbon fiber spiral placed in formwork and Figure 2-7 showed dimensions and specimens reinforcement details. The results showed that GFRP reinforcing bars had very small contribution in concrete columns capacities and using a CFRP warps as a spiral stirrups provides adequate lateral restraint for the longitudinal reinforcing bars.

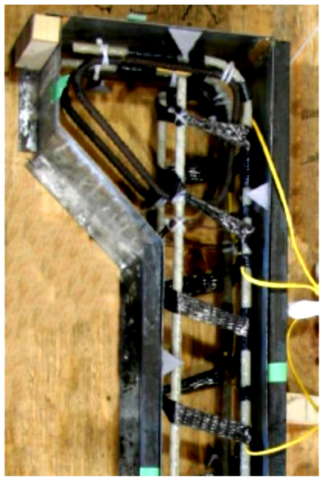

**Figure 2-6-**GFRP reinforcement cage with carbon fiber spiral placed in formwork (Tikka et al., 2010)

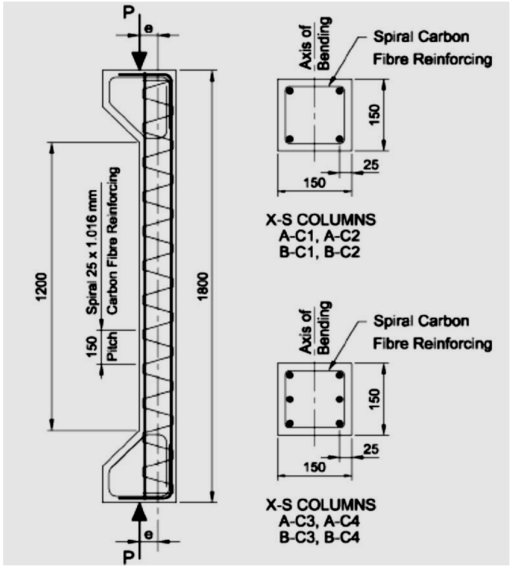


**Figure 2-7-**Dimensions and specimens reinforcement details (Tikka et al.,2010)

- **Issa et al. (2012)**

Issa et al. (2012) Conducted an experimental program on six columns of 150*150 mm cross section to explore the behavior of GFRP and steel reinforced concrete columns when subjected to eccentrically axial loads. Four of them had GFRP reinforcement and two had steel reinforcement. The concrete strength of the GFRP reinforced columns was either 24.73 MPa

or 38.35 MPa while for the steel reinforced columns it was 24.73 MPa. The eccentricity was either 50 mm or 25 mm and the tie spacing was either 80 mm or 130 mm. Figure 2-8 show the test specimen. In general, all the specimens failed by sudden crushing of the most compressed concrete fibers on the compression face. It was concluded that:

1. Steel reinforced columns deform lesser than GFRP reinforced columns.
2. Columns with greater tie spacing deform more than those with smaller tie spacing. The difference in deformations is clear for GFRP reinforced columns and is small for steel reinforced columns.
3. In this research, tie spacing had no notable effect on the maximum lateral deflection.
4. For the tested columns with initial eccentricity equal to 50 mm, the average maximum stress was about 60% of the concrete compressive strength
5. The GFRP bar strain is smaller for the medium strength specimens compared to normal strength specimens.
6. Steel bar strains were generally smaller than GFRP bar strains.
7. At high loads, the GFRP and steel bar strains are larger when the tie spacing is larger.

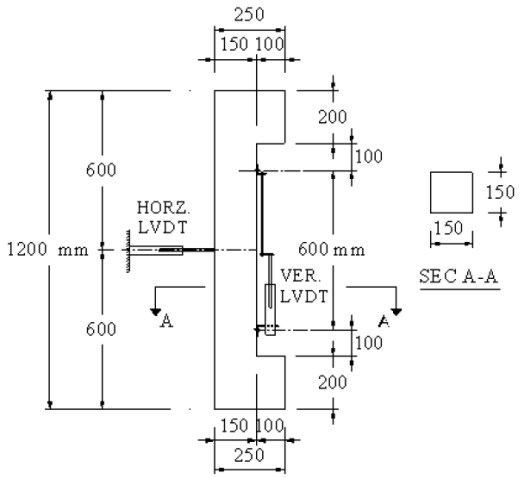


**Figure 2-8-**Test Specimens (Issa et al., 2011)

- **Hadi et al. (2016a)**

Hadi et al. (2016a) investigated the use of GFRP bars and GFRP helices (spirals) as longitudinal and transversal reinforcement, respectively, in RC columns. A total of 12 circular concrete specimens with 205-mm diameter and 800-mm height were cast and tested under different loading conditions. The effect of replacing steel with GFRP reinforcement and changing the spacing of the GFRP helices on the behavior of the specimens was investigated. Nine specimens were tested as columns under eccentricity as shown in Figure 2-9 and three specimens were tested as beams under flexure. It was concluded that:

1. Replacing the steel bars and helices with the same amount of GFRP bars and helices led to reductions in the axial load-carrying capacity and bending moment of the specimens under different loading conditions. Also, an increase in the applied initial eccentricity caused a reduction in the performance of the column specimens in terms of axial load-carrying capacity and ductility;
2. The load-carrying capacity and bending moment of the GFRP RC specimens can be calculated by the same principles used for the conventional steel-RC specimens. Also, ignoring the contribution of the GFRP bars in compression may result in a large discrepancy between the experimental and analytical results.

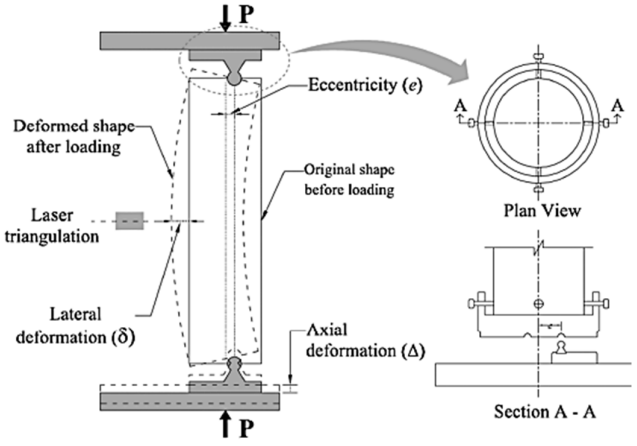


**Figure 2-9-**Test Specimens (Hadi et al., 2016)

## 2.5 Confinement Models

Early research on tested concrete cylinders by Richart et al. (1928) and Richart et al. (1929) provided some of the basic information on concrete confinement. The first set of tests included concrete cylinders confined by uniform fluid pressure (Richart et al. 1928), followed by cylinders confined by circular spirals (Richart et al.1929). Subsequently, (King 1946) studied the effect of confinement on ultimate strength of reinforced columns. Column confinement was a topic for many researchers. (Chan 1955) and (Roy & Sozen 1965) experimentally investigated the behavior of confined concrete, and proposed analytical models to describe stress-strain relationships for confined concrete. The main variables considered were the size, strength, amount and spacing of lateral reinforcement (Moussa, 1993). Other variables considered included cross-sectional size and shape, and rate of loading. In 1988, Mander et al. reported test results of circular, square, and rectangular columns with different volumetric ratios and spacings of confinement reinforcement (Mander et al. 1988)

The first models proposed to understand the behavior of FRP confined concrete were based on the models derived for steel confined concrete. Initial studies to model FRP confined concrete was carried out by (Fardis & Khalili 1981). The model is based on the triaxial failure criterion proposed by Richart et al. (1929). (Saadatmanesh et al. 1994) developed a model, based on

Mander et al.'s model (1988), for columns that are partially confined using FRP strips. The enhancement of the confined concrete was defined as a function of confining pressure which was considered constant throughout the test. As FRP behaved differently from steel under axial loading, the steel confinement models can't be applied on FRP confined models, the main reason of that is the non-yielding behavior of FRP.

Researchers showed in appropriate implementation of steel confinement models (Mirmiran and Shahawy (1996)) and (Spoelstra & Monti 1999). Consequently, more models, based on FRP confined specimen, were introduced (Nanni & Bradford 1995); (Samaan et al. 1998);( Spoelstra and Monti 1999),(Lam & Teng 2003).

For circular FRP confined reinforced concrete (RC) columns, several stress -strain models have been proposed to model the constitutive behavior of concrete. These stress–strain models can be classified into two categories: design-oriented and analysis-oriented models (Lam and Teng 2003). Design-oriented models (Fardis and Khalil (1982), (Samman et al. 1998), ((Xiao & Wu 2000), (Ozbakkaloglu & Lim 2013) provide closed-form equations directly calibrated on experimental results for predicting the compressive strength, ultimate axial strain, and stress–strain behavior of FRP-confined concrete. Analysis-oriented models (Mirmiran et al. 1996), (Spoelstra el al. 1999), (Fam & Rizkalla 2001b) derive stress–strain relation that are generated using incremental numerical procedures typically used within nonlinear FE models. Among the two categories, design-oriented models generally performed better than the analysis-oriented models in predicting the ultimate strength enhancement and strain enhancement ratios. This is primarily because these models were calibrated from test data of FRP-confined concrete that enabled them to directly interpret the important parameters that influence the behavior of FRP-confined concrete. It should be noted that the confinement models proposed for the FRP wraps and jackets are applicable for modelling the stress-strain models for the CFFT members. (Ozbakkaloglu et al. (2013))

A review of examples of the past researches conducted to study the stress-strain confinement model of FRP confined concrete columns are presented as follows:

- **Fardis et Khalil ( 1981)**

Fardis and Khalil (1981) focused on concentrically loaded short circular columns. They performed short term compression tests on 3 *6 in. and 4*8 in. cylinders and concluded that there is agreement between the strength and the axial stress suggested by Richart et al. (1928).

Ultimate condition expressions for strength and strains were as follows:

$$\frac{f'_{cc}}{f'_c} = 1 + 4.1\,\frac{f_{l,a}}{f'_c} \qquad 2\text{-}1$$

$$\varepsilon_{cu} = 0.002 + 0.001\left(\frac{E_f t_f}{D f'_c}\right) \qquad 2\text{-}2$$

Axial stress –strain curve expression:

$$f_c = \frac{E_c\,\varepsilon_c}{1 + \varepsilon_c\left(\frac{E_c}{f_{lu}} - \frac{1}{\varepsilon_{cu}}\right)} \qquad 2\text{-}3$$

Where $f'_{cc}$the ultimate confined stress of FRP is confined concrete, $f'_c$ is ultimate unconfined concrete stress, $f_c$ is the axial compressive stress of concrete, $\varepsilon_c$ is the axial strain of unconfined concrete and $\varepsilon_{cu}$ is the ultimate axial strain of FRP confined concrete.

- **Samman et al. ( 1998)**

Samman et al. (1998) introduced a model that depends mainly on the relation between the dilation rate and confining material hoop stiffness where 30 cylindrical specimens (152.5*305mm) were tested under uniaxial compression. The proposed model adapted Richard and Abbott equation (1975) as follow:

The stress–strain behavior of FRP-confined concrete was described by two slopes, namely the slope of the elastic portion of the initial ascending branch ($E_1$) and the post-peak second branch ($E_2$)

$$f_c = \frac{(E_1 - E_2)\varepsilon_c}{(1 + (\frac{(E_1 - E_2)\varepsilon_c}{f_o})^n)^{\frac{1}{n}}} + E_2\varepsilon_c \qquad n = 1.5 \qquad 2\text{-}4$$

Ultimate condition expressions for strength and strains:

$$f'_{cc} = f'_c + 6(f_{lu})^{0.7} \qquad 2\text{-}5$$

$$\varepsilon_{cu} = \frac{f'_{cc} - f_o}{E_2} \qquad 2\text{-}6$$

Where $f_o$ is the intercept stress which is a function of the strength of the unconfined concrete and the confining pressure of the tube.

$$f_o = 0.872f'_c + 0.371f_{lu} + 6.258 \quad 2\text{-}7$$

$$E_1 = 3950\sqrt{f'_c} \qquad 2\text{-}8$$

$$E_2 = 254.61\, f'^{0.2}_c + 1.3456\, \frac{E_f t_f}{D} \qquad 2\text{-}9$$

- **Lam et Teng (2003)**

Lam and Teng (2003) developed a model for confined concrete where they assumed that the stress–strain curve consists of two parts: the first is a parabolic section and the second is a straight line. The slope of the parabola at $\varepsilon_c$=0 (initial slope) is the same as the elastic modulus of unconfined concrete $E_c$ and the nonlinear part of the first portion is affected to some extent by the presence of an FRP jacket. The parabolic first portion joins the linear second portion smoothly (i.e. there is no change in slope between the two portions where they join) and the linear second portion ends at a point where both the compressive strength and the ultimate axial strain of confined concrete are reached. The proposed stress –strain model is defined by two equations:

$$f_c = E_c\,\varepsilon_c - \frac{(E_c - E_2)^2}{4f_o}\varepsilon_c{}^2 \qquad 0 \le \varepsilon_c \le \varepsilon_l \qquad 2\text{-}10$$

$$f_c = f_o + E_c\,\varepsilon_c \qquad \varepsilon_l \le \varepsilon_c \le \varepsilon_{cu} \qquad 2\text{-}11$$

The second linear part of the stress strain curve joins the first part at a transition strain$\varepsilon_l$ which is given by:

$$\varepsilon_l = \frac{2f_o}{(E_c - E_2)} \qquad 2\text{-}12$$

where $E_2$ is the slope of the linear second part of the stress-strain curve and is given by

$$E_2 = \frac{f'_{cc} - f_o}{\varepsilon_{cu}} \quad 2\text{-}13$$

Where $f_o$ is the intercept stress which is a function of the strength of the unconfined concrete and the confining pressure of the tube and was calculated from Samman et al, 1998:

$$f_o = 0.872f'_{co} + 0.371f_{lu} + 6.258 \quad 2\text{-}14$$

- **Mohamed and Masmoudi (2010)**

Developed a model to account for the confinement using FRP tubes is proposed to predict the peak stress of the CFFT cylinders as follows:

$$f'_{cc} = f'_c\left[0.7 + 2.7\left(\frac{f_{lu}}{f'_c}\right)^{0.7}\right] \qquad 2\text{-}15$$

The proposed model was calibrated using the regression analysis method and based on the test results of 23 CFFT specimens were tested under axial compression load. The accuracy of the proposed model depends significantly on the ultimate hoop strength of the FRP tubes. Also, this model accounts for the variation in the unconfined concrete compressive strength in the range of 25–60 MPa.

- **Wei and Wu (2012)**

Wei and Wu (2012) presented a unified stress–strain model of concrete for circular, square, and rectangular columns confined by fibre-reinforced polymer (FRP) jackets. The proposed model was built on gathering 432 specimens, 100 of which from the authors work and the rest are from literature. The model developed has the following equations:

$$f_c = E_c\,\varepsilon_c - \frac{f_o - E_c\varepsilon_o}{{\varepsilon_o}^2}{\varepsilon_c}^2 \qquad 0 \le \varepsilon_c \le \varepsilon_o \qquad 2\text{-}16$$

$$f_c = f_o + E_2\,(\varepsilon_c - \varepsilon_o) \qquad \varepsilon_o \le \varepsilon_c \le \varepsilon_{cu} \qquad 2\text{-}17$$

where the transitional strain, $\varepsilon_o$ is calculated from the second aforementioned condition to give:

$$\varepsilon_o = \frac{(f_o + f_{cu} + E_c\varepsilon_{cu}) - \sqrt{(f_o + f'_{cc} + E_c\varepsilon_{cu})^2 - 8f_oE_c\varepsilon_{cu}}}{2E_c} \qquad 2\text{-}18$$

$$E_2 = \frac{f_{cu} - f_o}{\varepsilon_{cu} - \varepsilon_o} \qquad 2\text{-}19$$

The proposed model has three parameters, ultimate stress$f_{cu}$, ultimate strain$\varepsilon_{cu}$ , and transitional stress$f_o$, which are determined as follows:

$$\frac{\varepsilon_{cu}}{\varepsilon_o} = 1.75 + 12\left(\frac{f_{lu}}{f'_c}\right)^{0.75}\left(\frac{f_{30}}{f'_c}\right)^{0.62}\left(0.36\,\frac{2r}{b} + 0.64\right)\left(\frac{h}{b}\right)^{-0.3} \qquad 2\text{-}20$$

$$f_o = f'_c + 0.43\left(\frac{2r}{b}\right)^{0.68}\left(\frac{h}{b}\right)^{-1} f_{lu} \qquad 2\text{-}21$$

where *f30* is the concrete strength of unconfined grade *C30* concrete.

- **Ozbakkaloglu et al (2013)**

Ozbakkaloglu et al.(2013) presented a design oriented model to quantify the influence of important parameters on the behavior of FRP-confined concrete. The ultimate stress and strain conditions were calculated as follow:

The ultimate strength:

$$f'_{cc} = C_1 f'_c + 3.2[f_{lu} - f_{lo}] \quad 2\text{-}22$$

Where $f_{lu}$ is the reduced actual confining pressure, $f_{lo}$ is the threshold confining pressure

$$C_1 = 1 + 0.0058 \frac{K_l}{f'_c} \quad 2\text{-}23$$

$$f_{lo} = K_l \varepsilon_{l1} \quad 2\text{-}24$$

$$\varepsilon_{l1} = (0.43 + 0.009 \frac{K_l}{f'_c}) \varepsilon_o \quad 2\text{-}25$$

$$K_l = \frac{2E_f t_f}{D} \qquad K_l \geq f'^{0.65}_c \quad 2\text{-}26$$

The Ultimate strain:

$$\varepsilon_{cu} = C_2 \varepsilon_o + 0.27(\frac{K_l}{f'_c})^{0.9} \varepsilon_{h,rup}^{1.35} \quad 2\text{-}27$$

where $\varepsilon_{h,rup}$ is the hoop rupture strain.

$$C_2 = 2 - \left(\frac{f'_c - 20}{100}\right) \qquad C_2 \geq 1 \quad 2\text{-}28$$

$$\varepsilon_o = \left(-0.067 f'^2_c + 29.9 f'_c + 1053\right) * 10^{-6} \quad 2\text{-}29$$

## 2.6 Finite Element Modelling

In modern structural engineering research, finite element analyses (FEA) are essential for interpretations to the experimental results and providing insights into structural behavior of FRP-confined RC columns. Good numerical models can predict the crack initiation and propagation and help in understanding of the various failure mechanisms, the influence of the important governing parameters and provide explanations to experimental observations, where

the test measurements are impossible. Realistic and reliable models must be able to account for the numerous complexities of concrete behavior such as the nonlinear response in compression, post-cracking behavior in tension, and the bond-slip relationships associated with FRP/concrete interfaces.

In early work, linear elastic analyses were implemented, while the recent trend has been towards the use of nonlinear finite element models. Recently various commercial finite element packages have been used for the analysis of the behavior of FRP confined concrete columns. These include ABAQUS (Hu et al, 2003; Jiang et al., 2013 ; Teng et al., 2015 ; Hassanein et al.,2015 ; Lin et al., 2017), ANSYS ( Mirmiran et al., 2000; Feng et al.,2002; Li et al.,2003; Chakrabarti et al.,2008; Son et Fam, 2008; Pan et al.,2017) and In other studies, in-house numerical codes have been developed based on various approaches (Montoya et al., 2004).

A review of past studies on the application of finite element analysis for the modelling of FRP confined concrete columns is presented in this section. A description of concrete constitutive models, concrete cracking behavior, and various techniques for modelling FRP strengthening materials is presented.

- **Mirmiran et al (2000)**

Mirmiran et al (2000) conducted a nonlinear finite element model for FRP confined concrete using non associative Drucker–Prager plasticity model (Drucker and Prager 1952) that was developed to account for restraint pressure sensitivity of concrete and assumes an elastic perfectly plastic response. The model was developed in ANSYS and used one quarter model of the circular and square column specimens. Concrete is modelled by an 8-noded SOLID65 element, which consists of a single solid material and up to three smeared reinforcing materials in three different orientations. The solid material, i.e., plain concrete, is treated as an initially isotropic homogeneous material with different tensile and compressive strengths. It is also capable of cracking in tension and crushing in compression. Cracking can occur in any of the three orthogonal directions. The element can also accommodate plastic deformations and creep. The jacket is modelled by a 4-noded linear elastic membrane SHELL41 element, which is a three dimensional shell element with membrane stiffness and three translational degrees of freedom per node. However, it does not have any bending stiffness, nor any rotational degree

of freedom. The element can accommodate variable thickness, orthotropic behavior, stress stiffening, large deflection, and cloth option, the last of which is a nonlinear feature that constitutes wrinkling of the element in compression in one or both orthogonal directions.

It was concluded that while the Drucker Prager plasticity can be calibrated fairly well for predicting the axial stress strain response, it does not properly establish the true dilation tendencies of the FRP-confined concrete, simply because the DP model corresponds to an elastic perfectly plastic material.

- **HU et al. (2003)**

Hu et al. (2003) proposed proper material constitutive models for concrete-filled tube (CFT) columns and verified it by the nonlinear finite element program ABAQUS against experimental data. The cross sections of the CFT columns in the numerical analysis are categorized into three groups, i.e., circular section, square section, and square section stiffened by reinforcing ties. As the concrete in the CFT columns is usually subjected to triaxial compressive stresses, the failure of concrete is dominated by the compressive failure surface expanding with increasing hydrostatic pressure. Hence, a linear Drucker-Prager yield criterion (Figure 2-2) is used to model the yield surface of concrete. Via the numerical analyses, it is shown that for circular CFT columns, the tubes can provide a good confining effect to the concrete especially when the width-to-thickness ratio $D/t$ is small say ($D/t$<40). For square CFT columns, the tubes do not provide a large confining effect to the concrete especially when the width-to-thickness ratio $B/t$ is large say ($B/t$>30).

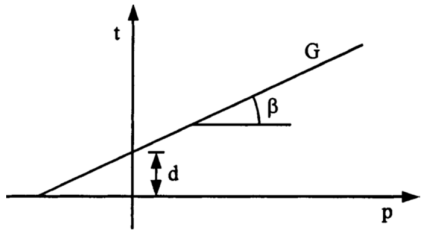


**Figure 2-10-**Linear Drucker-Prager yield criterion for concrete (Hu et al, 2003)

- **Montoya et al (2004)**

Montoya et al. (2004) presented a new constitutive model for confined concrete that were formulated and implemented into in-house nonlinear finite element programs at the University of Toronto where a program for analysis of axisymmetric solids was specifically developed. The confinement models proposed follow a compression field modelling approach that combines nonlinear elasticity and plasticity- type modelling, the formulations were corroborated by examining the behavior of reinforced concrete columns confined with fibre reinforced polymers (FRP), steel, or a combination of both. The nonlinear elastic analysis procedure in VecTor3 and VecTor6 was implemented. The Mohr–Coulomb criterion is used to determine the cracking stress of concrete, in triaxial states of stress. The main objective of the work was to evaluate the capabilities of the compression field modelling to reproduce the behavior of confined concrete at the structural level. The analytical and experimental results were found to agree reasonably well.

- **Son and Fam (2008)**

Son and Fam (2008) developed a finite element model using ANSYS to predict the flexure behavior of both hollow FRP tubes and CFFTs. It accounts for cracking and plasticity of the concrete-fill and includes the effects of both materials and geometric nonlinearities. For the concrete core in CFFTs, an eight-node 3-D Reinforced Concrete Solid (SOLID65) element was used, the element is based on a constitutive model for the triaxial behavior of concrete, the element includes a smeared crack analogy for cracking in tension zones and a plasticity algorithm to account for the possibility of concrete crushing in compression. The concrete material is assumed to be initially isotropic, before cracking or crushing. Each element has eight integration points at which cracking and crushing checks are performed. Cracking or crushing occur once one of the element's principal stresses exceeds the tensile or compressive strength of concrete. Cracked or crushed regions are formed perpendicular to the relevant principal stress direction. FRP material failure is detected through the Tsai–Wu failure criteria. The model agreed well with the provided experimental data.

- **Yu et al. (2010)**

Yu et al. (2010) presented a modified plastic-damage model within the theoretical framework of the Concrete Damaged Plasticity Model (CDPM) in ABAQUS for the modelling of confined concrete under non-uniform confinement. The modifications proposed for the CDPM include a damage parameter, a strain-hardening/softening rule and a flow rule, all of which are confinement-dependent, and a pressure- dependent yield criterion. The distinct characteristics of non-uniformly confined concrete are also included in this model by defining an effective confining pressure. Finite element models incorporating the proposed CDPM model were developed for concrete in a number of confinement scenarios, including active confinement, biaxial compression, FRP-confined circular and square columns, and hybrid FRP-concrete-steel double-skin tubular columns. The finite element predictions were shown to be in close agreement with the existing test results.

- **Lim and Teng (2016)**

Lim and Teng (2016) presented a three dimensional finite element modelling of FRP-confined circular concrete columns under eccentric loading using ABAQUS finite element program. The approach is based on Yu et al. (2010) plastic-damage model for the compressive behavior of FRP-confined concrete. The FE approach has been shown to provide accurate predictions for FRP-confined circular concrete columns tested by previous researchers. Based on the results and discussions presented in the paper, the following conclusions was drawn:

1. The concrete in an eccentrically-loaded FRP-confined column is subjected to non-uniform confinement, and this non uniformity increases as the load eccentricity increases.

2. The direct use of a concentric-loading stress–strain model in the analysis of eccentrically-loaded columns can lead to significant errors in deformation/ductility predictions, but the corresponding errors in the prediction of load-carrying capacity are small for columns with a relatively small load eccentricity; for columns with a large load eccentricity, both the load capacity and the ultimate deformation/ductility are significantly underestimated. Therefore, it is important to include the effect of strain

gradient on the stress–strain behavior of confined concrete in the strengthening/retrofit design of FRP jackets.

## 2.7 Summery

By reviewing the past studies on CFFT members, it can be found concluded that there is a research gap in understanding the behavior of reinforced CFFT columns under concentric and eccentric loading. Moreover, introducing appropriate equations is still needed for the design of reinforced CFFT columns.

# CHAPTER 3

# Analytical Modeling of Moment-Curvature Behavior and P-M Diagram of Steel and CFRP RC Circular Columns Confined with GFRP Tubes

(***Composite Structures Journal, 189 (2018), p. 473-487***.)

## Abstract

Enhancing the behavior, strength, durability and stiffness of concrete columns is achieved through integrating the fiber-reinforced-polymer (FRP) reinforcement into concrete-filled FRP tube (CFFT) technique. Yet, the eccentric behavior of CFFT columns reinforced with FRP bars was not well investigated. This paper reports on the results of an experimental investigations and theoretical models of CFFT columns reinforced with steel and carbon-FRP (CFRP) bars under concentric and eccentric compressive loads. The experimental test parameters were the type of the internal reinforcement (CFRP versus steel) and eccentricity to diameter ratios. It was found that the CFRP reinforced CFFT columns successfully maintained the axial load capacities under different eccentricities as compared with the steel reinforced CFFT columns. However, the strength and behavior of the steel and CFRP CFFT test specimens were mainly affected by the eccentric loading. The average compressive strength of CFFT columns was reduced by 42% to 75% with increasing the e/D ratio from 10 to 40%. Theoretical models using two approaches to predict the axial-moment interaction diagrams and moment curvature relationships were developed and validated through comparison with the experimental results.

A nonlinear moment-curvature (M-φ) response was observed regardless the type of reinforcement and the applied eccentricity ratio. Furthermore, a comprehensive parametric study was performed to investigate the influence of different design variables on the moment capacity by creating numerous moment curvature relationships.

## 3.1 Introduction

Concrete-filled fibre-reinforced-polymer (FRP) tubes (CFFTs) provide an innovative alternative system to conventional materials for several structure applications, including structures piles, bridge columns and piers, overhead sign structures, poles, posts, traffic signs, traffic lights, beams, and bridge girders. The concept of CFFT was developed for different purposes including, the development of non-corrosive piles for marine environments to replace the reinforced, prestressed, and concrete-filled steel tube piles (Mirmiran and Shahawy 1996, Parvathaneni et al. 1996). The concrete filling also significantly enhances the ductility of the system, therefore, they can be used as bridge columns and piers in seismic zones. Several experimental and analytical investigations have addressed the behaviour of CFFT columns under axial loading (Mohamed and Masmoudi 2008, Mohamed et al. 2010, Hong and Kim 2004, Mohamed and masmoudi 2010, Ozbakkaloglu and Vincent 2014). It was concluded that CFFT technique increases strength and stiffness in both the axial and transverse directions for concrete columns under axial compressive loads due to the lateral confinement provided by the FRP tube. Despite the fact that most of the structure columns under axial loads exhibited to eccentric loads due to unintentional load eccentricities, possible construction error, lateral deformation and buckling phenomenon, limited investigations have been carried on to study the behavior of CFFT columns under eccentric loading (Lillistone and Jolly1997, Fam et al. 2003b, Hadi et al. 2016b). On the other hand, the behavior of FRP bars as longitudinal reinforcement in compression members is still a relevant issue to be addressed and it is not recommended by ACI 440.1R-15 to resist compression stresses. Current guidelines and codes of practice do not recommend the use of FRP bars as internal reinforcement in either compression members or eccentrically-compression loaded members. However, standards and guides (CAN/CSA S806-12) allow using FRP bars in the compression zone of flexural members, provided that they are neglected in determining the member's axial or flexural

strength. Recent research investigations have been conducted on the use of FRP bars in concrete columns under axial compressive and eccentric loads (Deluca et al. 2010, Mohamed et al. 2014, Hadhood et al. 2016). Few studies stated that columns reinforced with FRP bars behaved very similar to the conventional steel reinforced columns (Zadeh and Nanni 2013). Fan and Zeng (2016) studied the behavior of inorganic polymer concrete columns reinforced (IPCC) longitudinally with basalt FRP under eccentric loading. The mechanical behavior of short IPCC under eccentric compression was experimentally investigated and compared with control steel reinforced ordinary Portland cement concrete columns (OPCC). They have indicated that the load-carrying capacity of IPCC was approximately 30% lower than that of OPCC, while the ultimate displacements of IPCC were 65% and 15% larger than those of OPCC under large and small eccentricities, respectively. In addition, a recent research by Hadi et al. (2016a) was conducted to investigate the behavior of FRP reinforced CFFT columns under eccentric loads. They concluded that FRP reinforced CFFT specimens sustained higher peak axial loads, axial and lateral deformations at peak loads than steel RC specimens. Therefore, they recommended the use of FRP tube confined concrete in combination with FRP bars. Further research work is required to investigate the ultimate strength and moment capacity of steel and FRP reinforced CFFT columns. In this study, 10 reinforced CFFT columns, 5 steel reinforced CFFT and 5 CFRP reinforced CFFT columns, were tested under axial and eccentric loads. The effects of the eccentricity-to-diameter (*e/D*) ratios and the type of internal reinforcement on the behavior of CFFT columns are presented in terms of failure modes, ultimate load carrying capacities and load-deformation characteristics. A theoretical model has been developed for the axial-bending moment interaction diagrams and moment-curvature curves. The analytical models have been validated with the experimental results. In addition, a parametric study was conducted to study the effect of design variables on moment capacity of reinforced CFFT columns.

## 3.2 Research Significance

The main objective of this study is to understand the behavior of steel and carbon FRP reinforced CFFT columns under eccentric loading. The following points summarize the different objectives of this research work:

1. To experimentally investigate the performance of steel and CFRP reinforced CFFT columns under eccentric loading.
2. To experimentally investigate the effect of different parameters including the eccentricity-to-diameter (*e/D*) ratios and the type of internal reinforcement on the behavior of CFFT columns.
3. To theoretically develop analytical models for axial-bending moment and moment-curvature diagrams.
4. To investigate the effect of different parameters including unconfined concrete strength, longitudinal reinforcement ratio, and number of GFRP tube layers on the moment capacity.

## 3.3 Experimental Program

In this study, 10 reinforced CFFT columns (5 CFRP reinforced and 5 steel reinforced) were tested under concentric and eccentric loading. One CFRP CFFT column and one steel CFFT column were tested under concentric loads while the remaining 8 were tested under eccentric load. All specimens were 152 mm in diameter and 912 mm in height.

### 3.3.1 Materials

Glass-fibre reinforced polymer (GFRP) tubes were used as structural formwork for the CFFT specimens. The GFRP tubes were fabricated using filament winding technique; E-glass fibre and epoxy resin were utilized for manufacturing these tubes. The tubes had a core diameter of 152 mm and a wall thickness of 2.65 mm (6 layers). The fibre orientations of the tubes were mainly in the hoop direction (±60 degree with respect to the longitudinal axis). The split-disk test and coupon tensile test were performed according to ASTM D-2290-08 and ASTM D638-

08] standard, respectively, on five specimens of the tubes. Figure 3-1.a presents the axial tensile stress-strain response resulted from the coupon tests. In addition, Figure 3-1.b shows the average stress-strain relationship for the split-disk test in the hoop direction. All specimens of this study were constructed using normal concrete strength. Concrete batch was supplied by ready mix concrete supplier. The 28-day average concrete compressive strength was found equal to 30 ±0.6 MPa. Two types of reinforcing bars were used as longitudinal reinforcement for the CFFT columns; deformed steel bars No. 10 M (11.3 mm nominal diameter) and sand-coated carbon FRP (CFRP) bars No. 3 (9.52 mm nominal diameter). The reinforcement ratios used for steel and CFRP reinforced CFFT columns were 3.3% and 2.4%, respectively. For the purpose of comparison, it should be noted that the CFRP bar No.3 was chosen based on the nearest available diameter to give nearly the same bar tension side reinforcement ratio as the steel bar No.10M. The steel and CFRP reinforcement ratios in the tension side were 1.6%and 1.3%, respectively. Thus, the difference between the sizes of the two bars diameters was considered insignificant in this study. The mechanical properties of the steel bars were obtained from standard tests that were carried out according to ASTM A615/A615M-09, on five specimens for each type of the steel bars. The average values of the yield tensile strength, $f_y$ was 462±7 MPa with an ultimate tensile strength, $f_{su}$, 577±5 MPa. On the other hand, the CFRP bars were manufactured and developed by Pultrall Inc., Quebec, Canada. The bars were made of continuous fibre impregnated in vinylester resin with a fibre content of 73%, using the pultrusion process. The elastic modulus and ultimate tensile strength were 128 GPa and 1431 MPa with an ultimate tensile strain 1.2±0.09%.

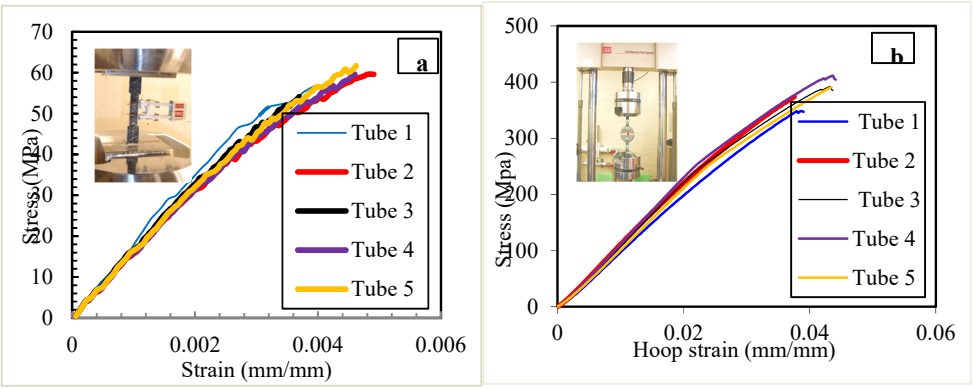


**Figure 3-1-** Setup and Stress-strain relationship, (a) coupon tensile test and (b) split-disk test.

### 3.3.2 Test Specimens

Table 3-1 summarizes different configurations of the tested specimens. The experimental program was carried out on ten reinforced CFFT specimens. The ten specimens were included through two series. The tested columns had a circular cross-section of 152 mm diameter. Series No. 1 and 2 present reinforced CFFT columns with a total height 912 mm, reinforced longitudinally with 6 steel or CFRP bars, respectively. The bars were distributed uniformly inside the cross section of the GFRP tube. The bars in all column specimens were fixed using two steel stirrups of 3.2 mm diameter at a distance of 25mm from the top and the bottom of the height, to fix the bars during casting, where the type will prevent the bars from buckling. The distance between the bars and the tubes was 8 mm. Figure 3- 2 shows an overview of the cages of steel and CFRP bars along with the location of the stirrups used. A concrete cover of 10 mm was provided between the ends of the longitudinal bars and the end surfaces to avoid the stress concentration at the bars area. Specimens ID were shown in the second column of Table 3-1, the numbers indicate the eccentricity (e) in mm and the letter S or C refers to the type of internal reinforcement, respectively, steel or CFRP bars. The load eccentricity-to-diameter (e/D) ratios for the reinforced CFFT columns were 0, 0.1, 0.2, 0.3 and 0.4. $f'_{cc}$ values were calculated from the experimental work as a ratio between the ultimate load and the area. It should be noted that replicas for the concentric specimens were found in the literature (Mohamed and Masmoudi, 2010), where they found that the variation of the results was very small.

**Table 3-1–** Test matrix and summery of test results

| Series No. | Specimen ID | *(e/D)* | *Bar type* | $P_u$ (kN) | $\Delta_h$ (mm) | $M_\Delta$ (kN.m) | $M_e$ (kN.m) | $M_u$ (kN.m) | $(f'_{cc}/f'_c)$ |
|---|---|---|---|---|---|---|---|---|---|
| 1 | S-00 | 0 | Steel | 1480 | 7.30 | --- | --- | --- | 2.30 |
| | S-15 | 0.1 | Steel | 825.0 | 31.00 | 13.14 | 12.38 | 25.51 | 1.04 |
| | S-30 | 0.2 | Steel | 620.0 | 45.5 | 9.40 | 18.60 | 28.00 | 0.65 |
| | S-45 | 0.3 | Steel | 466.0 | 60.00 | 6.87 | 20.97 | 27.84 | 0.36 |
| | S-60 | 0.4 | Steel | 367.0 | 73.00 | 4.70 | 22.02 | 26.72 | 0.17 |
| 2 | C-00 | 0 | CFRP | 1343 | 3.20 | --- | --- | --- | 2.20 |
| | C-15 | 0.1 | CFRP | 771.7 | 22.1 | 5.47 | 11.58 | 17.05 | 1.12 |
| | C-30 | 0.2 | CFRP | 614.5 | 43.46 | 8.28 | 18.44 | 26.71 | 0.82 |
| | C-45 | 0.3 | CFRP | 454.9 | 59.55 | 6.61 | 20.47 | 27.08 | 0.52 |
| | C-60 | 0.4 | CFRP | 375 | 75.32 | 5.74 | 22.50 | 28.24 | 0.37 |

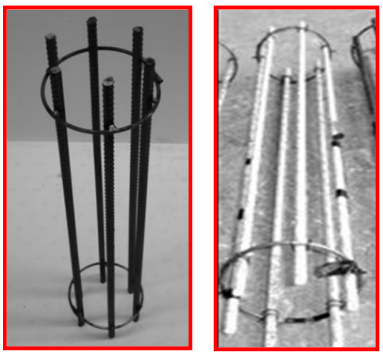

Steel bars CFRP bars

**Figure 3-2**-Overview of steel and CFRP bars cages

### 3.3.3 Instrumentation and Test Setup

The Vertical and horizontal displacements of all specimens at their mid-height were monitored using linear variable displacement transducers (LVDTs), two in each side. Strains in the longitudinal bar reinforcement and FRP tubes were recorded using electric strain gauges, 6.0 mm in length. Two strain gauges were bonded to the mid-height of two longitudinal steel or CFRP bars, 180 degree apart. Two axial and two transversal strain gauges were installed on the FRP tubes on two opposite sides at the mid height of each column. The concentrically and eccentrically loaded CFFT specimens were tested under monotonically increasing axial

compressive loading condition (load-controlled). The specimens were prepared before the test by a thin layer of high strength Sulphur capping on the top and bottom surfaces beside spherical head on the top to insure the uniform stress distribution during the test. For concentrically loaded CFFT columns, steel collars (4.0 mm thickness and 60.0 mm width) were attached to the ends of the specimens to prevent premature failure at these locations. For eccentrically loaded CFFT columns, the load was applied with specific eccentricities using specially designed two rigid steel end caps and roller bearing assembly. The two rigid steel end caps were designed and fabricated from high strength steel plates and semicircular section of thicknesses 30 mm and 5 mm, respectively. The steel plates and semicircular section were welded together with outward radiating stiffeners of thickness equal to 25 mm. The CFFT specimens were tested under four variable eccentric loads. Therefore, four lines holes were drilled at the top and bottom surfaces of the steel plate of the two caps at distance 15, 30, 45, 60 mm from the center of specimen's position to fix the roller steel rod. The caps sections were placed over the two ends of the CFFT specimens and clamped together 15 mm with high strength steel bolts. The specimens were tested using a 6,000 kN (1350 kips) capacity FORNEY machine, where the CFFT columns were setup vertically at the center of loading plates of the machine. Figure 3-3 shows the rigid steel caps details and test setup for eccentrically and concentrically loaded CFFT columns.

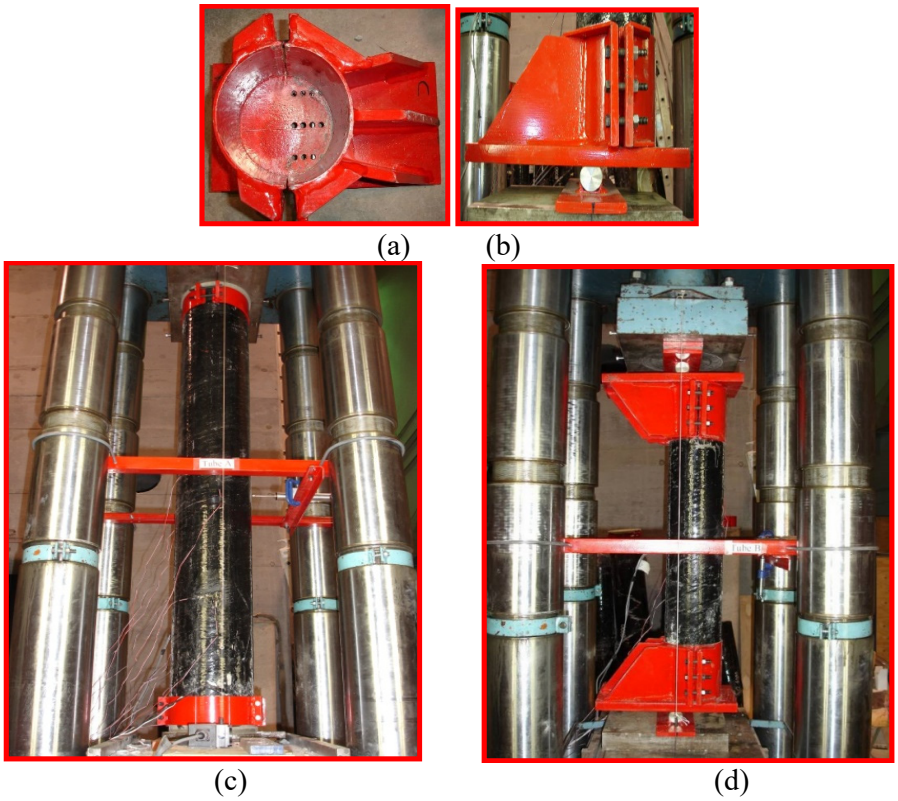

(a) (b)

(c) (d)

**Figure 3-3**-Test set up for concentric and eccentric axial load: (a) Front view for rigid-steel frame; (b) Plane for rigid-steel frame; (c) Specimen under concentric axial load; (d) Specimen under eccentric axial load

## 3.4 Observed Behavior and Test Results

### 3.4.1 Test Results and Discussion

The test results indicated that the CFRP reinforced CFFT columns under eccentric loads behaved similarly to that the counterpart reinforced with steel bars, in terms of load carrying capacities and deformations. However, the load carrying capacities of steel and CFRP reinforced CFFT columns were reduced due to the presence of the moment resulting from the applied load with eccentricity. Table 3-1 presents the peak loads ($P_u$), the primary moment ($M_e$) computed based on the initial (nominal) eccentricity, the secondary moment ($M_\Delta$) caused by the lateral midheight displacement at peak load, total moment at peak load ($M_u$) and the corresponding horizontal displacements at the mid-height of the columns ($\Delta_h$). The table also includes concentrically loaded reinforced CFFT columns of the same materials as a reference to emphasize the effect of load eccentricity on the behavior of the reinforced CFFT columns. The reported total maximum moment $M_u$ at mid-height, in Table 3-1 for all eccentrically loaded specimens, is composed of the primary moment, based on the initial eccentricity, and the secondary moment due to the lateral deflection at peak load at mid-height.

### 3.4.2 Strength and Failure Modes

The failure mode of the tested columns was affected mainly by the level of the applied eccentricity. As shown in Figure 3-4, the failure mode of the concentric columns (S-00 and C-00; Zero eccentricity) was due to rupture of GFRP tube. For column (S-00) the rupture of GFRP tube was accompanied by local buckling of the internal steel bars at the column mid-height. Figure 3-5 shows that the mode of failure of eccentrically loaded Steel and CFRP reinforced CFFT columns was compression control. The failure of the steel reinforced CFFT columns was generally marked by a soft and gradual failure as compared to those reinforced with CFRP bars. As the ultimate load was reached, horizontal flexural cracks propagated quickly through tension side. Significant decrease in the strength was observed for all eccentrically specimens as compared to the strength of concentrically loaded CFFT columns. Excessive horizontal

deformation at the mid height of the CFFT columns was observed beyond the peak load. The final failure mode for the eccentrically loaded CFFT columns was permanent with a single curvature in the direction of the tension side. Beyond the peak load, the failure was marked by the tensile rupture of the FRP tube at the tension side in the axial direction. On the other hand, minor local buckling in the compression side for the FRP tubes at the mid height was observed for Specimen S-60 due to the increases in the lateral deformations. In addition, for the specimens C-45 and C-60, fracture of CFRP bars occurred in the compression side beyond the peak load.

S-00 C-00

**Figure 3-4–** Failure modes of the concentrically loaded columns (S-00, C-00)

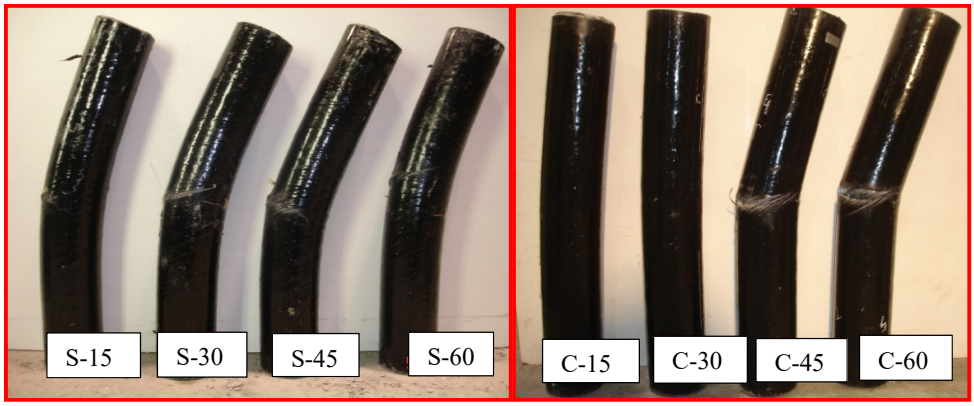


**Figure 3-5**– Failure modes of the eccentrically loaded column

### 3.4.3 Axial and Lateral Deformations

The plotted results in Figure 3-6 represent the load–shortening relationships of the steel and CFRP-CFFT columns. It can be seen that the load-axial deformation curve of CFFT columns typically consisted of three stages. The first branch of these curves was almost linear and it defined the initial stiffness of the FRP-confined concrete columns. The load–shortening relationships of CFRP reinforced CFFT columns typically coincided with the counterpart of steel reinforced CFFT columns. However, we found that the initial stiffness depended only on the eccentricity-to-diameter ratios regardless the type of longitudinal reinforcements (refer to Figure 3-6). For example, the decrease of the initial stiffness (tangent stiffness) of the Specimens S-15, S-30, S4-5 and S-60 (with an eccentricity to diameter ratio changed from 0.1 to 0.4) compared to Specimens S-00 was, respectively, 65%, 73%, 82% and 85%. The corresponding values for CFRP reinforced CFFT specimens were 62%, 71%, 84% and 83%., respectively. The second stage of the curve presented transition stage to the third branch of the load-axial deformation curve. With the propagation of the lateral cracks and because of the confining pressure, the load-deflection curve distinguished with a hardening region until the failure point, which is the third branch of the curve for concentrically loaded columns (S-00 and C-00). However, the third branch of the curve for eccentrically loaded columns distinguished with a softening region with a significant decrease in the ultimate load. This reflects the fact that the confinement effectiveness of the FRP tubes was not effective for eccentrically loaded columns as compared to that of concentrically loaded columns. Figure 3-

7 shows the load-lateral deformation relationships of the steel and CFRP reinforced CFFT tested columns. For concentrically loaded columns, no lateral deformation was recorded up to 85% of the ultimate load due to axial loading, however for eccentrically loaded columns; the lateral displacement of the columns was significant indicating instability of the columns. The lateral deformation of the eccentrically columns increased gradually with the load increase up to the peak load. After that the deformation increased progressively with a significant decrease in the load carrying capacities up to the complete instability of the column.

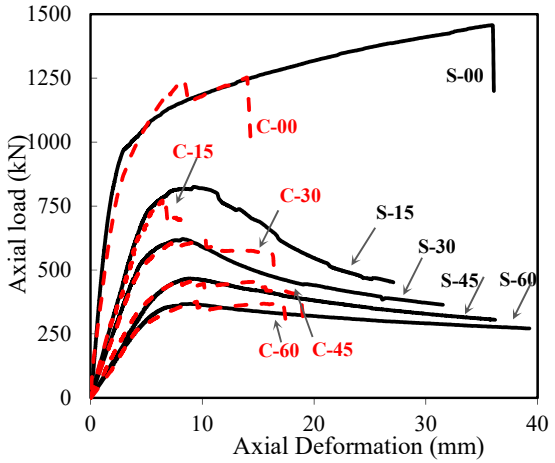


**Figure 3-6-** Load-axial displacement curves for the steel and CFRP reinforced CFFT columns.

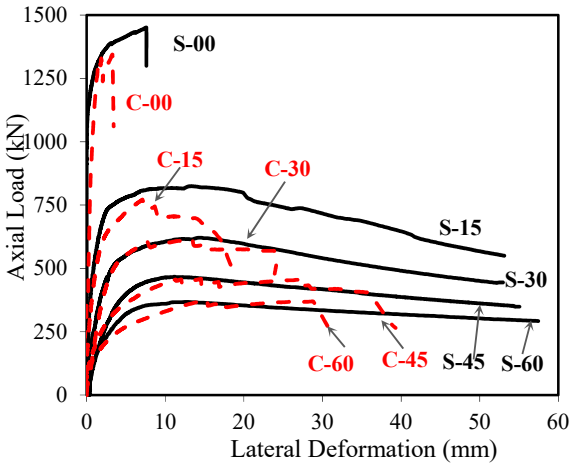


**Figure 3-7**- Load-lateral deformation relation for steel and CFRP reinforced CFFT columns

### 3.4.4 Ultimate Load Carrying Capacity and Eccentricity Effect

The ultimate capacity of all specimens was depicted versus the eccentricity to diameter (e/D) ratios values in Figure 3-8. The figure shows that CFRP reinforced CFFT columns maintained approximately the same load carrying capacities of the counterparts steel reinforced CFFT specimens. The ultimate capacities of Specimens C-00 and C-15 were 9% and 6.5% (less), respectively, than that reinforced with steel bars S-00 and S-15. Increasing the e/D ratios from 0.2 to 0.3, the ultimate load carrying capacities of the CFRP reinforced CFFT columns were similar (2% less) to the counterparts steel reinforced CFFT columns. However, the ultimate load of Specimens C-60 with e/D = 0.4 was higher (2%) than that of Specimens S-60. On the other hand, Figure 3-8 confirms the fact that the ultimate load capacities of the CFFT specimens significantly decreased with increasing the eccentricity to diameter (e/D) ratios. For example, the decrease of the ultimate capacity of the Specimens S-15, S-30, S-45 and S-60 (with an eccentricity to diameter ratio changed from 0.1 to 0.4) compared to Specimens S-00 was, respectively, 44%, 58%, 68% and 75%. The corresponding values for CFRP reinforced CFFT specimens were 42%, 54%, 66% and 72%, respectively, for Specimens C-15, C-30, C-45 and C-60. The confined concrete compressive strength to the unconfined concrete compressive strength ratio ($\frac{f'_{cc}}{f'_c}$) is given in Table 3-1. It was found that the gain in the confined strength decreased significantly with increasing the eccentricity-to-diameter ratios. The ($\frac{f'_{cc}}{f'_c}$) of steel

reinforced CFFT columns decreased from 2.3 to 0.17 with increasing the e/D ratios from zero to 0.4, respectively. The corresponding values for CFRP reinforced CFFT columns were 2.2 to 0.37.

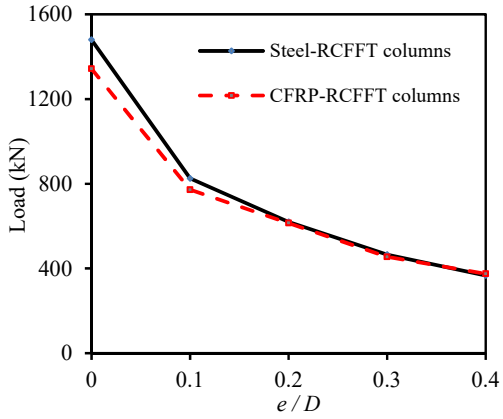


**Figure 3-8-** Load versus the eccentricity to diameter ratios

### 3.4.5 Steel and CFRP Bars Strain Profiles

The longitudinal bar strain was measured through two strain gauges, 180 degree apart bonded at the mid-height of outermost steel and CFRP bars, where the maximum stresses were expected. Figure 3-9 shows the bars strain profiles for the two series. At low eccentric loading (e/D=0.1), the ascending branch of the load strain profile was almost linear up to 86% and 82% of the peak load for S-15 and C-15, respectively, and the strains in the outermost bars changed from compression to tension with progressive increase until the peak load was reached. At the peak load for S-15 the tensile strain in the outermost steel bar was 2,500 microstarins (με) which was nearly equal to the yield strain of the steel bar (2200 με), While for C-15 the tensile strain in the outermost bar was 960 με which is less than 10 % of the ultimate strain (12,000 με) of the CFRP bar. For (e/D=0.2) the initial load – tensile strain behavior for S-30 and C-30 coincide and was linear up to 75% of the peak load. Afterward a semi linear behavior was observed for both specimen until the peak load where the strain increases progressively. At the peak load the tensile strains were 5,000 με and 4,000 με for S-30 and C-30 respectively. For

high eccentric loads (e/D=0.3 and e/D=0.4), non-linear behavior was exhibited for all specimens where the tensile strain at the peak load was 7,000 με 6,600 με , 8,000 με, 6,400 με for S-45 , C-45, S-60 and C-60 respectively. Thus, the recorded tensile strain of the CFRP bars can develop up to 0.65% tensile strain (55% of the ultimate bar tensile strain). Moreover, the maximum observed tensile strain for CFRP bar was 10,400 με which is 87% of the ultimate strain of the bar. By observing the strain results for CFRP bars, it can be indicated that the CFRP longitudinal reinforcement exhibit high tensile strains and can sustain the eccentric loads as well as the longitudinal steel reinforcement.

To examine the contribution of the CFRP bars in compression, Figure 3-10 shows the longitudinal compression strains of CFRP bars versus the axial load. The average compression strains recorded for the outermost bars, at peak, were -4000, -3600, -4200, and -3800 με for C-15, C-30, C-45, and C-60, respectively. Moreover, at peak the strain results of the CFRP compression bars develop up to 0.45% compression strain which is about 36% of the ultimate tensile bar strain.

In brief, the results show that the CFRP reinforcement can be used an internal reinforcement in CFFT columns subjected to eccentric loads, taking into consideration limiting the maximum compression strength to 35% of the ultimate tensile bar strength.

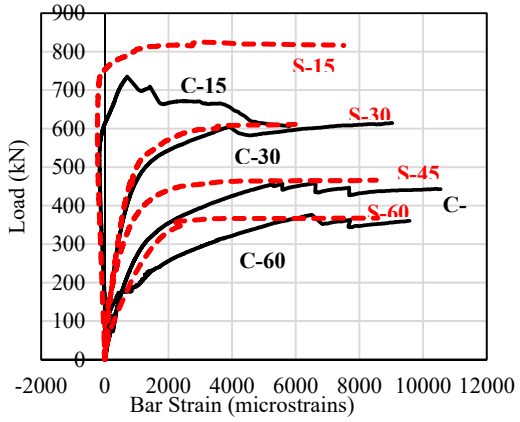


**Figure 3-9**-Load versus tensile bar strain (Steel & CFRP)

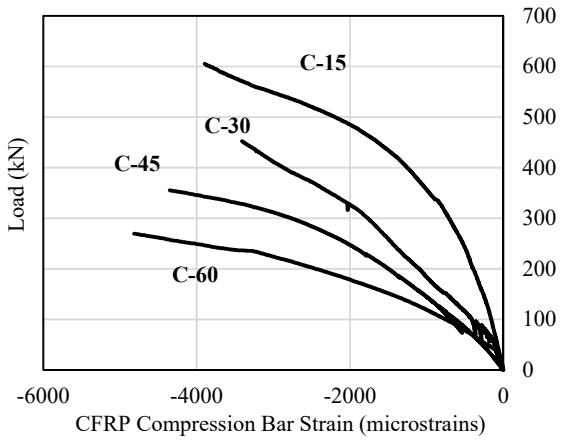


**Figure 3-10-**Load versus compression CFRP bar strain

### 3.4.6 GFRP Tube Strain Profiles

The strain behavior of the tube in the longitudinal and hoop directions is a good indicator of the confinement effect and failure mechanism of the specimens. Figure 3-11 shows the longitudinal and hoop strains of the FRP tube measured by two axial and two transversal strain gauges at the mid height of the column 180 degrees apart. The load strain behavior was generally linear up to nearly a range of (70% to 85 %) of the peak load followed by a non-linear response till the peak load. It was clear that the confinement effect of the tube decreases by increasing the eccentricity. Figure 3-11.a shows the load- longitudinal strain relation for specimens of series (1 &2), where the longitudinal tube strain confirms the tensile rupture of the GFRP tube of the eccentrically loaded columns, since the longitudinal strains of all specimens reached a range of (13,000 to 18,000) microstrains. In addition, Figure 3-11.b shows the load-tube hoop strain relation for specimens of series (1 &2) and it was indicated that the hoop strain developed mainly tensile strain, where the maximum measured tensile strains after peak on average ranged from 6,000 to 12,000 microstrain. These values are quiet lower than the FRP hoop strain of the used GFRP tube calculated from the split desk test and equals 38,000 microstrain.

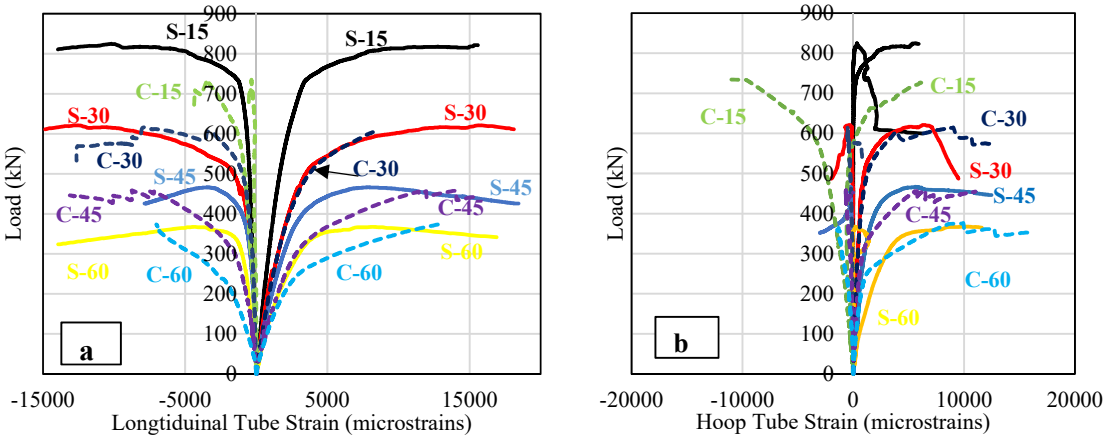


**Figure 3-11-** Load versus longitudinal and hoop tube strain

## 3.5 Experimental and Theoretical models of (P-M) Interaction Diagrams

### 3.5.1 Experimental (P-M) Interaction Diagrams

For the two series (1 and 2) the experimental normalized axial -moment interaction diagrams were drawn as shown in Figure 3-12, where the normalized axial force $P_u$ and $M_u$ the normalized bending are calculated using the following equation;

$$P_n = \frac{P_u}{f'_{cc} A_g} \quad 3\text{-}1$$

$$M_n = \frac{M_u}{f'_{cc} A_g D_o} \quad 3\text{-}2$$

Where $f'_{cc}$ is the confined concrete strength and is calculated using confined concrete model modified by lam and teng (2003) and discussed in details in the following section, $A_g$ is the

gross sectional area, $D_o$ is the diameter of the tube. $M_u$ is the moment resulting from applied load with initial eccentricity ($e$) and lateral deformation ($\Delta$), therefore the mid-height moment can be described by the equations below;

$$M_u = M_e + M_\Delta \quad 3\text{-}3$$

$$M_e = P_u e \quad 3\text{-}4$$

$$M_\Delta = P_u \Delta \quad 3\text{-}5$$

It can be observed that the steel reinforced CFFT columns interaction diagrams have specific pattern, where a reduction in the axial load is accompanied by an increase in the moment strength from pure axial load to the balance point condition where ($\varepsilon_c = \varepsilon_{cu}, \varepsilon_s = \varepsilon_y$), followed by a reduction in the axial load and moment strength till the pure flexure point. Unlike the steel reinforced CFFT columns, the FRP reinforced CFFT columns have no unique pattern and it will not exhibited a balanced point, this may refer to the linear elastic stress-strain behavior of FRP bars.

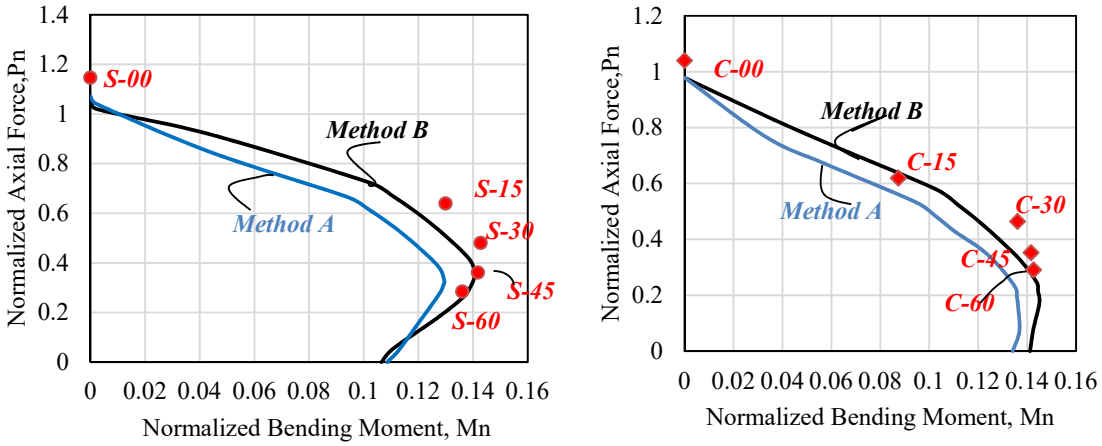


**Figure 3-12-**Normalized interaction diagrams for all columns

## 3.5.2 Theoretical Modeling

A Several researchers have developed the P-M interaction diagram for reinforced columns based on simplified sectional analysis either by layer by layer numerical integration method (Hadi et al.2016b, Choo et al. 2006) or by strain compatibility and force resultant (Bisby and Ranger 2010). Thus, a theoretical study using the two simplified sectional analysis methods was conducted to evaluate the axial load- moment (P-M) interaction strength of both steel and FRP reinforced CFFT columns. The results were compared with the experimental results on the basis of the following assumptions: (a) Plane sections remain plane under bending, (b) tensile strength of concrete is neglected, (c) the existence of the a perfect bond between concrete, reinforcement and GFRP tube, (d) the area of the concrete displaced by reinforcement in compression will be subtracted, (e) distribution of concrete compressive stress can be described by the equivalent rectangular stress block defined as in ACI318-14, (f) distribution of strains within the circular CFFT cross section is linear. Adequate material modelling of different parts of the concrete filled FRP tube columns assures the accuracy of the developed theoretical methods. Different material models are illustrated on the following sections.

### 3.5.2.1 Modelling of Confined Concrete

The confined concrete strength $f'_{cc}$ was calculated using the stress-strain model suggested by Lam and Teng (2003) for circular confined concrete columns under concentric load. It was assumed that the model used for calculating the stress-strain curve for circular confined columns under concentric loads could be used for circular confined eccentrically loaded columns (Jiang and Teng 2012). Though this model was validated using finite element modelling by Abdallah et al. (2017) for similar group of specimens under concentric loading. The model proved to be one of the most accurate models to predict the maximum confined stress and strain for confined RC circular columns (Ozbakkaloglu 2013). In this model, they assumed that the stress–strain curve consists of two parts: the first is a parabolic section and the second is a straight line. The slope of the parabola at $\varepsilon_c$=0 (initial slope) is the same as the elastic modulus of unconfined concrete $E_c$ and the nonlinear part of the first portion is affected to some extent by the presence of an FRP tube. The parabolic first portion joins the linear

second portion smoothly (i.e. there is no change in slope between the two portions where they join) and the linear second portion ends at a point where both the compressive strength and the ultimate axial strain of confined concrete are reached. The proposed stress–strain model shown in Figure 3-13 is defined by two equations;

$$\sigma_c = E_c\,\varepsilon_c - \frac{(E_c - E_2)^2}{4f_o}\varepsilon_c{}^2 \qquad 0 \le \varepsilon_c \le \varepsilon_l \qquad 3\text{-}6$$

$$\sigma_c = f_o + E_c\,\varepsilon_c \qquad \varepsilon_l \le \varepsilon_c \le \varepsilon_{cu} \qquad 3\text{-}7$$

The second linear part of the stress strain curve joins the first part at a transition strain$\varepsilon_l$ which is given by;

$$\varepsilon_l = \frac{2f_o}{(E_c - E_2)} \qquad 3\text{-}8$$

where $E_2$ is the slope of the linear second part of the stress-strain curve and is given by;

$$E_2 = \frac{f\prime_{cc} - f_o}{\varepsilon_{cu}} \qquad 3\text{-}9$$

Where $f_o$ is the intercept stress which is a function of the strength of the unconfined concrete and the confining pressure of the tube and was calculated from Samman et al 1998;

$$f_o = 0.872f'_c + 0.371f_{l,a} + 6.258 \qquad 3\text{-}10$$

$f'_c$ is the unconfined concrete strength and $f_{l,a}$ is the lateral confining pressure of GFRP and is equal $\frac{2f_f t_f}{D}$; $f_f$ is the tensile strength of GFRP in the hoop direction, $t_f$ is the total thickness of GFRP tube.

The maximum confined concrete strength is given by:

$$f'_{cc} = f'_c + 3.3\,f_{l,a} \qquad 3\text{-}11$$

The corresponding ultimate confined concrete strain ($\varepsilon_{cu}$) can be determined by:

$$\varepsilon_{cu} = \varepsilon_{co}\left(1.75 + 12\left(\frac{f_{l,a}}{f'_c}\right)\left(\frac{\varepsilon_{fe}}{\varepsilon_{co}}\right)^{0.45}\right) \qquad 3\text{-}12$$

$\varepsilon_{co}$ is the unconfined concrete strain and is taken = 0.003 (ACI318-14)

$\varepsilon_{fe}$ is the effective strain level in the FRP at failure, according to ACI 440procedures $\varepsilon_{fe}$ should

not be taken more than 0.004 in members subjected to combined axial compression and bending moment to ensure shear integrity of the confined concrete.

According to ACI440.2R-08 $\varepsilon_{cu}$ should not exceed a value of 0.01 to prevent excessive cracking and the resulting loss of concrete integrity .

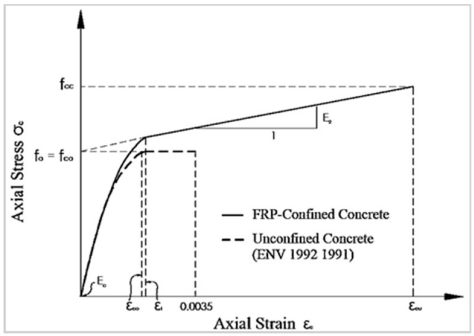


**Figure 3-13-** Stress-Strain curve for FRP-confined concrete

### 3.5.2.2 Modelling of Steel bars

The stress-strain values of the steel bar were calculated based the elastic-perfectly plastic theory where the axial stress at a given strain is calculated as follow;

$$f_s = E_s \varepsilon_s \qquad f_s \leq f_y \qquad \text{3-13}$$

$E_s, f_y$ are the young's modulus and yield strength of the steel bar respectively.

### 3.5.2.3 Modelling of CFRP bars

Based on the linear-elastic until rupture theory (Kobayashi and Fujisaki 1995), the axial stress at a given strain of CFRP bar is calculated as follows;

$$f_{fb} = E_{fb} \varepsilon_{fb} \qquad \text{3-14}$$

$E_{fb}$ is the modulus of elasticity of the CFRP bar.

### 3.5.3 Detailed Proposed Sectional Analysis Methods

#### 3.5.3.1 Method A (Strain Compatibility and Force Equilibrium)

The difficulty of the analysis of the circular concrete filled FRP tube columns refers to the variable stresses over the section depth and its distribution along an area of variable width, also the FRP tube is continuous around the perimeter and the steel or FRP bars are usually distributed around the depth. Thus to simplify the analytical calculations a straightforward analysis procedures based on the using the internal tension and compression forces of concrete, steel or FRP bars and GFRP tubes equilibrium and strain compatibility as shown in Figure 3-14.a were presented. Where in tension the concrete is assumed not to contribute to the internal forces after cracking, while in compression the concrete is accounted by using the circular compression block proposed by Whiteny (1942). A trigonometric integral approach for the concrete compression block was presented in Figure 14.b and was calculated as follows;

Area of segment = $A_{segment} = \int_0^{\alpha} 2(\frac{D}{2}\sin\theta)\ (\frac{D}{2}\sin\theta)d\theta$

$$= \frac{D^2}{2}\int_0^{\alpha}\sin^2\theta\ d\theta$$

$$= \frac{D^2}{2}\left[\frac{\alpha_{rad}}{2} - \frac{1}{4}\sin 2\alpha\right] \qquad 3\text{-}15$$

The location of the centroid of the circular compression block ($\bar{Y}$) is calculated as;

$$\bar{Y} = \frac{\int_0^{\alpha} 2(\frac{D}{2}\sin\theta)(\frac{D}{2}\cos\theta)\ (\frac{D}{2}\sin\theta)d\theta}{A}$$

$$\bar{Y} = \frac{\frac{D^3}{4}(\sin^3\frac{\alpha}{3})}{A} \qquad 3\text{-}16$$

Thus, the concrete internal compression force ($C_c$) was presented as follows;

$$C_c = \xi * f'_{cc} * A_{segment} \qquad 3\text{-}17$$

$\xi$ is a reduction factor to account for the concrete area displaced by the internal reinforcement to avoid over estimation of the column strength, according to ACI-318-14, the reduction factor was taken as 15% in the maximum ($\xi = 0.85$) to give more conservative results.

The strain in the internal bars and GFRP tube can be calculated by considering the distribution of the bars and the effective resistance of the compression and tension forces by the GFRP tube above and below the neutral axis respectively. By referring to Figure 3-14 to calculate the strain of the different components. Firstly, it was assumed that $\varepsilon_{top} = \varepsilon_{cu}$, and the strain in the internal bars was calculated as follows;

$$\varepsilon_{bi} = \varepsilon_{cu}\left(\frac{c-d_i}{c}\right) \qquad i = 1,2,3,4 \qquad 3\text{-}18$$

$$\varepsilon_{bottom} = \varepsilon_{cu}\left(\frac{c-D_0}{c}\right) \qquad 3\text{-}19$$

The internal compression and tensile forces in the GFRP tube and steel or FRP bars were calculated as;

$$C_{tube} = 0.5 * E_{FRP} * \varepsilon_{top} * C * t_{FRP} \qquad 3\text{-}20$$

$$T_{tube} = 0.5 * E_{FRP} * \varepsilon_{bottom} * (D_0 - C) * t_{FRP} \qquad 3\text{-}21$$

$$C_{bi}\ or\ T_{bi} = A_{bi} * E_{bar} * \varepsilon_{bi} \qquad 3\text{-}22$$

Compressive forces are assumed to be positive and the moment to be applied around the center line (C.L.) of the cross section, Therefore the nominal axial force and the nominal moment strength were calculated as follows;

$$P_n = \sum C_{bi} + C_{tube} + C_c - \sum T_{bi} - T_{tube} \qquad 3\text{-}23$$

$$M_n = \sum C_{bi}\left(\frac{D_o}{2} - d_i\right) + C_{tube}\left(\frac{D_0}{2} - \frac{C}{3}\right) + C_c * \bar{Y} - \sum T_{b4}\left(\frac{D_0}{2} - d_i\right) - T_{tube}\left(\frac{D_o}{6} + \frac{C}{3}\right) \qquad 3\text{-}24$$

For the nominal axial load point where ($M_n$=0), $P_n$ can be calculated using the following equations;

*For Steel bars*

$$P_n = 0.85 f'_{cc}\left(A_g - A_s\right) + f_y A_s \qquad 3\text{-}25$$

*For FRP bars*

$$P_n = 0.85f'_{cc}\left(A_g - A_{bar}\right) + E_{bar}\varepsilon_{fe}A_{bar} \qquad 3\text{-}26$$

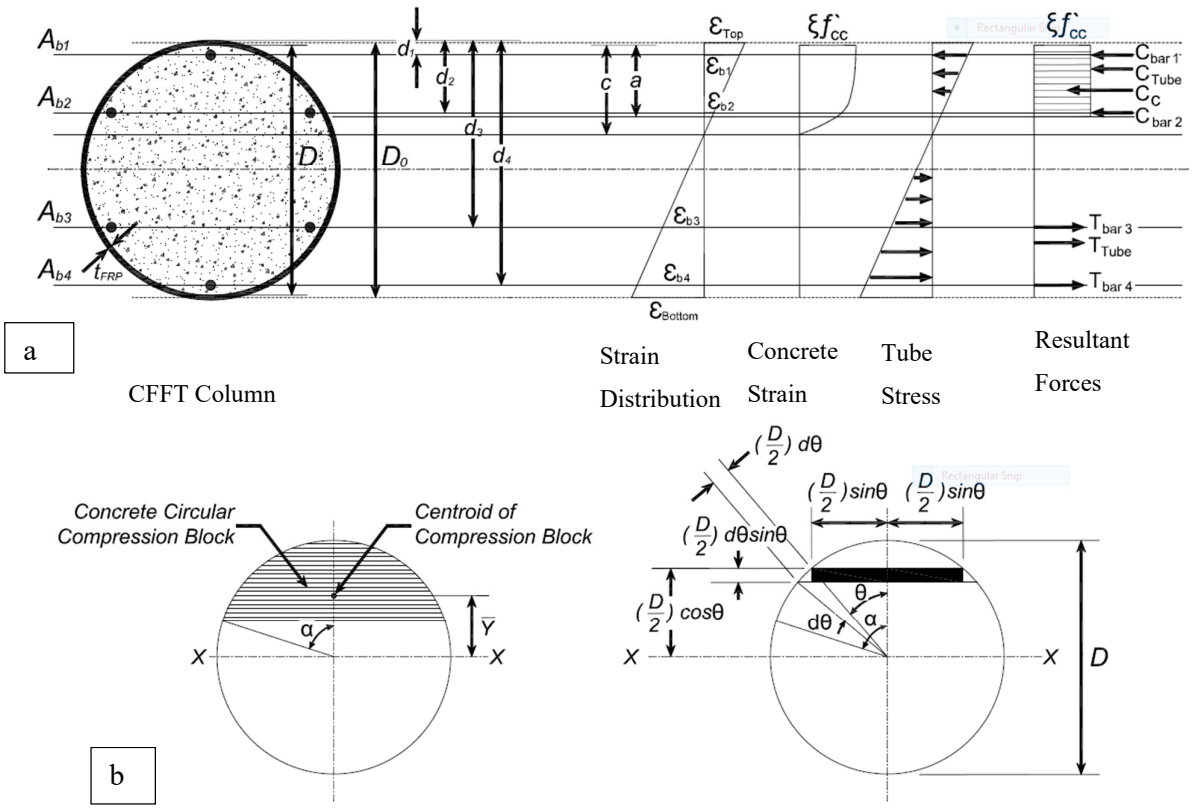


**Figure 3-14-** (a) Equivalent stress-strain distribution for CFFT columns; (b) Circular concrete compression block trigonometric approach

### 3.5.3.2 Method B (Layer by Layer Numerical Integration Method)

The layer by layer numerical procedure include discretizing the cross section into a number of multi-layers, each layer was assigned a material type linking that layer's material to its corresponding material model. The discretized section for circular columns was shown in Figure 3-15. The area of each concrete layer and the distance of its center to the top edge of concrete were donated as $A_{c\_seg(i)}$ and $d_{c(i)}$ , respectively. The $i$ represents the $i_{th}$ concrete segment. For the GFRP tube the index $j$ represents the $j_{th}$ tube segment where $A_{t\_seg(j)}$ and $d_{t(j)}$ represents the corresponding segment area and the distance of the center to the top edge of concrete. The area of the longitudinal bars (Steel or FRP) at different layers was donated by

$A_{b\_seg(k)}$ and $d_{b(k)}$ , where $k$ represents the $k_{th}$ bar layer. Based on the assumption of the plane section remains plane during bending, the strain $\varepsilon_{cc(i)}$ at the center of $i_{th}$ concrete segment can be calculated as,

$$\varepsilon_{cc(i)} = \varepsilon_{top}\left(1 - \frac{d_{c(i)}}{c}\right) \qquad 3\text{-}27$$

where $\varepsilon_{top}$ is the assumed compression strain in the outermost fiber of the concrete section, and $c$ is the distance from neutral axis to top of concrete edge. Similarly, the strain at the center of each tube segment $\varepsilon_{t(j)}$ and at the center of each bar $\varepsilon_{b(k)}$ were calculated as,

$$\varepsilon_{t(j)} = \varepsilon_{top}\left(1 - \frac{d_{t(j)}}{c}\right) \qquad 3\text{-}28$$

$$\varepsilon_{b(k)} = \varepsilon_{top}\left(1 - \frac{d_{b(k)}}{c}\right) \qquad 3\text{-}29$$

Using the material constitutive models, calculate the stresses in the middle of each layer for concrete, tube, and bars ($f_{cc(i)}$,$f_{t(j)}$ , $f_{b(k)}$ ) respectively. Accordingly, after considering axial equilibrium $P_u$ and $M_u$ about the top edge of concrete can be calculated as,

$$P_u = \sum_i f_{cc(i)} A_{c\_seg(i)} + \sum_j f_{t(j)} A_{t\_seg(j)} + \sum_k f_{b(k)} A_{b\_seg(k)} \qquad 3\text{-}30$$

$$M_u = \sum_i f_{cc(i)} A_{c_{seg(i)}} d_{c(i)} + \sum_j f_{t(j)} A_{t_{seg(j)}} d_{t(j)} + \sum_k f_{b(k)} A_{b_{seg(k)}} d_{b(k)} \qquad 3\text{-}31$$

A flow chart illustrating the analysis procedure steps to calculate $P_u$ and $M_u$ is shown in Figure 3-16. Consequently, through repeating the flow chart steps, the complete axial load-moment interaction diagram can be generated by increasing the compressive strain $\varepsilon_{top}$ to its ultimate state ($\varepsilon_{cu}$).

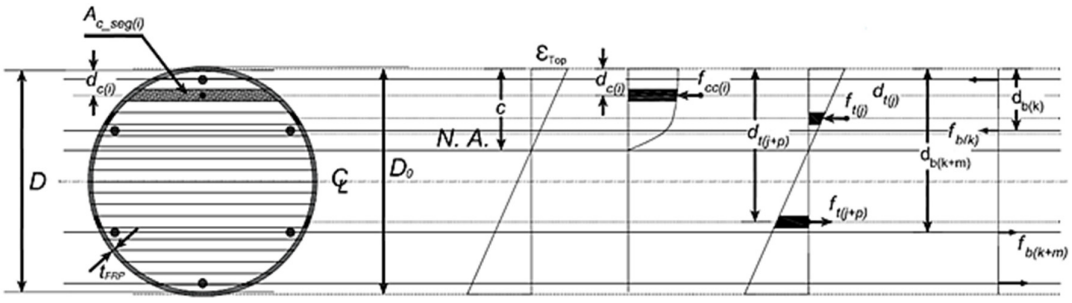


**Figure 3-15-** Discretized section for CFFT column and its strain and stress Profile

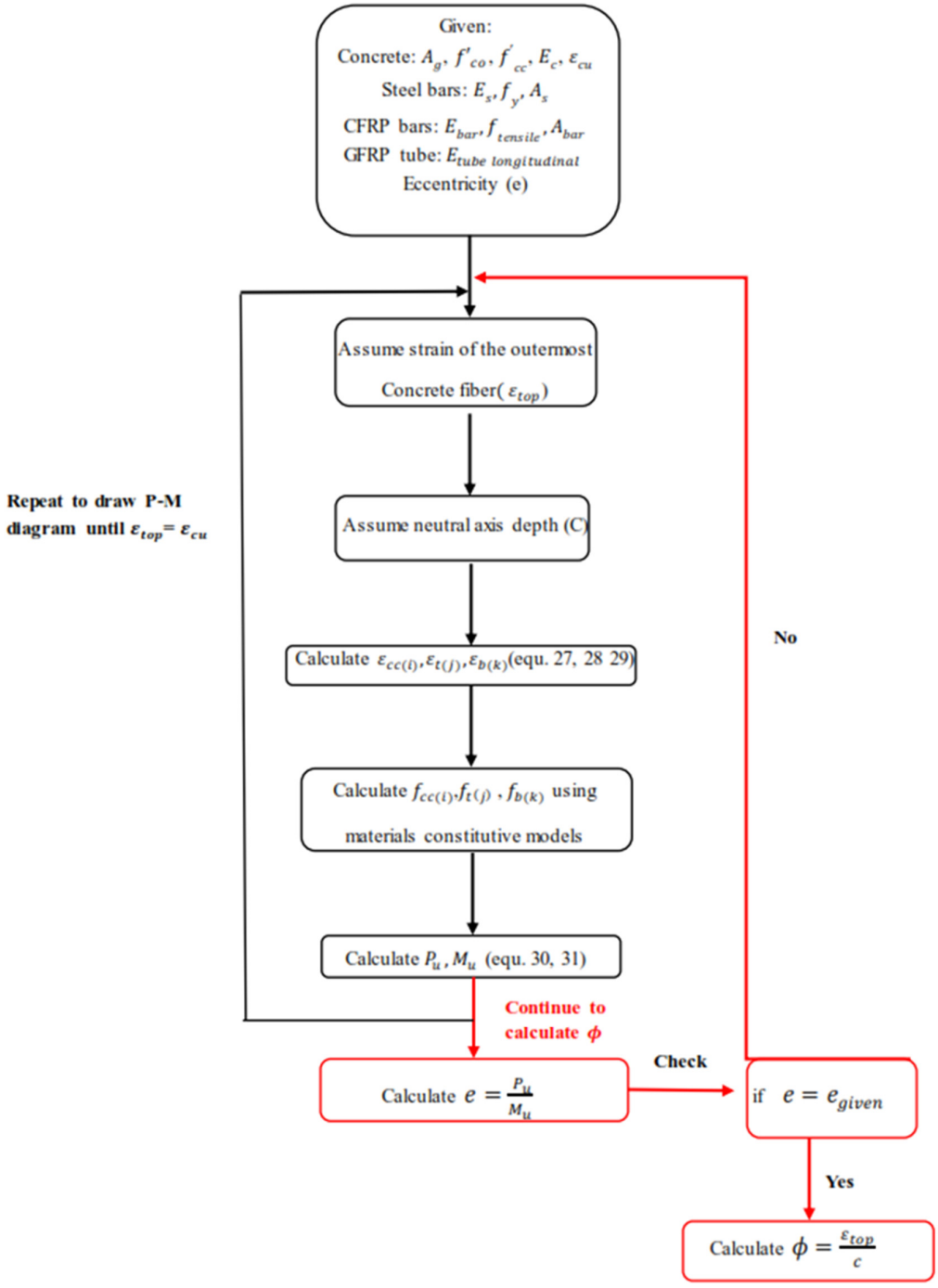


**Figure 3-16-** Flow chart illustrating steps for calculating axial load- moment -curvature

### 3.5.1 Comparison between Experimental and Theoretical P-M Interaction Diagrams

Figure 3-12 shows the comparison between the experimental and the two theoretical P-M interactions for both steel and FRP reinforced CFFT columns, respectively. It was found that the predicated failure envelope for both series agreed well with the theoretical counterparts with a more accurate predication using method B. The experimental results gave an upper bound with a little margin, which means that the theoretical P-M interaction models estimated well the axial loads and bending moments of the experimental P-M interaction. To summarize the analytical results the ratio of the experimental axial force to the theoretical axial force ($P_{exp}/P_{Theo}$) for the two series was shown in Table 3-2. It was found that the average ratio ($P_{exp}/P_{Theo}$) was (1.175, 1.06) for series 1 and (1.2, 1.05) for series 2 using method A and B, respectively. In addition, the ratio of the experimental moment to the theoretical moment ($M_{exp}/M_{theo}$) for both series was also indicated in Table 3-2. It was found that the corresponding value for estimating the moment resistance in terms of the average of ($M_{exp}/M_{theo}$) was (1.12, 1.025) for series 1 and (1.1, 1.035) for series 2 using method A and B, respectively.

Another comparison was conducted using the experimental data presented by Khan et al. (2017). In this study, experimental axial-moment interaction diagrams of 3 circular CFFT columns confined by CFRP tube and reinforced with CFRP bars were presented. The 3 CFFT columns (CTCR-0, CTCR-25, and CTCR-50) were tested under concentric and eccentric loads with eccentricity 25mm and 50 mm, respectively. Figure 3-17 shows the experimental P-M diagram compared with the theoretical P-M diagrams using the two suggested theoretical models. It was clear that the theoretical models matched well the experimental data, thus, the diagram ensures the accuracy of the proposed theoretical models.

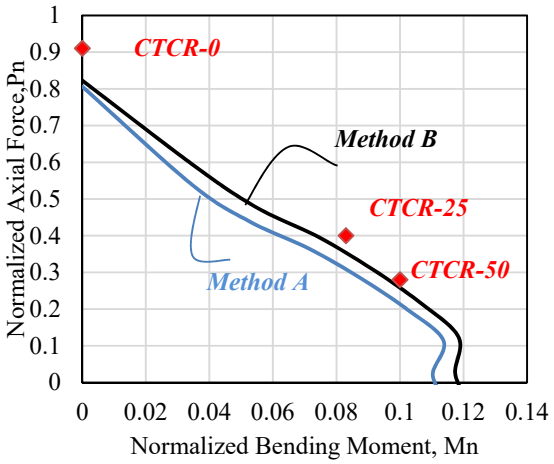


**Figure 3-17-** Comparison of experimental and theoretical axial and moment resistances

**Table 3-2-** Comparison of experimental and theoretical axial and moment resistances

| ID | Exp. | | Method 1 | | Method 2 | |
|---|---|---|---|---|---|---|
| | $P_{exp}$ (kN) | $M_{exp}$ (kN.m) | $P_{exp}/P_{theo}$ | $M_{exp}/M_{theo}$ | $P_{exp}/P_{theo}$ | $M_{exp}/M_{theo}$ |
| S-00 | 1480 | 0 | 1.07 | 0 | 1.07 | 0 |
| S-15 | 825 | 25.51 | 1.4 | 1.09 | 1.08 | 1.06 |
| S-30 | 620 | 28 | 1.25 | 1.12 | 1.05 | 1.03 |
| S-45 | 466 | 27.84 | 1.15 | 1.2 | 1.01 | 1 |
| S-60 | 367 | 26.72 | 1 | 1.06 | 1.08 | 1.01 |
| Mean | | | 1.175 | 1.12 | 1.06 | 1.025 |
| C-00 | 1343 | 0 | 1.065 | 0 | 1.065 | 0 |
| C-15 | 771.7 | 17.05 | 1.16 | 1.13 | 1.03 | 1 |
| C-30 | 614.5 | 26.71 | 1.3 | 1.15 | 1.02 | 1.1 |
| C-45 | 454.9 | 27.08 | 1.2 | 1.095 | 1.085 | 1.05 |
| C-60 | 375 | 28.24 | 1.25 | 1.05 | 1.06 | 1 |
| Mean | | | 1.2 | 1.1 | 1.05 | 1.035 |

## 3.6 Experimental and Analytical moment-curvature for steel and CFRP reinforced CFFT columns

Figures 18 and 19 show the experimental moment-curvature diagrams for series 1 & 2 which were plotted by calculating the curvature $\phi$ using the following equation:

$$\phi = \frac{|\varepsilon_{tension}|+|\varepsilon_{compression}|}{D_o} \qquad 3\text{-}32$$

Where $\varepsilon_{tension}$ and $\varepsilon_{compression}$ are the compressive and tensile strains measured from the two longitudinal strain gauges installed on the FRP tubes on two opposite sides at the mid height of each column. The midheight moment is calculated as mentioned in the previous section by Equation 3-3

### 3.6.1 Moment-Curvature Analytical Model

Due to its high accuracy, the layer by layer numerical integration method was used for creating the analytical moment curvature diagrams for both series. Following the same steps illustrated in the flow chart Figure 3-16, and after calculating $P_u$ and $M_u$ the associated curvature can be calculated after doing the required checks as,

$$\phi = \frac{\varepsilon_{top}}{c} \qquad 3\text{-}33$$

Consequently, through repeating the flow chart steps, the complete moment-curvature diagram can be generated by increasing the compressive strain $\varepsilon_{top}$ to its ultimate state ($\varepsilon_{cu}$). Figures 3-18, 3-19 show that good agreement between the experimental and theoretical results was observed and moment capacities were accurately estimated. In addition, regardless the type of reinforcement and the eccentric ratio, all specimens exhibited nonlinear moment-curvature (M-φ) responses. The moment-curvature curves mainly consist of 3 zones, the first zone represents the initial portion of both series of moment-curvature diagrams where they are nearly identical for curvature between 0 and 0.00002 1/mm as the stiffness depends mainly on the initial stiffness of concrete. This zone exhibit small curvatures and the load combination was not large enough to cause concrete cracks, thus the tube confining mechanism was not fully engaged. The second zone is the transition zone between initial concrete stiffness and the confined concrete stiffness, this zone corresponds to curvatures between 0.00002 and 0.000045 1/mm except for C-15 where the curvature range is between 0.00001 and 0.00002 1/mm. The third zone is with curvature of 0.000045 1/mm up to failure. A detailed discussion of the effect of the type of internal longitudinal reinforcement on the three zones is presented in the following section.

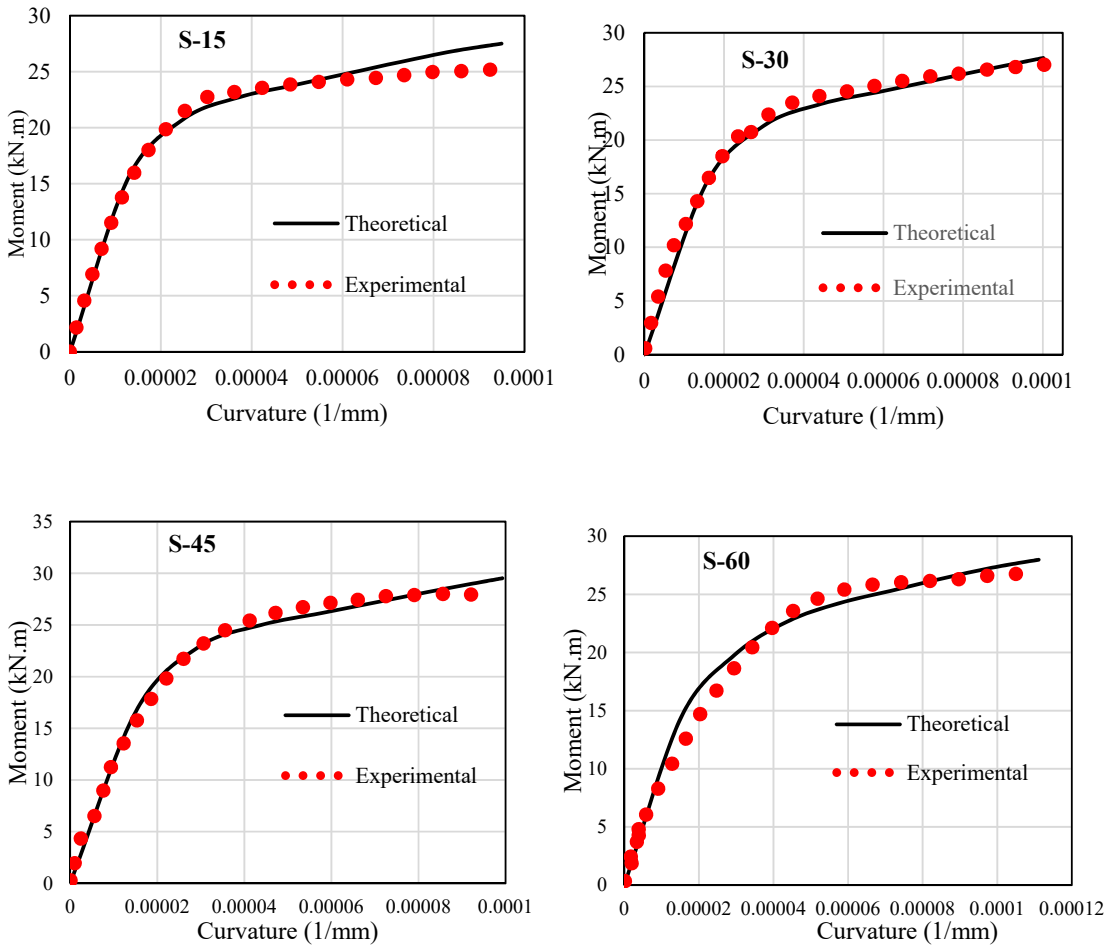


**Figure 3-18**- Experimental and theoretical moment-curvature diagrams for Steel CFFT columns

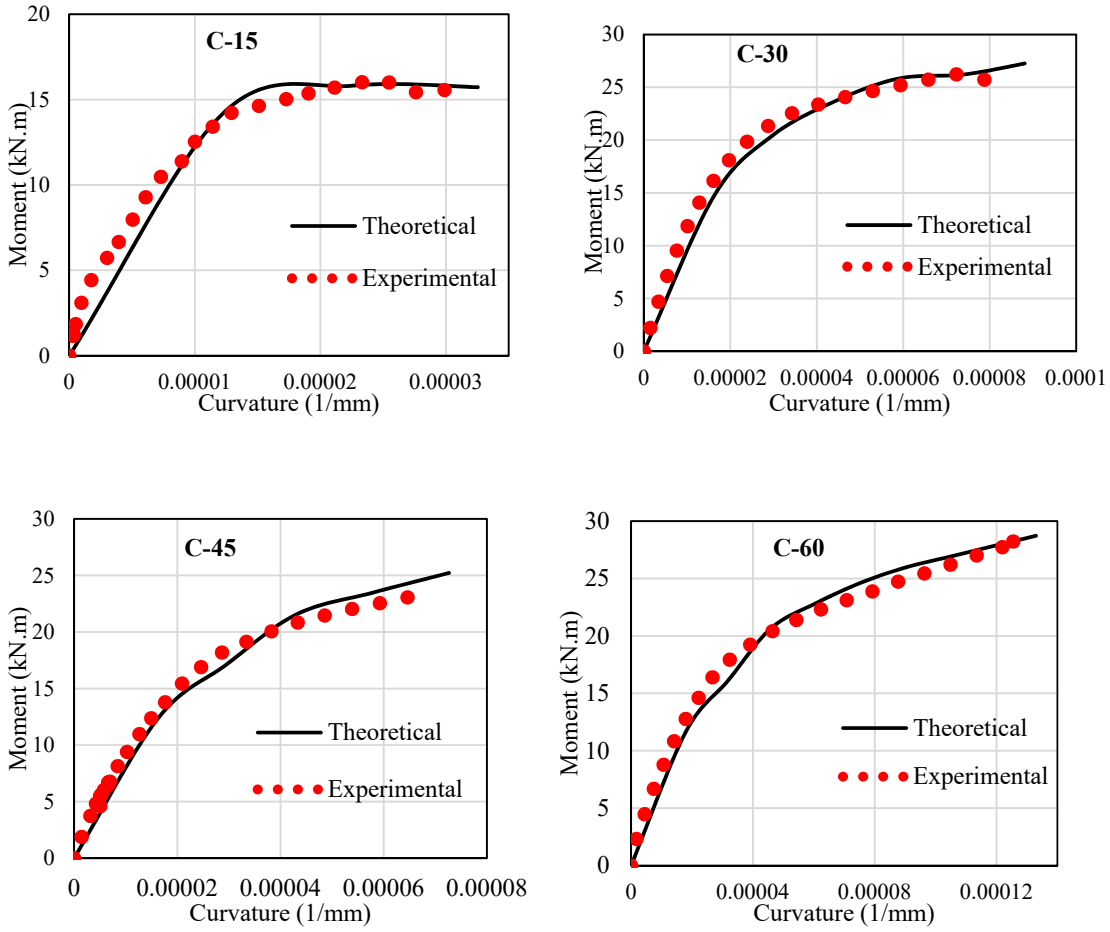


**Figure 3-19-** Experimental and theoretical moment-curvature diagrams for CFRP CFFT columns

### 3.6.1.1 Effect of Reinforcement Type on Moment-Curvature Behavior

To account for the effect of using different longitudinal reinforcement (Steel or CFRP), a comparison between moment curvature diagrams for specimens (S-60 & C-60) was indicated in Figure 3-20. Zone 1 represented by point 0 to point 1 for both specimens is the region of uncracked section. At this level, the behavior of all constituent materials is linear-elastic and small curvature occurred, though the stiffness of the cross section is controlled by the initial stiffness of the concrete. Zone 2 represented by point 1 to point 2 for both specimens is the cracked section region where the cracks start and increase causing the section to lose strength

and stiffness and start to dilate laterally where the tube start to engage and control this dilation by preventing the concrete core from losing more strength and failing. Thus, the moment curvature diagram at the end of this region is controlled by the confined concrete stiffness. Hence, the cracking curvature of the column section $\phi_{cr}$ can be calculated by:

$$\phi_{cr} = \frac{M_{cr}}{EI_e} \qquad 3\text{-}34$$

At point 2 in S-60 moment curvature diagram, the steel bars reached the yield point (a point with yield moment $M_y$) and an increase in the moment capacity of the section occurred till failure at point 3 (Zone 3). The value of yield curvature $\phi_y$ corresponding to the "yield moment" $M_y$ can be calculated by the following equation,

$$\phi_y = \frac{\varepsilon_{sy}}{d - c_y} \qquad 3\text{-}35$$

Where $\varepsilon_{sy}$ strain in the extreme tension longitudinal bar at yield; $d$ is distance from extreme tension bar to top concrete edge; and $c_y$ neutral axis at $M_y$. The effective flexural stiffness is then calculated as:

$$EI_e = \frac{M_y}{\phi_y} \qquad 3\text{-}36$$

$I_e$ is the effective section inertia.

While for the CFRP CFFT column (C-60), the CFRP bars don't exhibit a yield point instead a linear elastic behavior from point 2 to 3 controls the specimen till failure. This region could be refereed at by the softening region where the effective flexure stiffness can be calculated as:

$$EI_e = \left(\frac{M}{\phi}\right)_{Softening} \qquad 3\text{-}37$$

Where $\left(\frac{M}{\phi}\right)_{Softening}$ in C-60 correspond to $\frac{M_y}{\phi_y}$ in S-60.

Also, it was observed that C-60 exhibited nearly the same ultimate moment capacity as that of S-60 with a slightly smaller reinforcement ratio ($\rho_{steel} = 3.3\%$ while $\rho_{frp} = 2.4\%$ ) taking into consideration that this similarity is somehow fictitious due to the difference in the effective flexural stiffness between the two specimens , where $(EI)_{CFRP} \ll (EI)_{Steel}$. Thus, it is important to study the effective flexural stiffness to define the relation between moment and stiffness of the reinforced CFFT columns.

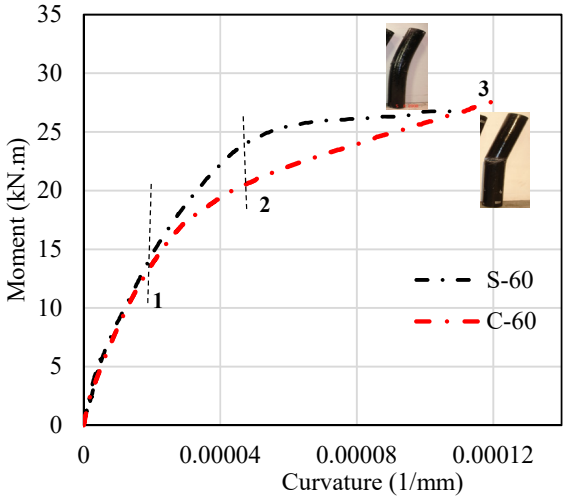


**Figure 3-20-** Comparison for experimental moment curvature diagrams for S-60 &C-60

### 3.6.1.2 Variation of Effective Flexural Stiffness for Steel and CFRP Reinforced CFFT Columns

Figure 3-21 shows the variation of the effective flexural stiffness along the applied moment where the effective flexural stiffness was calculated from the experimental moment curvature curve according to the following equation;

$$EI_e = \frac{M}{\phi} \qquad 3\text{-}38$$

As it can be seen from Figure 3-21, in the pre-cracking region, the specimens showed the highest flexural stiffness, once the cracks initiated, the flexural stiffness was notably reduced till the failure. In addition, the difference in the effective stiffness between Steel and CFRP

reinforced CFFT specimen can be clearly noticed, this difference occurs mainly after the pre-cracking stage. This is attributed to the different behavior of the internal bars, as the steel bars reached the yielding state while the CFRP bars behave linearly elastic till failure and the higher young's modulus of steel than that of CFRP.

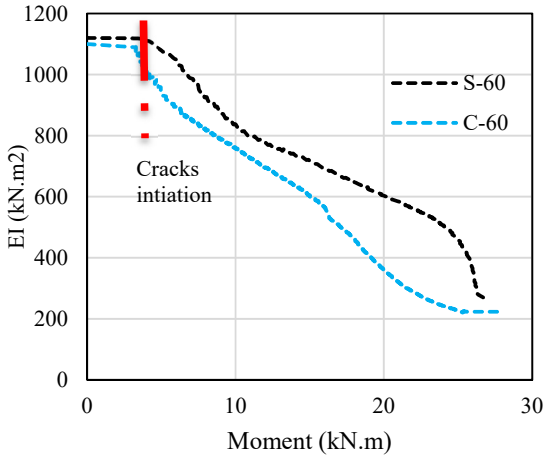


**Figure 3-21**-Effective flexure stiffness variations

## 3.7 Parametric Investigation

The parametric investigation was done to identify the trends between design variables and column's moment capacity, this was achieved through studying the structure performance in terms of moment-curvature diagrams for reinforced CFFT columns. The design variables include the unconfined concrete strength ($f'_c$), longitudinal reinforcement ratio ($\frac{A_{bar}}{A_g}$), and the thickness of the GFRP tube. The $f'_c$ parameter study analyzes the unconfined concrete strength as (25, 30 and 40 MPa). The reinforcement ratio ($\rho_b = \frac{A_{bar}}{A_g}$) parameter is recommended by ACI 318-14 in the range between 1% and 8%, thus in this study limits (1, 3, 6, 8 %) are considered so the widest range of recommended values are reviewed. Finally, the thickness of the tube is controlled by the number of layers of the GFRP tube, thus (3, 6 and 8 layers) are considered with thickness (1.325, 2.65, 3.53 mm) respectively. Figure 3-22 shows the

theoretical moment curvature curves considering the different design variables for both steel and CFRP reinforced CFFT columns. It was clear that increasing $f'_c$ increases the specimen moment capacity where for steel reinforced CFFT column increasing $f'_c$ from 25 MPa to 30 and 40 MPa increases the moment capacity by 11% and 14% respectively, while for CFRP reinforced CFFT column increasing $f'_c$ from 25 MPa to 30 and 40 MPa increases the moment capacity by 13% and 16% respectively. Also, increasing the percentage of longitudinal reinforcement has a great influence on the moment capacity of the column. For steel reinforced CFFT column increasing ($\frac{A_{bar}}{A_g}$) from 1% to 3%, 6% and 8% increases the moment capacity by 40%, 62% and 68% respectively, while for CFRP reinforced CFFT column increasing ($\frac{A_{bar}}{A_g}$) from 1% to 3%, 6% and 8% increases the moment capacity by 25%, 60% and 68% respectively. In addition, the effect of increasing the number of layers has a small influence on the moment capacity of reinforced CFFT specimen. For steel reinforced CFFT columns increasing the number of layers from 3 to 6 and 8 layers increases the moment capacity by 5% and 7% respectively and by 4% and 6% respectively for CFRP reinforced CFFT columns.

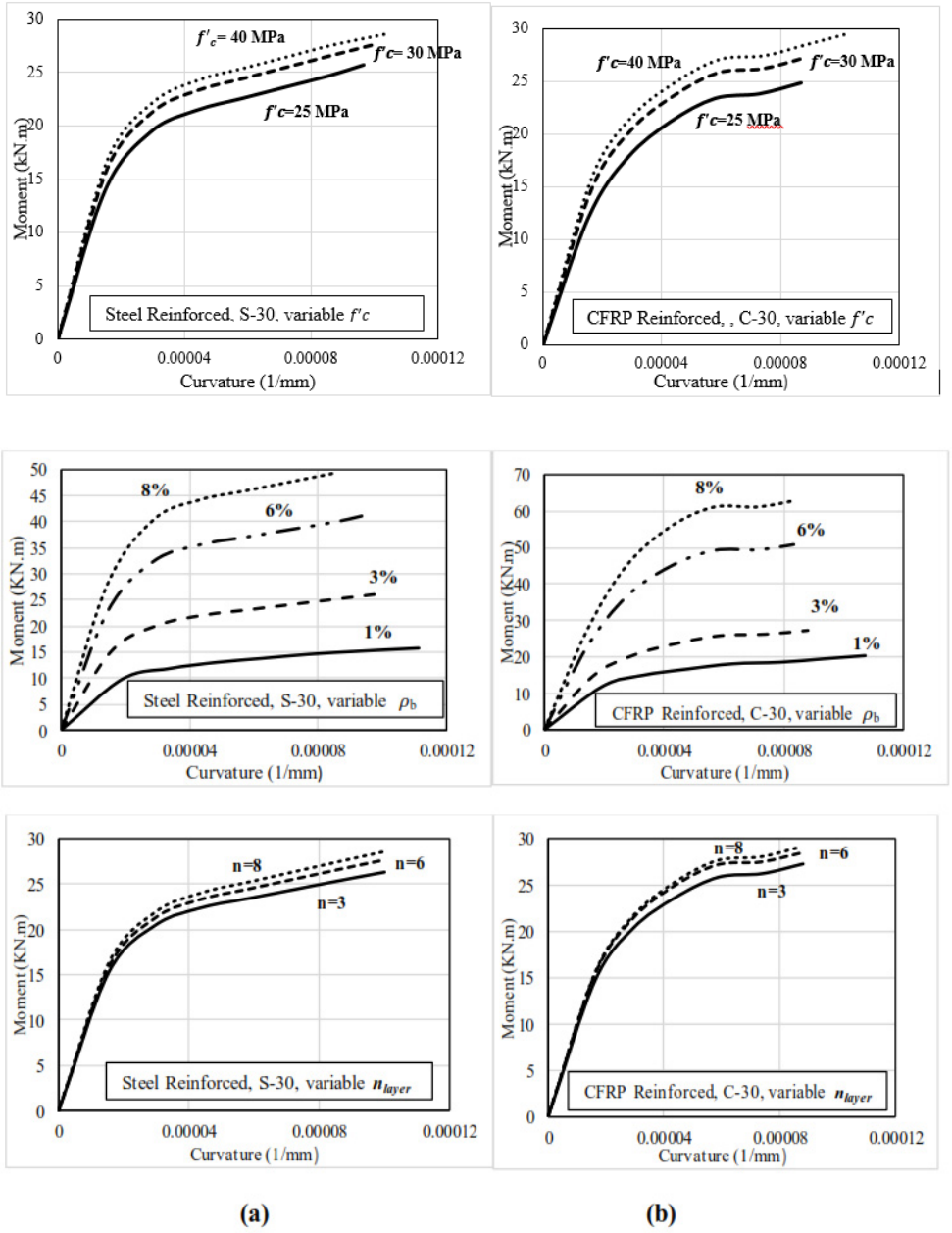


**Figure 3-22-** Theoretical moment curvature diagrams considering design variables, (a) Steel reinforced CFFT columns; (b) CFRP reinforced CFFT columns

## 3.8 Conclusions

A total of full scale 10 reinforced CFFT columns were constructed and tested under concentric and eccentric compression loads to investigate the behavior of steel and CFRP reinforced CFFT columns. The axial-bending moment curvature behavior was also investigated experimentally and analytically for the 10 specimens. The test parameters were the internal reinforcement type and the eccentricity to diameter ratio *(e/D)*. Based on the presented experimental work and theoretical models, the following conclusions can be drawn as follows:

1. The behavior of steel and CFRP reinforced CFFT columns under eccentric loads is completely different as compared to those tested under concentric loads in terms of ultimate load capacities and failure modes, where the load carrying capacities of CFFT columns under load eccentricities, *e/D* ratios ranged from 0.10 to 0.4 were reduced by 42 to 75%, respectively, as compared to that of the same CFFT columns under concentric load. In addition, rupture of the FRP tube in the hoop direction and local buckling of internal bars are the dominant in case of concentric loading. While overall instability of the columns along with the combination of tensile rupture of the FRP tubes and CFRP bars or steel yielding in the tension side with excessive axial and lateral deformations are the dominant in case of eccentric loading.
2. The axial and lateral deformations were increased progressively with increasing the eccentricity values.
3. The experimental investigation conducted in this study indicated that the CFRP bars could be used as a longitudinal internal reinforcement for CFFT columns under eccentric loads, provided that the maximum compression strength is limited to 35% of the ultimate tensile bar strength.
4. The recorded bar strain at peak can reach up to 0.65% and 0.45% ultimate tensile and compressive strains, respectively. These values proved the effective contribution of the CFRP bars in resisting tensile and compressive stresses.
5. Experimental axial-moment interaction diagrams showed that the failure envelope of the FRP reinforced CFFT columns was unlike the steel reinforced CFFT columns where no balance point was indicated. This was due to the variation of the linearly elastic stress strain

response of CFRP bars until failure while for the steel bars a well-defined yield plateau behavior occurred.

6. Constructing a theoretical *P-M* diagrams based on strain compatibility -force resultant and layer-by-layer methods predict quiet well the axial load bending moment for both steel and FRP reinforced CFFT columns and pertained reasonably close values to the experimental results.

7. The developed analytical model for computing the moment-curvature diagram based on the layer by layer numerical integration provided accurate predictions compared to the experimental results. It also shows that regardless the type of reinforcement and the eccentric ratio all specimens exhibit nonlinear moment-curvature (M-φ) responses.

8. Studying the variation of flexure stiffness along the applied moment shows that CFRP reinforced specimen exhibits a more significant reduction of stiffness after initiation of cracks in comparison with steel reinforced specimen. This returned to the higher young's modulus of steel than that of CFRP.

9. The parametric investigation showed that the increase in the unconfined concrete strength, longitudinal reinforcement ratio and number of layer of FRP tube increase the moment capacity of the columns. Increasing ($\frac{A_{bar}}{A_g}$) and $f'_c$ has a significant influence on the moment capacity of the columns which increased by 68% on changing ($\frac{A_{bar}}{A_g}$) from 1% to 8% and increased by average 15 % on increasing $f'_c$ from 25 MPa to 40 MPa. Yet increasing the number of FRP tube layers shows insignificant increase in the moment capacity of the columns which increased on average 6% when increasing the number of layers from 3 to 8 layers.

# CHAPTER 4

# Experimental and Theoretical Development of Effective Flexural Stiffness for Concrete-filled FRP Tube columns

(***Engineering Structures Journal,*** Submitted, under review)

## Abstract

Recent years, concrete-filled fibre-reinforced-polymer (FRP) tubes (CFFTs) have been widely investigated. It proved to have significant effect when used as an external confinement in improving the strength and ductility of concrete columns. Nonetheless, the effective flexure stiffness of such members has not yet been defined. This paper introduces an extensive study on the effective flexure stiffness of slender (CFFT) columns. Current codes and design provisions on the effective stiffness ($EI_e$) are reviewed along with past studies considering the external FRP confinement on the effective stiffness expressions. On the basis of an experimental parametric study and theoretical simulation, variables influencing the effective stiffness expressions are discussed. The main parameters considered are: the eccentricity ratio ($e/D$), slenderness ratio ($l/D$), and the axial load ratio $(P_u/P_o)$. Two nonlinear design equations are developed and proposed to compute ($EI_e$) of steel and FRP reinforced CFFT circular columns. The proposed equations are applicable for any load levels including both service and ultimate loads. A nonlinear design equation for unreinforced CFFT columns is also developed. A comparative study is conducted using the available experimental data to ensure the accuracy of the proposed equations.

**Keywords:** Concrete; Eccentricity; Load; Moment; CFFT circular column; FRP bars; Stiffness.

## 4.1 Introduction

When designing a concrete–filled fibre-reinforced-polymer (FRP) tube (CFFT) column, structural engineers must take into consideration the impact of second order or P-Δ effects to determine if loads applied to a structure in its deformed position significantly increase internal forces (i.e. by more than 5%). Typically, second order effects of this magnitude occur when a CFFT column is slender; that is, when its slenderness ratio is greater than or equal approximately 12 (Mohamed et al. 2010). Thus, when a CFFT column with length (L) subjected to eccentric load, it deflects laterally and exhibit an additional eccentricity (midheight deflection) which results in an additional moment along its height. This additional moment is considered as the second order moment which controls the maximum moment acting on the column, as shown in Figure 4-1. It may be noted that a CFFT column under single curvature bending is considered the worst case scenario for causing secondary moments. The accuracy of evaluating the effect of the second order effects depend mainly on the realistic determination of the effective flexure stiffness of the column ($EI_e$).

Over the past three decades, many authors and codes have proposed different techniques and equations to calculate the effective stiffness of RC columns (Mavichak and Furlong 1976, Mirza 1990, Westerberg 2002, Bonet et al. 2004, Tikka and Mirza 2005, Tikka and Mirza 2008). Due to the importance of strength and stiffness for structure members, different design codes provide expressions to calculate these properties. However, there is no unified equation for calculating the stiffness of concrete members confined with FRP tube or sheet. The ACI Building Code 318-14 allows the use of the moment magnifier method to calculate the second order moments in columns. This approach is affected by the critical buckling load ($P_{cr}$) which is strongly affected by the effective flexure stiffness $EI_e$. The AISC design specification introduces an equation for stiffness of composite members (for example a member confined with steel tube). Tikka and Mirza have done extensive researches to study the effective flexure stiffness for different type of columns including slender, tied RC columns and composite sections. Those studies showed that the EI expressions currently used by the ACI Code have a high degree of variability and can be conservative for columns subjected to low eccentricities and unconservative for columns subjected to high eccentricities. In addition, investigations by

other researchers showed dependence of column flexural stiffness on the level of axial load (Khuntia and Ghosh 2004a, Khuntia ang Ghosh 2004b, Mehanny et al. 2001) as well as eccentricity ratio (Mirza 1990, Lioyd and Rangan 1996). To generalize the design of RC columns to include FRP bars and to account for the different mechanical properties of FRP including the reduced effectiveness of FRP bars in compression and their wide range of elastic modulus $E_f$ , Zadeh and Nanni (2017) studied the effect of using FRP bars on the $EI_e$ equation and derived analysis and design parameters for concrete columns reinforced with FRP bars, similar to those used for steel-reinforced columns. They concluded that the flexural stiffness of FRP columns, whether for analysis or for second-order effects may be approximately expressed as: GFRP-RC columns equals 60% of steel RC columns while CFRP-RC columns equals 80% of steel RC columns. They recommended these values for frames subjected to gravity loads (nonsway frame).

This paper aims to develop new expressions for effective flexure stiffness of steel and FRP reinforced and unreinforced slender CFFT columns under short term loads that take into consideration the confinement effect induced by FRP tube, in addition to the influences of various important parameters generated from a parametric study of an available experimental data base. The new equations will be developed with assistance of theoretical computational procedure consisted of more than 3400 isolated steel and FRP reinforced CFFT columns that were simulated to generate the required stiffness data. Comparison between available experimental stiffness data and developed stiffness equations at service and ultimate load levels will be conducted.

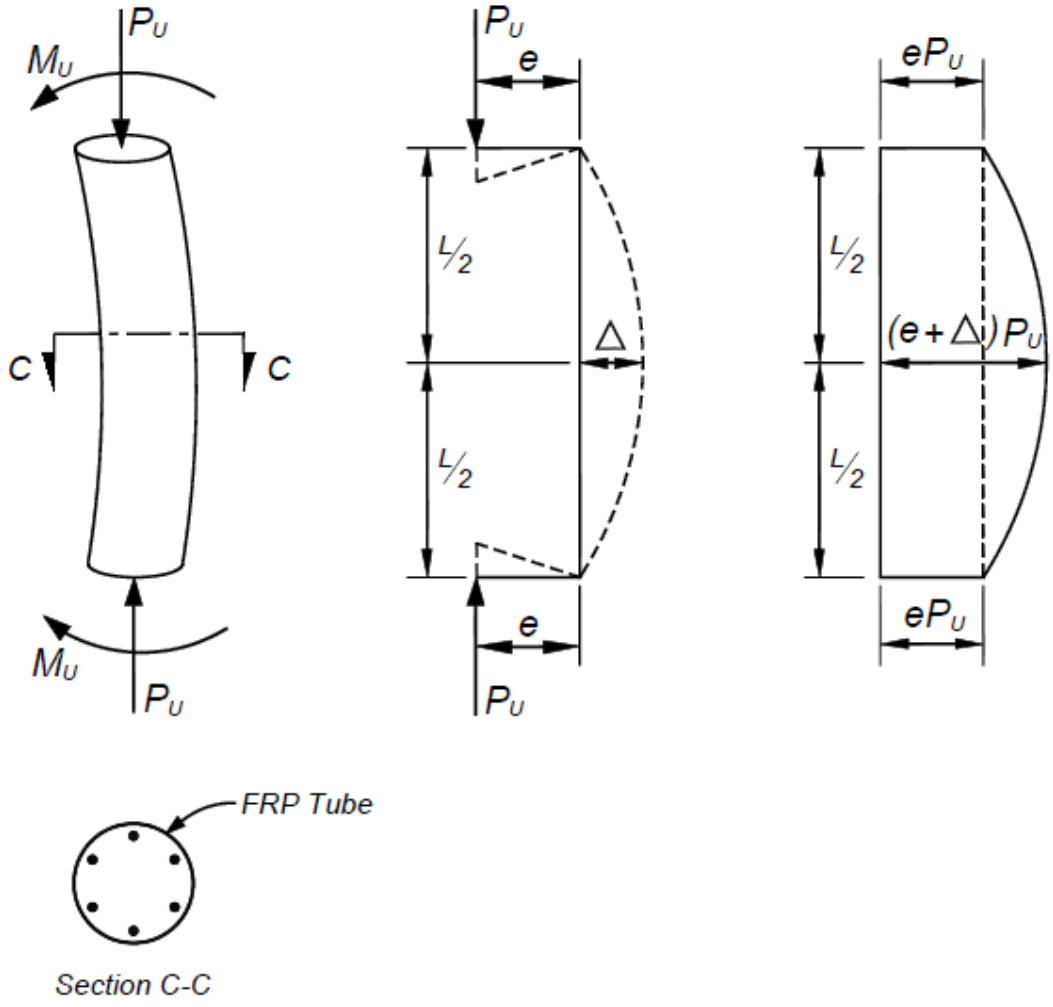


**Figure 4-1-** Type of CFFT Column Studied: (a) Symmetrical single curvature pin-ended CFFT column; (b) Forces on the column; (c) Bending moment diagram ($M= P_u (e+\Delta)$)

## 4.2 Research Objective

One of the major elements in design of slender CFFT column is a suitable assumption of flexural stiffness *EIe*. In this paper new nonlinear $EI_e$ equations based on experimental and theoretical statistical evaluations of parameters affecting the flexural stiffness is developed for steel and FRP reinforced and unreinforced slender CFFT columns. The effective flexure stiffness at service and ultimate loads predicted by the proposed $EI_e$ expressions show excellent agreement with available experimental results. The proposed equations can be used by design professionals, and it could be incorporated into codes and guidelines provisions concerned with the design and analysis of FRP confined and CFFT columns.

## 4.3 Review for Current Codes and Past Studies on Stiffness Expressions

Many codes and design provisions proposed several methods to determine the stiffness for different structure elements. They consider the stiffness as an important design parameter where it is required for defining buckling capacity, deflections, and serviceability criteria. For instance, column stiffness has been studied for either reinforced concrete columns or columns confined with steel tubes (Parbhu et al.2015). AISC (2016) suggested the following stiffness equation for composite columns confined with steel tube;

$$EI_e = C_1 E_c I_g + E_s I_s + E_s I_{st} \qquad 4\text{-}1$$

where $E_c, E_s$ = modulus of elasticity of concrete and steel, respectively.

$I_g$ = moment of inertia of gross concrete section, neglecting reinforcement, $mm^4$

$I_{st}$ = moment of inertia of steel tube about the elastic neutral axis of the composite section, $mm^4$

$I_s$ =moment of inertia of Steel reinforcing bars about centroid of section, $mm^4$

$C_1$ = coefficient for calculation of effective rigidity of an encased composite compression member = $0.25+3\left(\frac{A_s+A_{st}}{A_g}\right)\leq 0.7$ 4-2

In which, $A_g, A_s, A_{st}$ = cross-section area of concrete, steel bars and steel tube, mm$^2$

According to ACI 318-14, the moment magnifier method is used to calculate the second order moments in columns. This approach is affected by the critical buckling load ($P_{cr}$). For calculating the critical axial buckling load, the primary concern is the choice of a stiffness $EI_e$ that reasonably approximates the variations in stiffness due to cracking, creep, and nonlinearity of the concrete stress strain curve. Thus, to consider the maximum bending moment which includes the second order effects occurring along the height of the column the following equations are used;

$$M_{max}=\delta M_2 \qquad 4\text{-}3$$

$$P_{cr}=\frac{\pi^2 EI_e}{L^2} \qquad 4\text{-}4$$

$$\delta=\frac{C_m}{1-0.75\frac{P_u}{P_{cr}}} \qquad 4\text{-}5$$

where $M_2$ is the large factored end moment on a compression member, $C_m$ is coefficient accounting for non-uniform moment, $P_{cr}$, $P_u$ = critical axial force and ultimate axial force, respectively.

For a pin-ended column of length $L$ subjected to equal end moments with single curvature bending, $\delta$ can be approximated as:

$$\delta=\frac{1}{1-0.75\frac{P_u}{P_{cr}}} \qquad 4\text{-}6$$

$EI_e$ shall be calculated by the following equation

$$EI_e = 0.2E_cI_g + E_sI_s \quad 4\text{-}7$$

In brief, ACI 318-14 equation for $EI_e$ is independent from the load applied on the column while many other authors as confirm that the effective flexure stiffness depends on the loads applied by means of relative eccentricity. Several studies can be found in the literature to calculate the stiffness of RC columns in different forms either rectangular, slender, circular, or as a composite section (Mirza 1990, Tikka and Mirza 2005, Tikka and Mirza 2008, Khunita and Ghosh 2004a, Khuntia and Ghosh 2004b). Yet, for FRP confined RC columns there is a lack in the available studies concerning the calculation of the flexural stiffness. An expression suggested by Sadeghim and Fam (2014), based on ACI expression was introduced considering the contribution of external FRPs to the stiffness equation as follows:

$$EI_e = 0.2E_cI_g + E_sI_s + E_{fe}I_{fe} \quad 4\text{-}8$$

In which, $E_{fe}, I_{fe}$ = modulus of elasticity and moment of inertia of the external FRP.

Thus, they assume that contribution of the external FRP is the same as that of reinforcing steel in the overall stiffness of the column, the accuracy of this equation will be discussed later in this study. Also, based on ACI 318-14 expression, the effect of using FRP internal reinforcement instead of steel reinforcement on the effective stiffness have been discussed by Zadeh and Nanni (2013) and then modified in Zadeh and Nanni (2017) as follows:

$$EI_e = 0.2E_cI_g + 0.75E_fI_f \quad 4\text{-}9$$

$E_f, I_f$ = modulus of elasticity and moment of inertia of FRP reinforcing bars.

Thus, the equation can be simplified for using GFRP and CFRP internal bars as follows,

$$EI_e = 0.2E_cI_g + 0.03E_cI_g \qquad 4\text{-}10 \qquad \text{for GFRP internal bars}$$

$$EI_e = 0.2E_cI_g + 0.09E_cI_g \qquad 4\text{-}11 \qquad \text{for CFRP internal bars}$$

## 4.4 Experimental Data Base

An experimental data base presented in Table 4-1 was undertaken to calculate experimental $EI_e$ of CFFT columns which is given by the following equation;

$$EI_e = \frac{M}{\phi} \qquad 4\text{-}12$$

where $\phi$ is the curvature of CFFT column in (1/mm) and calculated using the following equation:

$$\phi = \frac{\left|\varepsilon_{tension}\right| + \left|\varepsilon_{compression}\right|}{D_o} \qquad 4\text{-}13$$

where $\varepsilon_{tension}$ and $\varepsilon_{compression}$ are the compressive and tensile strains measured from the two longitudinal strain gauges installed on the FRP tubes on two opposite sides at the mid height of the column. $D_o$ is the external diameter of the tube.

A parametric study was conducted using experimental results of tested CFFT specimens to investigate the effect of various parameters on the effective flexure stiffness. Table 4-1 shows the details of different configurations of the tested specimens. The experimental program was carried out on reinforced CFFT specimens under eccentric loads. Eight specimens were included through two series. The tested columns had a circular cross-section of 152 mm diameter. Series No. 1 and 2 present reinforced CFFT columns with a total height 912 mm, reinforced longitudinally with 6 deformed steel bars No. 10 M (11.3 mm nominal diameter) or sand-coated carbon FRP (CFRP) bars No. 3 (9.52 mm nominal diameter), respectively. The

bars were distributed uniformly inside the cross section of the glass FRP (GFRP) tubes. For the steel bars, the average values of the yield tensile strength, $f_y$ was 462 MPa with an ultimate tensile strength, $f_{su}$, 577 MPa. On the other hand, the CFRP bars were manufactured and developed by Pultrall Inc., Quebec, Canada. The bars were made of continuous fiber impregnated in vinylester resin with a fiber content of 73%, using the pultrusion process. The elastic modulus and ultimate tensile strength of the CFRP bars were 128 GPa and 1431 MPa, respectively, with an ultimate tensile strain 1.2±0.09. The average concrete strength was 30±0.6 MPa. The GFRP tubes were fabricated using filament winding technique; E-glass fiber and epoxy resin were utilized for manufacturing these tubes. The tubes had a core diameter of 152 mm and a wall thickness of 2.65 mm (6 layers). The fiber orientations of the tubes were mainly in the hoop direction (±60 degree with respect to the longitudinal axis). Specimens ID were shown in the second column of Table 4-1, the numbers indicate the eccentricity ($e$) in mm and the letter S or C refers to the type of internal reinforcement, respectively, steel or CFRP bars. The load eccentricity-to-diameter ($e/D$) ratios for the reinforced CFFT columns were 0.1, 0.2, 0.3 and 0.4. The main parameters investigated from the experimental work were; the axial load ratio $P_u/P_o$ (ranging from 0.05 to 0.65) and the eccentricity ratio (ranging from (0.1 to 0.4). A detailed analysis on the moment-curvature diagrams for tested CFFT specimens using a strain compatibility model with more experimental parameters and data including a parametric study has been developed and validated, but remains outside the scope of this paper. Figures (4-2, 4-3) show the variation of $EI_e/EI_g$ for the steel and CFRP reinforced CFTT columns, respectively, with changes in eccentricity ratio $e/D$ and the axial load level $(P_u/P_o)$. It is shown that for any axial load ratio $(P_u/P_o)$, $EI_e$ decreases with increasing $e/D$, this is expected as increasing the eccentricity ratio, leading to an increase in the bending moment which leads to an increase in flexural cracks and reduction in $EI_e$ of the section. In addition, increasing the axial load ratio always results in reduction in effective stiffness $EI_e$ for the CFFT column. Note that, $P_o$ is calculated using the following equation:

For Steel CFFT Column:

$$P_o = \phi f'_{cc}(A_g - A_s) + f_y A_s \qquad 4\text{-}14$$

For CFRP CFFT Columns:

$$P_o = \phi f'_{cc}(A_g - A_{bar}) + E_{bar}\varepsilon_{fe}A_{bar} \quad 4\text{-}15$$

Equation 4-15 was used by several researchers (Mohamed and Masmoudi ,2010) and it results in more conservative values for $P_o$.

$\phi$is the strength reduction factor that was suggested to be equal 0.8 for reinforced CFFT columns (Mohamed and Masmoudi, 2010)

$f'_{cc}$ is the confined concrete strength calculated from Lam and Teng (2003) confined concrete model

$\varepsilon_{fe}$is the effective strain level in the FRP at failure, according to ACI440-2R-08 procedures $\varepsilon_{fe}$ should not be taken more than 0.004 in members subjected to combined axial compression and bending moment to ensure shear integrity of the confined concrete.

Due to the lack of the available experimental data to cover all the important parameters that affect the accuracy of the effective flexure stiffness equation $EI_e$, a theoretical equation was used to generate stiffness data, this theoretical procedure will be discussed in details in the following sections.

**Table 4-1-** Specimens details and summary of test results (Abdallah et al.,2018)

| Series No. | Specimen ID | *(e/D)* | *Bar type* | $P_{u(exp)}$ (kN) | ($\Delta_+$e) (mm) | $M_{u(exp)}$ (kN.m) | $\phi_{exp}$ (1/m) |
|---|---|---|---|---|---|---|---|
| 1 | S-15 | 0.1 | Steel | 825.0 | 31.00 | 25.51 | 0.06 |
| | S-30 | 0.2 | Steel | 620.0 | 45.5 | 28.00 | 0.072 |
| | S-45 | 0.3 | Steel | 466.0 | 60.00 | 27.84 | 0.077 |
| | S-60 | 0.4 | Steel | 367.0 | 73.00 | 26.72 | 0.09 |
| 2 | C-15 | 0.1 | CFRP | 771.7 | 22.1 | 17.05 | 0.0∘ |
| | C-30 | 0.2 | CFRP | 614.5 | 43.46 | 26.71 | 0.1 |
| | C-45 | 0.3 | CFRP | 454.9 | 59.55 | 27.08 | 0.11 |
| | C-60 | 0.4 | CFRP | 375 | 75.32 | 28.24 | 0.125 |

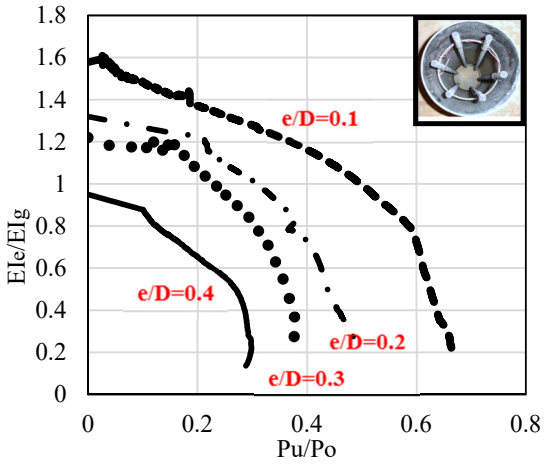


**Figure 4-2-** Influence of eccentricity ratio and axial load ratio on EIe for Steel CFFT columns

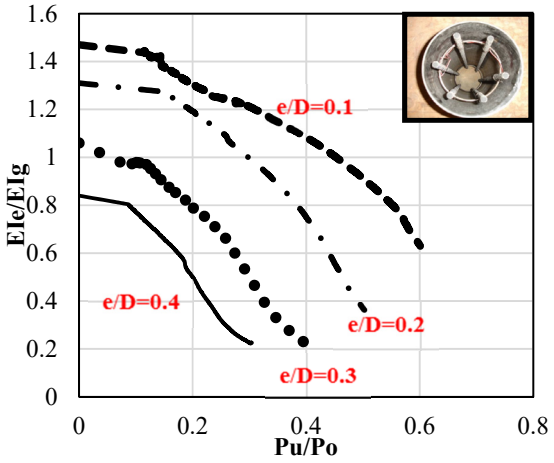


**Figure 4-3-** Influence of eccentricity ratio and axial load ratio on EIe for CFRP CFFT columns

## 4.5 Theoretical Stiffness Equation

A theoretical model based on secant formula developed by Timoshenko and Gere (1961) for pin-ended slender column subjected to end moments was used in this study as follows:

$$M_c = M_2 \sec\left(\frac{\pi}{2}\sqrt{\frac{P_u}{P_{cr}}}\right) \qquad 4\text{-}16$$

where $M_c$ is the design bending moment that includes second-order effects; $M_2$ is the applied column end moment calculated from a conventional elastic analysis. For the purpose of the current analysis $M_c$ is replaced by the cross section bending moment strength $M_{cs}$ and $M_2$ is replaced by the overall column bending moment strength $M_{col}$. By substituting Euler's buckling load equation into $M_c$ equation for pin-pin ended column ($k$=1), $EI_{th}$ could be simplified as follows:

$$EI_{th} = \frac{P_u l^2}{4\left[\sec^{-1}\left(\frac{M_{cs}}{M_{col}}\right)\right]^2} \qquad 4\text{-}17$$

$P_u$, $M_{cs}$, $M_{col}$ was shown in Figure 4-4, which presents the schematic cross section and column axial load-bending moment interaction diagrams explained in details in the following section.

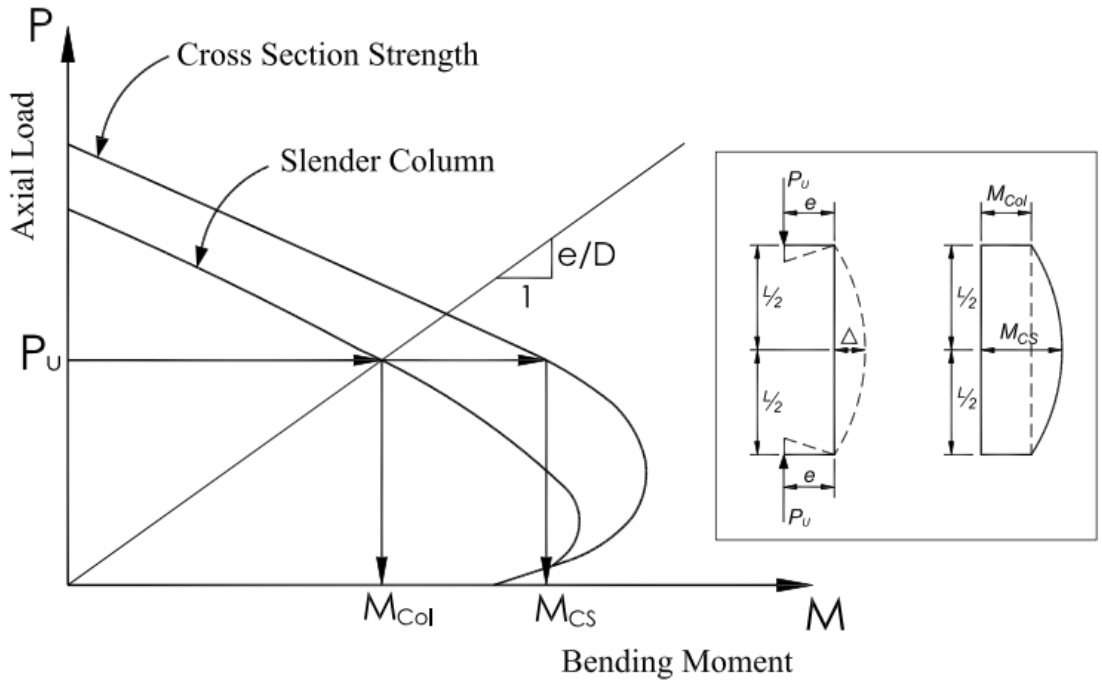


**Figure 4-4-** Schematic axial load-bending moment interaction diagram for cross section and slender CFFT column

### 4.5.1 Development of Theoretical Computational Method for Bending Moment Resistances Considering Second Order Effects

To account for the first and second order moments ($M_{col}, M_{cs}$), axial load-moment-curvature diagrams have to be created based on the following assumptions (Mohamed and Masmoudi 2010, Lam and Teng 2009):plane section remains plane under bending, the existence of a perfect bond between concrete, reinforcement and FRP tube, tensile strength of concrete is neglected, the area of concrete displaced by reinforcement is neglected and finally distribution of the strains with in the circular CFFT cross section is linear. Layer by layer method for a given circular CFFT column is presented in Figure 4-5, where the cross section was assumed to be consisted of three materials: (1) confined concrete, (2) FRP tube, (3) internal reinforcing bars (steel or FRP). The accuracy of the theoretical model depends mainly on the constitutive

material modeling of each element of the cross section. Thus, Lam and Teng (2003) model for confined concrete was chosen to model the stress-strain curve for the circular confined concrete, this model proved to be one of the most accurate model to predict the stress-strain curve of circular confined columns (Abdallah et al.2017, Ozbakkaloglu 2013). It was assumed that the model used for calculating the stress-strain curve for circular confined columns under concentric loads could be used for circular confined eccentrically loaded columns (Jiang and Teng, 2013). In this model, they assume that the stress-strain curve of the confined concrete consists of two parts, the first is parabolic, while the second is a straight line. More details of this model can be found in Lam and Teng (2003). For reinforcing steel bars an elastic plastic stress-strain relation was used (Ozbakkaloglu et al. 2012). For the FRP bars a linear elastic until rupture theory presented by Kobayashi et al. (1995) was used. In addition, for design purpose a reasonable assumption to consider the contribution of FRP bars in tension only while the bars in compression were replaced by the same area of concrete (Zadeh and Nanni 2013). Although there is an evidence against a full discount of FRP compression bars, still the guidelines don't recommend relying on FRP bars in compression. In brief, they agreed that, since no standard test is available to establish the compressive properties of FRP bars, this assumption for replacing compressive FRP bars by concrete is considered safe for design purposes. A linear elastic stress-strain relationship was adopted for FRP tube where the parts above and below the neutral axis are considered effective in resisting the compression and tension forces, respectively (Figure 4-5). The contribution of the FRP tube should be considered in tension and compression to give more conservative results. The determination of ($P_u, M_{cs}, M_{col}$) from axial-load- moment relationships is summarized with the help of Figure 5 in the following steps:

1- Divide the column cross section into N number of strips and assume the location of the neutral axis;
2- Select a small value of the concrete strain $\varepsilon_c$ at the outer most compression fiber;
3- From the linear strain distribution, determine the strains at the centers of all strips of concrete in compression , FRP tube, tension and compression steel bars in case of steel

reinforced CFFT columns, and tension FRP bars in case of CFRP reinforced CFFT columns;

4- Using the material constitutive models and stress-strain relationships to determine the stresses and consequently the forces in tension or compression in each reinforcing bar, and in each strip of FRP tube, in addition to each strip of concrete in compression zone;
5- The axial load (*P*) and bending moment (*M*) that the cross section will resist for the assumed strain distribution and curvature can be calculated by summing all the vertical forces and the moments around the centroid (Figure 4-5c);
6- The associated curvature ($\phi$) is calculated by dividing the strain $\varepsilon_c$ in step 2 by the distance *C* from the outermost fibre in compression to the neutral axis;
7- The value $\varepsilon_c$ is increased by a small amount $\Delta\varepsilon_c$, and the procedure from step 4 is repeated, step 4 to 7 are repeated until the compressive strain $\varepsilon_{cu}$ (maximum confined concrete strain) is reached. The value of $\varepsilon_{cu}$ is calculated from Lam and Teng model for FRP confined concrete. After the ultimate compressive strain has been used a new location for the neutral axis is selected and the procedure from step 2 is repeated. It was clear that the aforementioned steps account for the first order analysis as the value of $\Delta$ was neglected.

To consider the second order effects in terms of P-$\Delta$, a numerical procedure was used to obtain the lateral displacement of the column as shown in Figure 4-6. The lateral displacements $\Delta_i$ and the slopes $\theta_i$ at points $x_i$ on the column are successively calculated for an initial slope $\theta_o$ at $x_0$ for a given combination of *P* and *M*. The discrete points $x_1, x_2, ....., x_n$, are chosen at small intervals so that the displacement and the slope at any point may be approximated by the following numerical integration equation (Chen and Atsuta 1976);

$$\Delta_i = \Delta_{i-1} + \theta_{i-1}\left(x_i - x_{i-1}\right) - \frac{1}{2}\phi_{i-1}\left(x_i - x_{i-1}\right)^2 \quad 4\text{-}18$$

$$\theta_i = \theta_{i-1} - \phi_i\left(x_i - x_{i-1}\right) \quad 4\text{-}19$$

Thus, to calculate the mid height deflection, Harik and Gesund (1986) recommended the use of 10 segments along the column height for column bending in single curvature, where the

procedure is repeated by changing $\theta_0$ until the correct displacement is obtained. Once the slope at the mid height equals zero, the assumed displacement is considered correct. Then, the values of moments along the column, including the maximum moment, can be determined from the lateral displacements. Repeating the above procedure for increasing values of *P*, the corresponding displacements along the column can be computed and, thus, the axial force-maximum moment resistance diagrams can be generated.

CFFT column

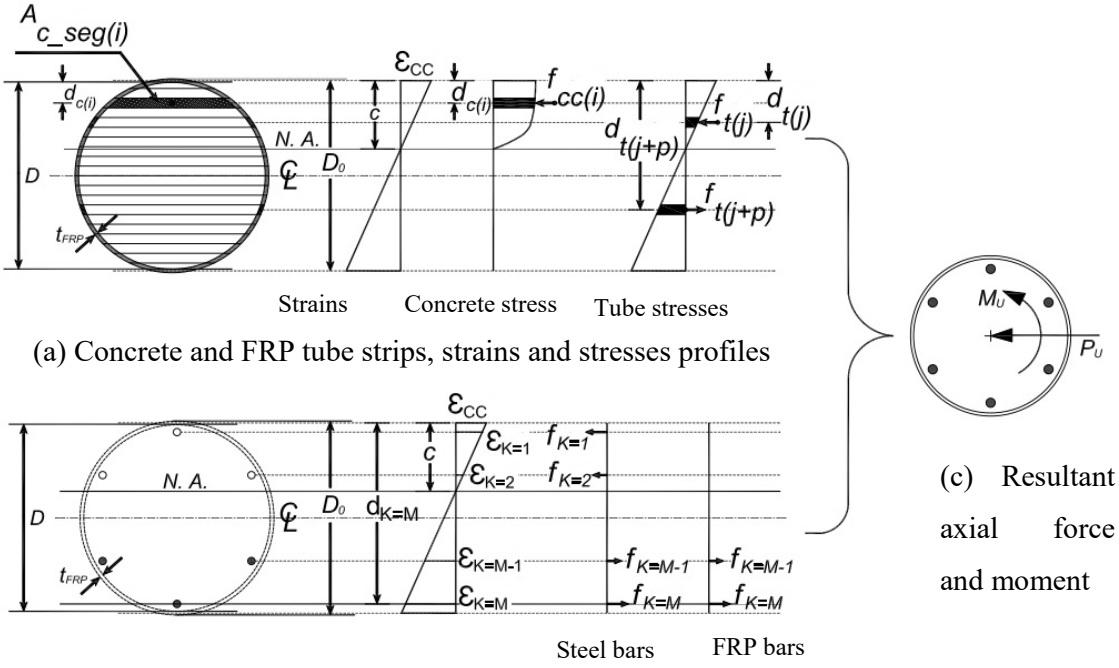


(a) Concrete and FRP tube strips, strains and stresses profiles

(b) Reinforcement Layout, strain distribution and stresses

(c) Resultant axial force and moment

**Figure 4-5-** Stress and strain profiles of reinforced CFFT columns

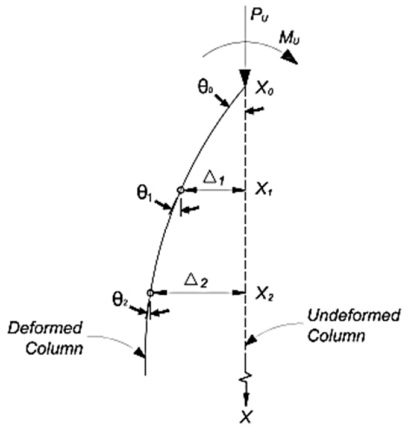


**Figure 4-6-** Numerical integration for CFFT column deflection

### 4.5.2 Parameters Used for Simulation of Theoretical Stiffness of CFFT Columns

To simulate the theoretical stiffness of CFFT columns, different combinations of specified parameters for the components of the circular CFFT columns are used. Table 4-2 shows the different parameters used in this study for concrete, reinforcing bars (steel & FRP), and FRP tube. Most of the parameters used were extracted from previous experimental data and mentioned as influence parameters in literature. For concrete, concrete compressive strengths ($f'_c$) is considered as an important parameter to be studied (Khuntia and Ghosh 2004a), while for reinforcing steel a specified yield strength ($f_y$) of 460 MPa was used with a variety in reinforcing ratio ($\rho_b$) (Mirza 1990). For FRP bars a tensile strength of 1400 MPa was used with the same reinforcing ratios used in the case of steel reinforced CFFT column. Three slenderness ratio *(L/D)* and ٨ eccentric ratio *(e/D)* were also used, the slenderness ratios used (10, 15 and 20) and the end eccentricity ratio *(e/D)* ranged from (0.05 to 0.65) as this is the practical range for reinforced concrete buildings (Mirza and Macgregor 1982). For the FRP tube, the important parameters shall be studied including the confinement reinforcement ratio ($\rho_t = \frac{4t}{D}$) which depends on the thickness ($t$) and internal diameter ($D$) of the tube, and the tensile strength and young's modulus the tube in the longitudinal direction ($f_t, E_t$) (Mohamed and Masmoudi 2011), where the longitudinal direction of the tube acts as longitudinal

reinforcement that resists the overall buckling of the column. The arrangement of the reinforcement used in the analysis was shown in Figure 4-5. The theoretical *EI* for each of CFFT column studied was computed from Equation (4-17) and using ( $M_{cs}$ & $M_{col}$) from the cross-section strength and slender column interaction diagrams.

**Table 4-2 -** Different parameters of reinforced CFFT Columns*

| CFFT Column Components | Properties Studied | Specified Values | No. of Specified Values |
|---|---|---|---|
| Concrete | $f'_c$ | 25,30,40 (MPa) | ٣ |
| Steel reinforcing bars | $f_y$ | 462 (MPa) | ١ |
| | $\rho_s$ | 1%, 3%,5% | 3 |
| FRP reinforcing bars | $f_b$ | 1431 (MPa) | ١ |
| | $\rho_b$ | 1%,3%,5% | 3 |
| FRP Tube | $f_t$ | 57.9, 146 (MPa) | 2 |
| | $E_t$ | 8785 ,12000 (MPa) | 2 |
| | D | 152, 320 (mm) | 2 |
| | t | 2.54, 6.4 (mm) | 2 |
| Section Properties | L/D | 10,15,20 | 3 |
| | e/D | 0.05;0.1;0.2;0.3;0.4;0.5;0.6;0.65 | 8 |

*Total number of simulated Steel or CFRP CFFT columns= 3*1*3*2*2*2*2*3*8= 1728, with each CFFT column has a different combinations of specified parameters shown above.

### 4.5.3 Comparison between available effective $EI_e$ equation and theoretical $EI_{th}$ values

It is important to study the accuracy of the available equations that consider the presence of external confinement on RC columns. Thus, Equation 4-8 will be compared to the theoretical $EI_{th}$ values computed from Equation 4-17 for all simulated steel reinforced CFFT columns. The result of this comparison is plotted in Figure 4-7, which shows histogram and statistics of the ratios of theoretical $EI_{th}$ to Equation 4-8 $EI_e$ values. Note that, stiffness ratio ($EI_{th}$/ $EI_e$) greater than one indicates that $EI_e$ is conservative, and values of ($EI_{th}$/ $EI_e$) less than one indicates that $EI_e$ is non conservative. It is shown that the average stiffness ratio equals 1.42 with a coefficient of variation of 0.28. These values are considered quite high, thus Equation (4-8) is considered an inaccurate equation and it is necessary to develop new equation that take into consideration all the important aforementioned parameters.

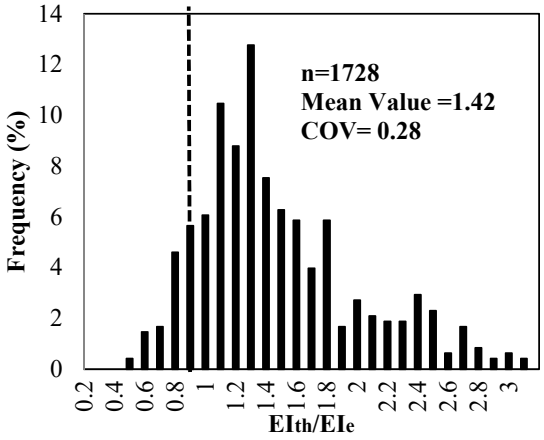


**Figure 4-7-** Comparison between equation (4-8) and theoretical equation

### 4.5.4 Requirements for Developing of Effective Flexural Stiffness $EI_e$ Equation

To develop the effective flexure stiffness equation for a slender CFFT column, several requirements have to be accounted to take into consideration the effect of cracking along the length of the column and the inelastic response in confined concrete, reinforcing bars and FRP tube. Thus, $EI_e$ should be referred as a complex function of a number of variables that can't be simplified to a simple analytical equations. Therefore, it is important to develop more accurate equation that take into account the effect of different variables on $EI_e$ of CFFT columns. This can be achieved through the following steps:

1- To include the variables affecting the flexure stiffness, a format of the proposed $EI_e$ equation was selected;
2- A multiple linear regression analysis of the generated theoretical stiffness ($EI_{th}$) date was conducted to evaluate the different coefficients related to the variables included in the proposed $EI_e$ equation;
3- The proposed $EI_e$ equation was then suggested and finalized by curve fitting and trial and error procedure of the generated theoretical stiffness data.

The following sections describe these steps in details.

### 4.5.5 Variables Used for Proposed $EI_e$ Equation

The variables used for developing of the $EI_e$ equation in this study were divided into three groups: 1) variables affecting the contribution of the confined concrete $E_cI_g$ to overall effective stiffness of CFFT columns; 2) variables affecting the contribution of longitudinal reinforcement either steel $E_sI_s$ or FRP $E_fI_f$ to the overall effective stiffness of CFFT columns; 3) variables affecting the contribution of the FRP tube $E_tI_t$ to the overall effective stiffness of

CFFT columns. Therefore, a modified version is proposed for steel reinforced CFFT column as follows;

$$EI_{e-s} = \alpha_c E_c I_g + \alpha_s E_s I_s + \alpha_t E_t I_t \quad 4\text{-}20$$

and for FRP reinforced CFFT column as follows;

$$EI_{e-FRP} = \alpha_c E_c I_g + \alpha_f E_f I_f + \alpha_t E_t I_t \quad 4\text{-}21$$

In which $\alpha_c, \alpha_s, \alpha_f, \alpha_t$ are dimensionless reduction factors (effective stiffness factors) for concrete, longitudinal steel or FRP bars and FRP tube, respectively. The reduction factor $\alpha_c$ represents the effect of different variables that influence the contribution of concrete to the overall column stiffness and can be linear or nonlinear function of these variables. If $\alpha_c$ is taken as a linear function of $x_1$ and $x_2$ and assumed to be equal to $(\alpha_k + \alpha_1 x_1 + \alpha_2 x_2 + \alpha_3 x_3)$, thus, equation for steel CFFT column becomes;

$$EI_{e-s} = (\alpha_k + \alpha_1 x_1 + \alpha_2 x_2 + \alpha_3 x_3) E_c I_g + \alpha_s E_s I_s + \alpha_t E_t I_t \quad 4\text{-}22$$

and for FRP CFFT column;

$$EI_{e-FRP} = (\alpha_k + \alpha_1 x_1 + \alpha_2 x_2 + \alpha_3 x_3) E_c I_g + \alpha_f E_f I_f + \alpha_t E_t I_t \quad 4\text{-}23$$

In Equations 4-22 and 4-23 $\alpha_k$ is a constant (equivalent to intercept of a simple linear equation) and the remaining $\alpha$ values are dimensionless factors corresponding to independent variables $x_1, x_2, x_3, E_s I_s, E_f I_f$ and $E_t I_t$. In addition to the parameters generated from the available experimental work affecting the effective stiffness of the CFFT columns, a correlation analysis of the theoretical *EI* data was conducted and the results indicated that both the eccentric ratio *(e/D)* and slenderness ratio *(L/D)* have the most significant effect on the stiffness beside the effect of the axial load ratio *($P_u/P_o$)*. These results agreed well with what was found before by several researchers on the factors affecting the contribution of concrete to the stiffness of slender columns (Mirza 1990, Tikka and Mirza 2005, Khunita and Ghosh 2004a, Khuntia and

Ghosh 2004b). Therefore, the following equations can be assumed, for steel and FRP reinforced CFFT columns, respectively;

$$EI_{e-s} = (\alpha_k + \alpha_1 e/D + \alpha_2 l/D + \alpha_3 P_u/P_o)E_c I_g + \alpha_s E_s I_s + \alpha_t E_t I_t \quad 4\text{-}24$$

$$EI_{e-FRP} = (\alpha_k + \alpha_1 e/D + \alpha_2 l/D + \alpha_3 P_u/P_o)E_c I_g + \alpha_f E_f I_f + \alpha_t E_t I_t \quad 4\text{-}25$$

To simplify the analysis a dimensionless equations are presented by dividing both sides for both equations by the gross concrete section stiffness;

$$\frac{EI_{e-s}}{E_c I_g} = (\alpha_k + \alpha_1 e/D + \alpha_2 l/D + \alpha_3 P_u/P_o) + \alpha_s \frac{E_s I_s}{E_c I_g} + \alpha_t \frac{E_t I_t}{E_c I_g} \quad 4\text{-}26$$

$$\frac{EI_{e-FRP}}{E_c I_g} = (\alpha_k + \alpha_1 e/D + \alpha_2 l/D + \alpha_3 P_u/P_o) + \alpha_f \frac{E_f I_f}{E_c I_g} + \alpha_t \frac{E_t I_t}{E_c I_g} \quad 4\text{-}27$$

### 4.5.6 Analysis of the Theoretical Stiffness Data using the Multiple Regression Method

It is important to conduct regression analysis of the theoretical stiffness data for both steel and FRP CFFT columns to estimate values of coefficients of key variables that affect the flexure stiffness of CFFT columns. The multiple regression analysis was conducted using the simulated theoretical flexure stiffness data $EI_{th}$ resulting from Equation 4-17 for steel and FRP CFFT columns and substituted in Equations 4-26 and 4-27, respectively. The resulting equations for steel and FRP CFFT columns, respectively are;

$$EI_{e-s} = (0.018 - 0.1e/D + 0.0184l/D - 0.0325P_u/P_o)E_c I_g + 0.82E_s I_s + 1.03E_t I_t \quad (n = 1728; S_e = 0.081; R_c = 0.8) \quad 4\text{-}28$$

$$EI_{e-FRP} = (0.0216 - 0.087e/D + 0.014l/D - 0.0273P_u/P_o)E_c I_g + 0.67E_f I_f + 0.94E_t I_t \quad (n = 1728; S_e = 0.066; R_c = 0.82) \quad 4\text{-}29$$

The accuracy of the regression of $EI_e$ was based on the standard error $S_e$ as a measured of sampling variability where the smaller the value of $S_e$, the smaller the sampling variability of the regression equation. In addition, $R_c$ is an index of the relative strength of the equation. From

the two equations, it was confirmed that increasing *(e/D)* is associated with decreasing the overall stiffness of the CFFT column. This is due to the decrease in the effect of the confinement of FRP tube as *(e/D)* increases, in addition to the increase in the bending moment, resulting in more cracking of the column. Although it was expected that the effective $EI_e$ of the CFFT column should increase when increasing the axial load as the depth of the flexure cracks increased, analysis proved the contrary where for a given *(e/D)* as $P_u$ increases, the compressive strain in the extreme compression fiber of concrete increases in high proportion than an increase in $(P_u/P_o)$. Thus, the regression analysis confirms what was concluded from the experimental parametric study that an increase in $(P_u/P_o)$ results in a reduction in the effective $EI_e$ for a CFFT column.

### 4.5.7 Proposed $EI_e$ Equation for Steel and FRP Reinforced CFFT Columns

The purpose of conducting the regression analyses of the theoretical stiffness data for both steel and FRP CFFT columns was to estimate the values of coefficients related to some variables that affect the flexure stiffness. Equation 4-28 shows a value of $\alpha_s = 0.82$. A value of 0.8 for $\alpha_s$ appears to be a reasonable approximation and was used for developing a more refined $EI_e$ equation through curve fitting to the simulated theoretical stiffness data. Similarly, for $\alpha_f$ Equation 4-29 shows a value of $\alpha_f$=0.67. Again, curve fitting to the simulated theoretical stiffness data shows a reasonable approximation of $\alpha_f$=0.7. $\alpha_t$ the dimensionless reduction coefficient for FRP tube appeared to be ranged from approximately 0.9 to 1, thus, to incorporate the parameters that affect the stiffness of FRP tube a simplified equation was suggested as follows;

$$\alpha_t = 0.6\beta + 0.9 \quad \text{4-30}$$

$$\beta = \rho_{tube}\left(\frac{f'_c}{E_c}\right)\Big/\left(\frac{f_t}{E_t}\right) \quad \text{4-31}$$

where $\rho_{tube}$ is the confinement reinforcement ratio ($\rho_{tube} = 4t/D$); $\beta$ is the strength-reinforcement index of the FRP tube and concrete; $f_t, E_t$ = the tensile strength of the FRP tube and modulus of elasticity of the FRP tube in the longitudinal direction, respectively. Concrete dimensionless reduction factor $\alpha_c$, is a function of eccentric ratio *e/D*, the slenderness ratio *L/D* and the axial load level $P_u/P_o$, thus with the aid of a spreadsheet and using trial and error procedure to develop an approximate equation for $\alpha_c$ using the theoretical stiffness data and the assumed dimensionless reduction factor for steel or FRP bars and for the FRP tube; the following equation for $\alpha_c$ was obtained;

$$\alpha_c = 0.2\left(\frac{l}{D}\right) - \frac{e}{D}\left(\frac{0.5}{1+e/D}\right) - 0.4\left(\frac{P_u}{P_o}\right) \quad \text{4-32}$$

Therefore, the proposed $EI_e$ equation for steel and FRP reinforced CFFT columns, respectively, can be written as follow;

$$EI_{e-s} = \alpha_c E_c I_g + 0.8E_s I_s + \alpha_t E_t I_t \quad \text{4-33}$$

$$EI_{e-FRP} = \alpha_c E_c I_g + 0.7E_f I_f + \alpha_t E_t I_t \quad \text{4-34}$$

Note that, these two equations can be used at any load level. To test the accuracy of these two equations $EI_{e)\ proposed}$ will be compared to the theoretical stiffness data and the available experimental data. Figure 4-8 shows comparison between Equations 4-33 or 4-34 and the theoretical stiffness data $EI_{th}$ in the form of histograms. It was found that the mean value for the two equations with the theoretical data is nearly equal one with a coefficient of variation of

0.1 for both figures. This indicates the accuracy of the proposed equations for both steel and FRP reinforced CFFT columns. Thus, in accordance to these two equations and due to the presence of different applications for using unreinforced CFFT columns, the previous equations can be written as follows for the unreinforced CFFT column;

$$EI_{e-unreinforced} = \alpha_c E_c I_g + \alpha_t E_t I_t \quad 4\text{-}35$$

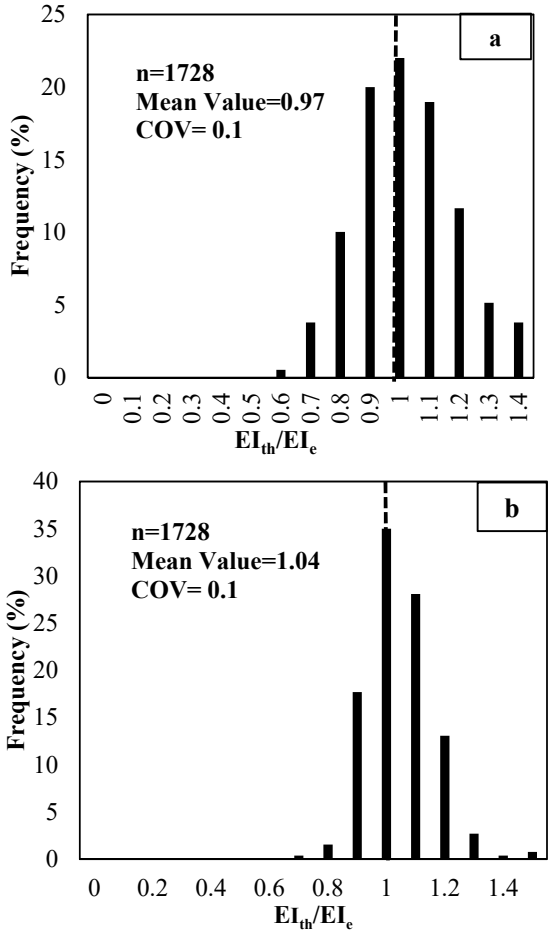


**Figure 4-8-** Comparison of proposed design equations with simulated theoretical data; (a) Steel reinforced CFFT columns (Eq. (4-33)); (b) CFRP reinforced CFFT columns (Eq. (4-34))

## 4.6 Comparison of Proposed $EI_e$ Equations and the Experimental Data at Service and Ultimate Loads

A comparative study was conducted using the present available experimental data (steel and CFRP reinforced CFFT columns) to ensure the accuracy of the proposed Equations 4-33 and 4-34. Since the proposed equations are applicable for all load levels of applied loads, both service and ultimate loads are considered in this study. The axial load capacity of reinforced CFFT columns was studied by Mohamed and Masmoudi (Mohamed and Masmoudi 2010), where they recommended that the design ultimate load for reinforced CFFT columns can be calculated as follows:

$$P_r = 0.57P_o \qquad 4\text{-}36$$

The ultimate load was conservatively defined as $0.6P_o$ for the tested specimens used in this study. The service load was taken as 0.7 of the ultimate load as recommended by ACI 318-14. Therefore, in this study the service load was defined as $0.4P_o$. For the purpose of comparison with the design equations, it is important to study the effective stiffness of the present experimental data at service and ultimate load levels. Thus, the relationship between the experimental ($EI_e$/ $EI_g$) and *e/D* for steel and CFRP CFFT columns at service and ultimate load levels were presented in Figures 4-9.a and 4-9.b. The mean values of ($EI_e$/ $EI_g$) for steel CFFT columns were 0.92 and 0.98 for service and ultimate load levels, respectively, while the mean values of ($EI_e$/ $EI_g$) for CFRP CFFT columns were 0.98 and 0.9 for service and ultimate load levels, respectively. It was clear that the stiffness of steel CFFT columns was higher than that

of CFRP CFFT columns, this refers to the fact that the young's modulus of steel is higher than that of CFRP.

Figure 4-10 shows comparison between ratio of experimental and proposed $EI_e$ with respect to eccentricity to diameter ratio $e/D$ for the steel and CFRP reinforced CFFT columns at service and ultimate loads. The results presented graphically by these figures are also tabulated in Table 4-3. The comparison at the service load level showed that the proposed equations had an excellent prediction compared to the experimental results. This was concluded by the means values of the ratios calculated by dividing the results from the experimental tests over those from the proposed equations. It was shown that the mean values at the service load levels were 1.15 and 1.16 for steel and CFRP reinforced CFFT columns, respectively. Similarly, the comparison at the ultimate load levels showed excellent agreement between the proposed equations and the experimental results with mean values equal 1.04 and 1.03 for steel and CFRP reinforced CFFT columns, respectively. Figure 4-11 shows another comparative study conducted using experimental data available in the literature (Khan et al. 2016, Khan et al. 2017). The experimental effective flexure stiffness of GFRP reinforced CFFT columns and CFRP reinforced CFFT columns were compared with the proposed effective flexure stiffness (Equations 4-33 and 4-34) at peak load. The comparison shows excellent agreement between the experimental results and proposed equation where the mean value at the peak load level was 1.15.

**Table 4-3–** Comparison of EIe for Steel and CFRP reinforced CFFT columns at service and ultimate loads

| Specimen ID | Experimental)$_{service}$ | | Experimental)$_{ultimate}$ | | Proposed Equations | | Ratio)$_{service}$ | Ratio)$_{ultimate}$ |
|---|---|---|---|---|---|---|---|---|
| | $EI_e/EI_g$ [1] | $P_s/P_o$ [2] | $EI_e/EI_g$ [3] | $P_u/P_o$ [4] | $(EI_e/EI_g)_s$ [5] | $(EI_e/EI_g)_u$ [6] | [7]=[1]/[5] | [8]=[3]/[6] |
| S-15 | 1.31 | 0.27 | 1.16 | 0.41 | 1.07 | 1 | 1.22 | 1.16 |
| S-30 | 1.26 | 0.2 | 1.01 | 0.3 | 1.06 | 1.02 | 1.19 | 0.99 |
| S-45 | 1.1 | 0.15 | 1 | 0.23 | 1.04 | 1.01 | 1.06 | 0.99 |
| S-60 | 0.81 | 0.12 | 0.73 | 0.18 | 0.73 | 0.7 | 1.11 | 1.03 |
| **Mean** | **0.92** | | **0.98** | | **0.98** | **0.94** | **1.15** | **1.04** |
| C-15 | ١.29 | 0.26 | 1.14 | 0.4 | 1.07 | 1.01 | 1.21 | 1.13 |
| C-30 | 1.22 | 0.21 | 1.01 | 0.32 | 1.05 | 1 | 1.16 | 1.01 |
| C-45 | 0.88 | 0.16 | 0.71 | 0.24 | 0.74 | 0.71 | 1.19 | 1 |
| C-60 | 0.76 | 0.13 | 0.69 | 0.19 | 0.72 | 0.7 | 1.06 | 0.99 |
| **Mean** | **1.04** | | **0.9** | | **0.9** | **0.87** | **1.16** | **1.03** |

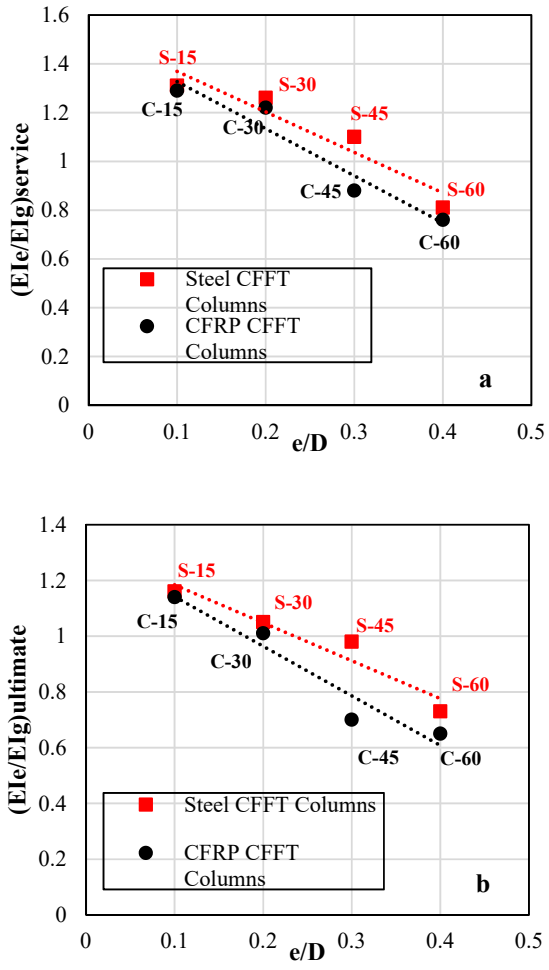


**Figure 4-9-** Flexure Stiffness of steel and CFRP reinforced CFFT columns as a function of eccentric ratio at: (a) service load; (b) ultimate load (Experimental results)

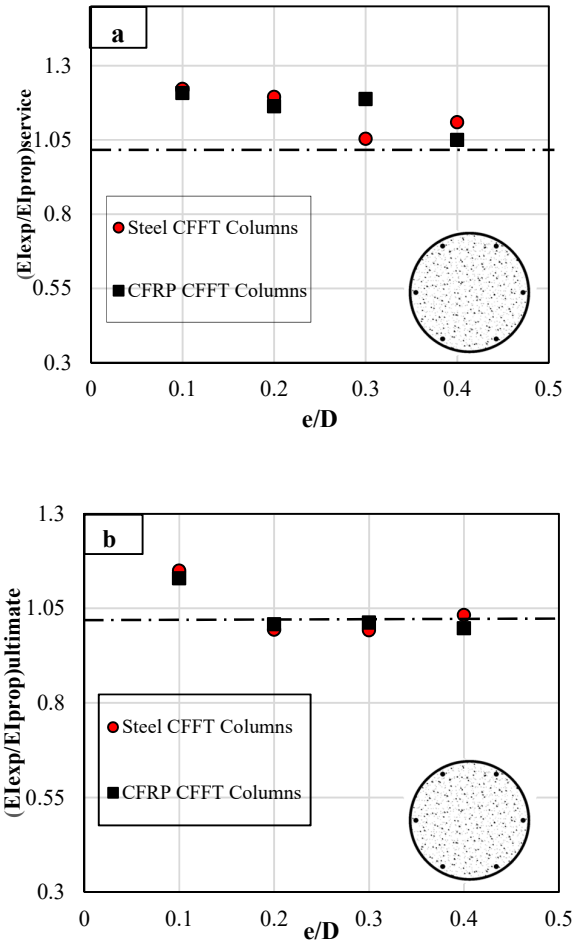


**Figure 4-10-** Comparison between ratio of experimental EIe and proposed EIe for steel and CFRP reinforced CFFT columns at: (a) service load; (b) ultimate load (Present Study)

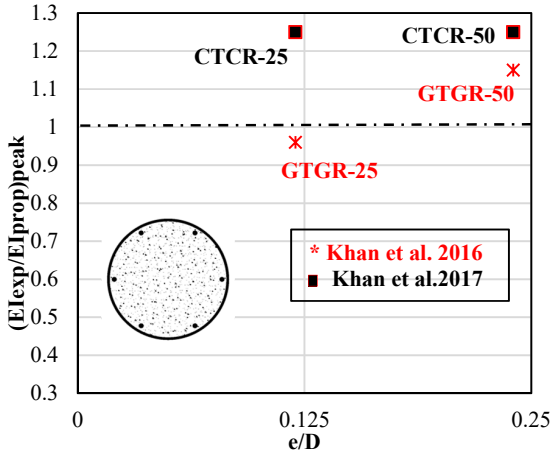


**Figure 4-11-** Comparison between ratio of experimental EIe and proposed EIe for GFRP and CFRP reinforced CFFT columns at peak load (Previous Studies)

## 4.7 Conclusions

This paper presents new design equations for the effective flexure stiffness of circular slender unreinforced and reinforced steel and FRP CFFT columns. The CFFT columns were subjected to short-term loads in a symmetrical single curvature bending. An experimental parametric study and a theoretical statistical simulation of the parameters that affect the flexure stiffness ($EI_e$) were conducted. The design equations take into consideration the variation in three parameters including; eccentricity to diameter ratio ($e/D$), slenderness ratio ($L/D$) and the axial load level ($P_u/P_o$), thus, the proposed equations are applicable for any axial load level including service and ultimate loads. Based on the results of this study, the following conclusions can be drawn:

1. The experimental effective stiffness results of steel and CFRP CFFT columns presented a clear evidence of the stiffness degradation over the load history. In addition, it was obvious that the steel CFFT specimens achieved higher stiffness than the CFRP CFFT specimens. This was attributed to their higher young's modulus than that of CFRP CFFT specimens.
2. The proposed design equations were developed using a simplified format to include all the parameters affecting the flexure stiffness of steel and FRP CFFT columns, respectively as follow;

$$EI_{e-s} = \alpha_c E_c I_g + \alpha_s E_s I_s + \alpha_t E_t I_t$$

$$EI_{e-FRP} = \alpha_c E_c I_g + \alpha_f E_f I_f + \alpha_t E_t I_t$$

where a multiple linear regression analysis was used to predict the coefficients of different variables included in the equations format. This type of analysis produced accurate estimation of the CFFT column stiffness equation.

3. Increasing the eccentricity and axial load ratios result in a reduction in the effective flexure stiffness ($EI_e$) of the slender CFFT column. Thus, a new stiffness reduction factor for concrete $\alpha_c$ was suggested, where $\alpha_c = 0.2\left(\frac{l}{D}\right) - \frac{e}{D}\left(\frac{0.5}{1+e/D}\right) - 0.4\left(\frac{P_u}{P_o}\right)$.
4. Stiffness reduction factors for reinforcing bars $\alpha_s = 0.8$ and $\alpha_f$=0.7 were proposed for steel and FRP reinforced CFFT columns, respectively.
5. The effectiveness of the confinement induced by the external FRP tube was taken into consideration in the formulation of the design equation where a new stiffness reduction factor for FRP tube $\alpha_t$ was proposed. $\alpha_t$ depends mainly on the strength-reinforcement ratio of FRP tube and concrete ($\beta$) and was formulated as ($\alpha_t = 0.6\beta + 0.9$).
6. The design equations were compared with the present experimental results and those available in the literature and proved to be reasonably accurate for practical engineering design applications.

# CHAPTER 5

# MODELLING OF BUCKLING INSTABILITY IN FRP REINFORCED CFFT COLUMNS

(***Construction and Building Materials Journal, 189 (2018), p. 473-487***.)

## 5.1 Introduction

Fibre reinforced polymers (FRPs) have, in the last two decades or so, become increasingly popular as materials for externally-bonded repair systems for deteriorated or under-strength reinforced concrete (RC) members. One application for which FRPs have shown significant promise, and have indeed been used in hundreds of field applications around the world, as external confining reinforcement for RC columns is the fibre reinforced polymers (FRP) tubes (Bisby et al. 2004). In recent years, some applications of concrete-filled FRP tubes (CFFTs) for different structural applications piles, columns, girders, bridge piers were accomplished. The fibre-reinforced polymers (FRP) tubes can play an important role in replacing transverse steel by providing ductility and strength for reinforced concrete columns (Mirmiran et al. 2001b, Mohamed and Masmoudi 2008; 2010, Toutanji and Safi 2002).

FRP bars are well known for their high tensile mechanical properties and its use in lieu of steel as reinforcing material in concrete is expected to extend the service life of constructed facilities because of better resistance to corrosion and higher damping properties than steel. FRP bars can also result in lower maintenance costs by eliminating corrosion induced damage. Furthermore, FRPs can non-destructively reveal their stress state and remaining life under service conditions (Wu 1990). Very few studies were conducted on the behavior of CFFT columns reinforced with FRP bars under uniaxial compression loads where most of the

available studies were oriented to steel reinforced columns CFFT. Moreover, the instability of such columns has not been studied yet.

The significant increase in the ultimate capacity of concrete columns proved that one of the critical parameters that control the mode of failure of such columns under pure axial compression is the slenderness ratio (Mirmiran and Shahawy 1997). Mohamed et al. (2010) conducted analytical nonlinear stability analysis beside an experimental investigation on the behavior of steel reinforced CFFT columns. They investigated the effect of three parameters and the parameters' interaction on the buckling behavior namely, the FRP tube thickness, concrete compressive strength, and slenderness ratio. The test results indicated that increasing the slenderness ratio from 8 to 20 the load carrying capacities of the CFFT specimens decreased by 30%. Also, the analytical study indicated that a slenderness value of 12 can be used as a limit value for design purposes for steel reinforced CFFT columns. Mirmiran et al. 2001a developed a rational method for the analysis of slender RC columns reinforced with FRP bars. They recommended that the slenderness ratio for columns reinforced with FRP bars, should be reduced from the current limits 22 (ACI 318-14) to 17, for columns bent in single curvature. Design of the slenderness ratio to avoid buckling of FRP reinforced CFFT columns has not been investigated yet. Moreover, experimental and theoretical investigations have to be conducted to understand the buckling instability behavior of FRP reinforced CFFT columns and to correlate their critical buckling loads to the material and geometric properties of the confining FRP tubes.

In this chapter a theoretical investigation was conducted to understand the instability buckling behavior of FRP reinforced CFFT columns where the accuracy of existing critical buckling load formulas were verified and then a threshold for the slenderness limit to prevent buckling instability failure mode for FRP-reinforced CFFT columns was proposed.

## 5.2 Overview of Past Experimental Work

Mohamed and Masmoudi (2010) conducted an experimental work to investigate the slenderness effects on behavior of Carbon FRP (CFRP) -Reinforced CFFT columns under pure

compression load using a 6,000 kN capacity FORNEY machine, where the CFFT columns were setup vertically at the centre of loading plates of the machine. Table 5-1 summarizes the different configurations and details of the test specimens.

The test specimens were identified by codes listed in the second column of Table 5-1. The first number presents the slenderness ratio of the specimens. The identification C were used to present the type of internal reinforcements as CFRP bars. The second number shows the height of the specimen by (cm), whereas, the height is ranged between 610 mm to 1520 mm. Groups No. 1 presents CFFT columns that reinforced internally w six CFRP bars (#3), with a longitudinal reinforcement ratio of 3.30%. All the CFFT specimens were cast using the same type of the FRP tube, with confinement reinforcement ratio (4t/D) equal to 7.0%, where (t and D) are respectively the thickness and the internal diameter of the tubes. The slenderness ratios of the specimens are varied from 8 to 20.

**Table 5-1—** Test matrix, specimens details and test results (Mohamed and Masmoudi,2010)

| Group No. | ID | $l$ (mm) | $kl/r$ | Internal reinforcement | $P_y$ (kN) | $P_u$ (kN) | $f'_{cc}$ (MPa) | $f'_{cc}/f'_c$ |
|---|---|---|---|---|---|---|---|---|
| 1 | 8-C-60 | 610 | 8 | CFRP bars 6 - #3 | -- | 1432 | 67.04 | 2.23 |
| | 12-C-90 | 912 | 12 | | -- | 1343 | 62.02 | 2.07 |
| | 16-C-120 | 1216 | 16 | | -- | 1138 | 50.44 | 1.68 |
| | 20-C-150 | 1520 | 20 | | -- | 1127 | 49.82 | 1.66 |

They observed that the FRP tube rupture and/or column instability were the dominant failure mode for the CFFT specimens depending on the slenderness ratio, where for the columns with a slenderness ratio 8 and 12 ($l$=610 mm and $l$= 912 mm, the failure modes were a combination of rupture of the confining FRP tubes and local buckling of internal reinforcing bars at the

column mid-height. However, the columns with slenderness ratios started to buckle at load level that was slightly less than the failure load of the column. Thus, they concluded that the ultimate failure of each column is usually caused by the inelastic behavior of the different component of CFFT columns.

## 5.3 Theoretical Investigation of Instability Buckling Behavior and Slenderness Effect of FRP Reinforced CFFT Columns

The inelastic behavior of the CFFT columns may sometimes affect the buckling behavior of the column taking into consideration the column geometry especially slenderness. When the column is not too slender, a significant reduction in the maximum load appeared at a relatively small deflections, therefore, it is important to understand quiet well the inelastic buckling and take it into consideration during design. In this section the critical slenderness ratio of the FRP reinforced CFFT columns is predicted. The theoretical analysis considers the confinement in the hoop direction of the tube as the fibre orientations were mainly in that direction (±60 degree with respect to the longitudinal axis). An elastoplastic response is considered for the CFRP reinforced CFFT columns distinguished by a softening limit corresponding to the yielding limit in steel reinforced CFFT columns. The elastoplastic behavior of the column has two important characteristics: (1) the tangent modulus $E_t$ for continued loading (i.e. the hardening region) which is smaller than the initial elastic modulus $E_o$, and (2) the unloading modulus $E_u$ in which it is assumed that no damage occurred during the axial loading, thus, $E_u = E_o$.

To ensure the accuracy of the theoretical analysis, the confinement effect of the tube on the behavior of concrete has to be precisely considered. Lam and Teng (2003) have introduced a model to represent the stress-strain curve for confined concrete. This model was verified by Ozbaklagu 2013 and proved to be one of the most accurate models in producing unified stress-strain model for FRP confined concrete. They assumed that the stress-strain curve was

consisted of two portions, a parabolic first portion that is distinguished with a smooth transition to the linear second portion. The initial slope of the parabolic portion is the same as the elastic modulus of the unconfined concrete and the linear second portion ends at a point where both the compressive strength and the ultimate axial strain of confined concrete are reached. Figure 5-1 shows the different young's modulus values ($E_t, E_u$) and the plastic limit stress $f_{co}$ (softening limit in the CFRP reinforced CFFT columns) which was assumed to be in the transition point between the parabolic and the linear portions. Moreover, $E_t$ was assumed to be equal $E_2$ in the hardening region of the stress strain curve as follow;

$$E_t = E_2 = \frac{f'_{cc} - f_{co}}{\varepsilon_{cu}} \qquad 5\text{-}1$$

where $f_{cc}'$ is the confined concrete stress and $\varepsilon_{cu}$ is the ultimate strain, these terms are calculated as follow;

$$f_{co} = 0.872 f_c' + 0.371 f_{l,a} + 6.258 \qquad 5\text{-}2$$

where $f_c'$ is the unconfined concrete strength and $f_{l,a}$ is the lateral confining pressure of GFRP and is equal $\frac{2 f_f t_f}{D}$ $f_f$ s the tensile strength of GFRP in the hoop direction, $t_f$ is the total thickness of GFRP tube.

The maximum confined concrete strength is given by:

$$f'_{cc} = f'_c + 3.3 f_{l,a} \qquad 5\text{-}3$$

The corresponding ultimate confined concrete strain ($\varepsilon_{cu}$) can be determined by:

$$\varepsilon_{cu} = \varepsilon_{co}\left(1.75 + 12\left(f_{l,a} \middle/ f'_c\right)\left(\varepsilon_{fe} \middle/ \varepsilon_{co}\right)^{0.45}\right) \qquad 5\text{-}4$$

$\varepsilon_{co}$ is the unconfined concrete strain and is taken = 0.003 (ACI318-14)

$\varepsilon_{fe}$ is the effective strain level in the FRP at failure, according to ACI 440 procedures $\varepsilon_{fe}$ should not be taken more than 0.004 in members subjected to combined axial compression and bending moment to ensure shear integrity of the confined concrete.

According to ACI440.2R-08 $\varepsilon_{cu}$ should not exceed a value of 0.01 to prevent excessive cracking and the resulting loss of concrete integrity.

In addition, the concrete initial tangent young's modulus can be expressed in SI units as;

$$E_c = 3950\sqrt{f_c'} \qquad 5\text{-}5$$

This equation has been modified to take into consideration the effect of the internal CFRP bars on the initial young's modulus to be used in the stability analysis in the following section , thus , the equivalent cross-sectional young's modulus equation is assumed as follows;

$$E_o = E_c[1+\rho_f(n-1)] \quad \text{(MPa)} \quad 5\text{-}6$$

where $\rho_f$ is the CFRP reinforcement ratio, $n$ donates the CFRP reinforcement modular ratio that is computed as $E_{fb}/E_c$ where $E_{fb}$ is the CFRP young's modulus.

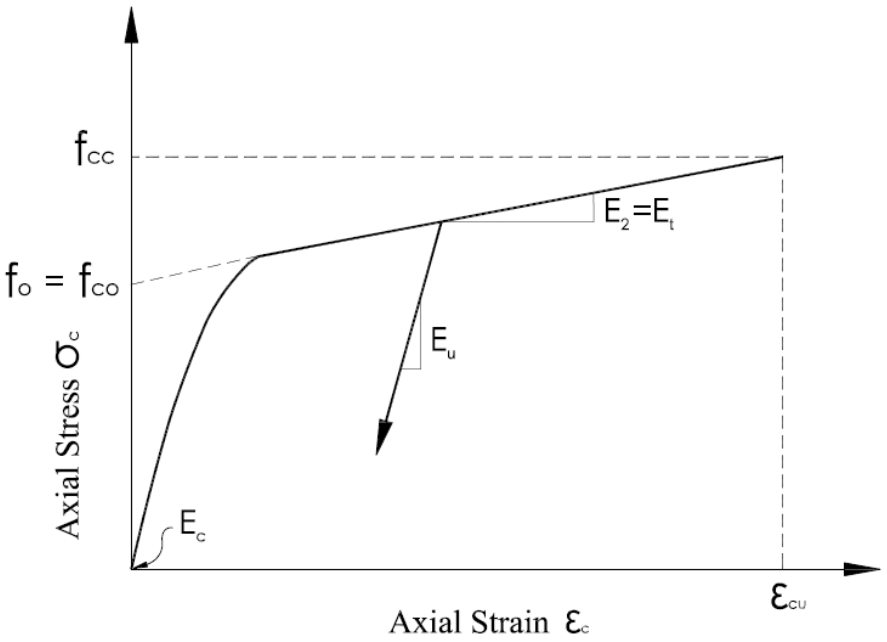


**Figure 5-1–** Stress-Strain curve for FRP confined concrete (Bazant and Cedolin, 1991)

### 5.3.1 Reduced and Tangent Modulus Loads

In this study, the investigated CFFT columns are considered not too short and not too slender, therefore, the inelastic buckling is considered relevant for the design purpose. Two formulas namely the tangent modulus load $P_t$ and the reduced modulus load $P_r$ are considered important characteristics in the theory of the inelastic columns (Bazant and Cedolin, 1991). These values give nearly an upper and lower bound for the critical buckling load (maximum applied axial load, $P_{max}$), where the reduced modulus load $P_r$ is considered the first buckling load and the tangent modulus load $P_t$ is considered the second buckling load (i.e. $P_t \leq P_{max} \leq P_r$). The maximum critical buckling load $P_{max}$ was illustrated by Bazant and Cedolin 1991 according to the type of loading, either under load or displacement control as follows;

$$P_{\max} = \begin{cases} \dfrac{2\xi}{\xi+1} P_t & \text{Under load control} \\ \dfrac{1+\xi}{2} P_t & \text{Under displacement} \end{cases} \qquad 5\text{-}7$$

where $\xi = \dfrac{E_u}{E_t}$.

Figure 5-2 shows an overview of fixed-fixed columns undergoes buckling under axial compressive load. To understand the buckling process, different assumptions must be considered as follow; (1) the plane section remains plane and normal to the deflected centerline of the column; (2) the position of the neutral axis of the cross-section is assumed at which the axial strain doesn't change. At the start of the buckling, the concave face of the column which is the face towards the center of curvature undergoes loading, while the convex face undergoes unloading, bilinear stress distribution is caused as shown in Figure 5-2 where the incremental stresses according to the plane cross section assumption are, $-E_u \, c/\rho$ and $-E_t \, (D_o - c)/\rho$,

($1/\rho$ = curvature due to buckling).

According to this case, the buckling load is assumed to remain constant. Therefore, the first critical buckling load ($P_r$, reduced load) is calculated as follows;

$$\mathrm{P_r} = \frac{\pi^2 E_r I}{(kl)^2} \quad \text{(kN)} \quad 5\text{-}8$$

$E_r$ is known as the reduced modulus, and assumed to be a function of both incremental moduli for loading and unloading ($E_t$, $E_u$) as (Bazant and Cedolin 1991);

$$E_r = \left[ 0.5 \left( 1/\sqrt{E_u} + 1/\sqrt{E_t} \right) \right]^{-2} \qquad 5\text{-}9$$

In contrary with the above assumption, in normal practical situation, the column doesn't buckle at a constant load, subsequently, there is no unloading anywhere in the cross section. In fact the column may start to buckle at a load that may lie significantly below the reduced modulus buckling load. Thus, at the beginning of buckling for which the normal stress distribution is still uniform, the incremental modulus may be assumed equal to the tangent modulus $E_t$ for all points of the cross section, and the tangent modulus load can be written as follows;

$$P_t = \frac{\pi^2 E_t I}{(kl)^2} \qquad 5\text{-}10$$

In brief, the column is considered in a stable state, when the deflection occurred at a load level greater than the tangent modulus load and less than the reduced modulus load , thus , the applied axial load will subsequently increase with the increase of the lateral deformation until reaching the critical load which lies somewhere between $P_t$ and $P_r$. This agreed well with what was mentioned in the experimental work by Moahmed and Masmoudi 2010 and taking Specimen 16-C-120 as an example. For this particular column the tangent buckling load is 1005 kN and the reduced buckling load is 2550 kN. The critical buckling failure load of this particular specimen is monitored as 1138 kN, which is 12% larger than $P_t$ and 55% less then $P_r$ ($P_t < P_{\max} < P_r$).

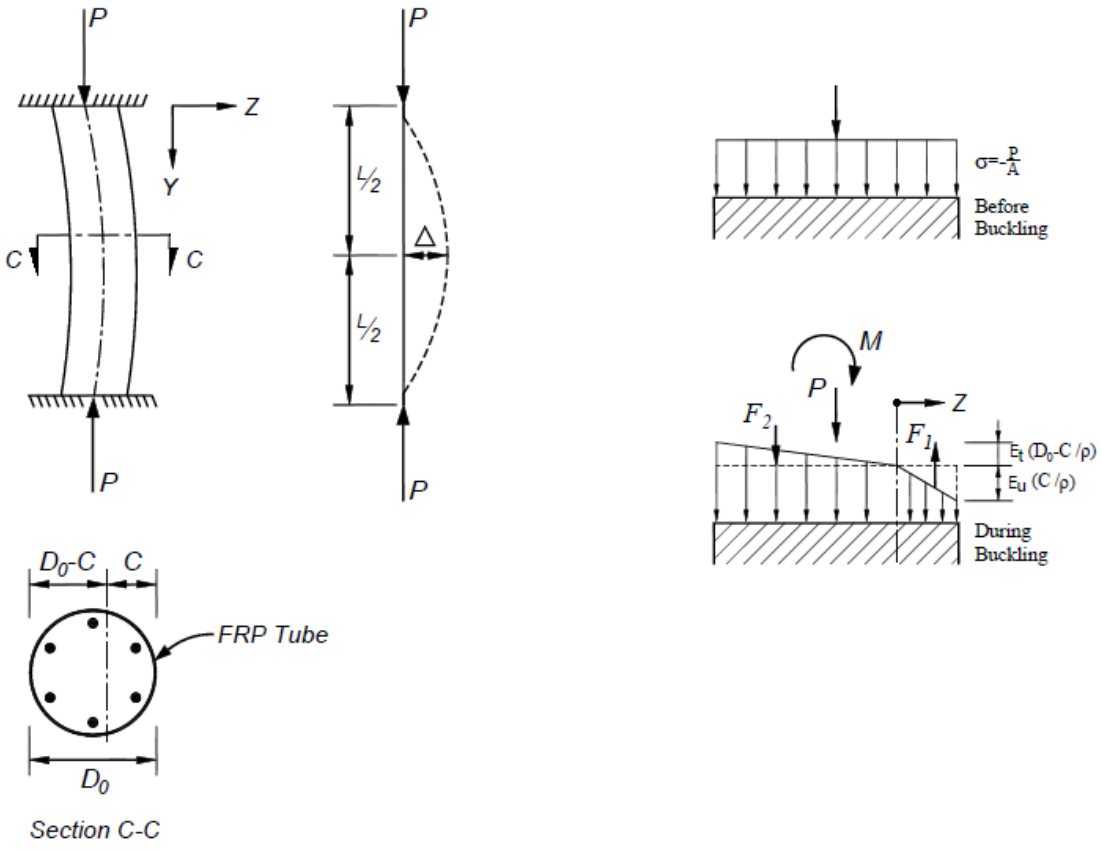


**Figure 5-2-** Overview of fixed -fixed CFFT column under axial compressive load and stress distribution before buckling and during buckling

## 5.4 Comparison between Experimental Values and Design Equations

Equations 5-8, 5-9 and 5-11 are compared to the experimental values as shown in Figure 5-3 where a relation between the critical stress ratio $\sigma_{cr}/E_t$ and the slenderness ratio $\lambda$ . It can be observed that specimens with slenderness ratios 8 and 12, the failure load ( $P_u$ ) is less than the Euler tangent load. This is due to the failure mechanism of these specimens which occurred

due to rupture of FRP tube (i.e. $P_u < P_t < P_{max}$). For specimens with higher slenderness ratios (16 and 20), the columns started to buckle at load level nearly corresponding to $P_t$, thus the critical buckling load (Eq. 5-8) occurred at a higher load level. In brief, it can concluded that, although the tangent Euler load can be used as a safe limit for the design ,it gives very conservative values, thus, the critical buckling load is considered more accurate in the instability analysis for FRP reinforced CFFT columns than the Euler tangent load.

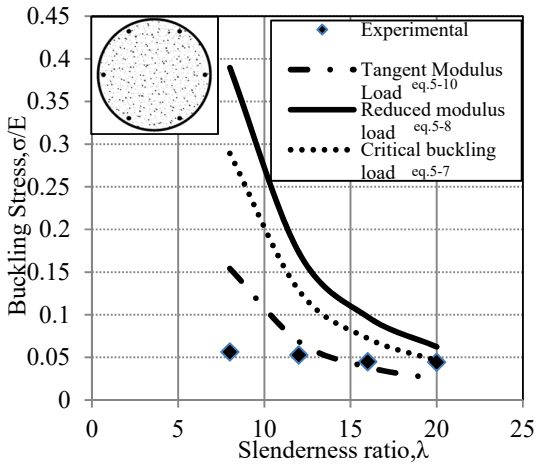


**Figure 5-3-** Experimental values versus design equations (in terms of critical buckling stress)

## 5.5 FRP CFFT Columns Strength Curve

In stability analysis, it is convenient to describe the buckling in terms of the columns Strength curve, which explains the dependence of the critical stress ratio on the slenderness ratio (kl/r). To construct this curve (Figure 5-4), the tangent Euler load and the critical buckling load are represented schematically as relation with the slenderness ratio, where the load based on the tangent modulus can be conservatively used as a safe limit for design. As it is observed from the experimental that the short FRP CFFT columns failure mechanism is controlled by rupture of FRP tube, in other word, maximum confined concrete strength ($f'_{cc}$) is reached (Eq. 5-4). This equation represent the horizontal limit for the ultimate strength of the FRP CFFT columns as shown in Figure 5-4. The critical slenderness ratio ($\lambda_{cr}$) is defined as the maximum

slenderness ratio corresponding to the ultimate strength of the column (intersection of the horizontal line with the design curve in Figure 5-4. Thus, it is clear that the critical slenderness ratio of CFFT columns depends on the properties of concrete and tube, and on the buckling load formulas which are the tangent Euler formula or the critical buckling load. An equation could be suggested for $\lambda_{cr}$ as follow;

$$\lambda_{cr} = \pi \sqrt{\frac{E_t}{f'_{cc}}} \sqrt{\frac{E_o}{E_o + E_t}} \qquad 5\text{-}11$$

By evaluating the experimental and theoretical results, it can be concluded that a slenderness limit of 14 can be considered as a safe value for design of FRP CFFT columns, this value is slightly higher than the value suggested by Mohamed et al. (2010) for steel reinforced CFFT columns, where they suggested a limit value of 12 for the slenderness limit.

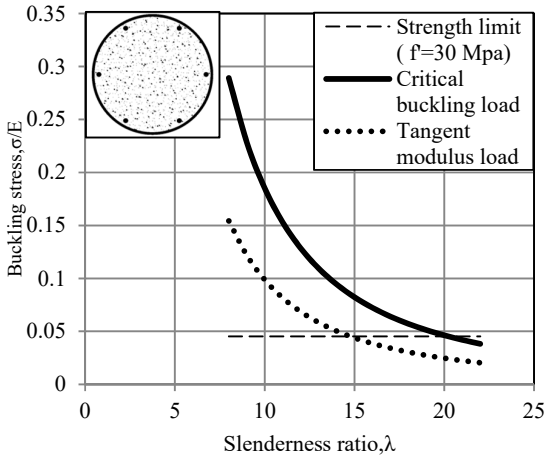


**Figure 5-4-** Design curves for FRP reinforced CFFT columns

## 5.6 Parametric Study

A parametric investigation was carried out to study the effect of different parameters on the critical slenderness ratio of FRP reinforced CFFT columns. These parameters could be divided into three categories as follows; (1) parameters related to concrete; (2) parameters related to

GRP tube; and (3) parameters related to the FRP bars. Three different tubes with different combination of tube parameters shown in Table 5-2 were used in this parametric study. The main parameter considered for the tube is the tube hoop stiffness which ranged from 50 to 250 (kN/mm). For concrete the main parameter considered is the concrete compressive strength $f_c'$ with a range between 10 MPa and 60 MPa. Moreover, it is important to consider the wide variation of the mechanical properties of the FRP bars. CFRP bars is the type of reinforcement considered in this study. According to ACI 440.1R-15 the tensile young's modulus of CFRP bar ranged from 120 to 580 GPa, these values were incorporated in the form of FRP modular ratio ($n = E_{fb} / E_c$) to study its effect on the slenderness limit. Thus, $n$was assumed between 4 and 20 to cover the range of young's modulus of CFRP bar. The investigated parameters also included different longitudinal reinforcement ratios (0.5%, 1%, 2%, 3%, 4%, 5%, and 6%) to respect the range provided by codes where the Canadian standards and guidelines (CSA/ CAN S806-12 and A23.3-14 allow the use of longitudinal reinforcement ratio smaller than 1%, provided that the bar area is not less than 0.005 times the gross area of the section. Figures 5-5 through 5-8 show different relations resulted from this investigation. Increasing the concrete compressive strength from 10 MPa to 60 MPa increases the critical slenderness by more than 40 % for different tube types. While increasing the hoop stiffness of FRP tube from 50 to 250 kN/mm, decreases the critical slenderness by nearly 30% for different concrete compressive strengths. In addition, it is obvious that the mechanical properties of the CFRP bars and their reinforcement ratio have insignificant influence on the critical slenderness of FRP reinforced CFFT columns.

**Table 5-2—** Properties of the tubes used in the parametric study

| **Properties** | **Tube I** | **Tube II** | **Tube III** |
|---|---|---|---|
| Diameter (mm) | 152 | 152 | 320 |
| Thickness (mm) | 2.65 | 6.4 | 4 |
| D/t | 58 | 24 | 80 |
| Stacking Sequence | $[\pm 60°]_3$ | $[\pm 65_3, \pm 45, \pm 65_3]$ | [88/+3/–88/–88/+3/ –88/+3/–88/+3/–88] |
| Young's Modulus-Hoop (MPa) | 20690 | 23630 | 21000 |
| Young's Modulus-Longitudinal (MPa) | 8785 | 9270 | 18000 |
| Ultimate Strength-hoop (MPa) | 345 | 390 | 401 |
| Ultimate Strength-Longitudinal (MPa) | 57.9 | 60.15 | 348 |
| $E_f t_f$ (kN/mm) | 55 | 151 | 84 |

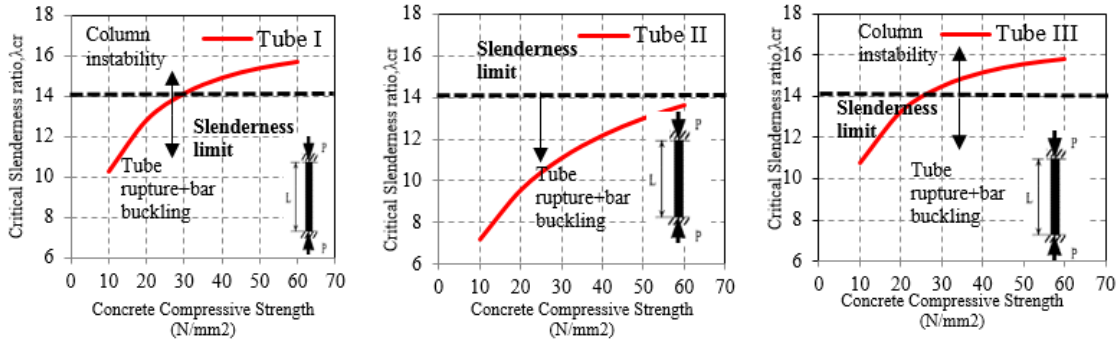


**Figure 5-5-** Effect of concrete compressive strength on critical slenderness ratio

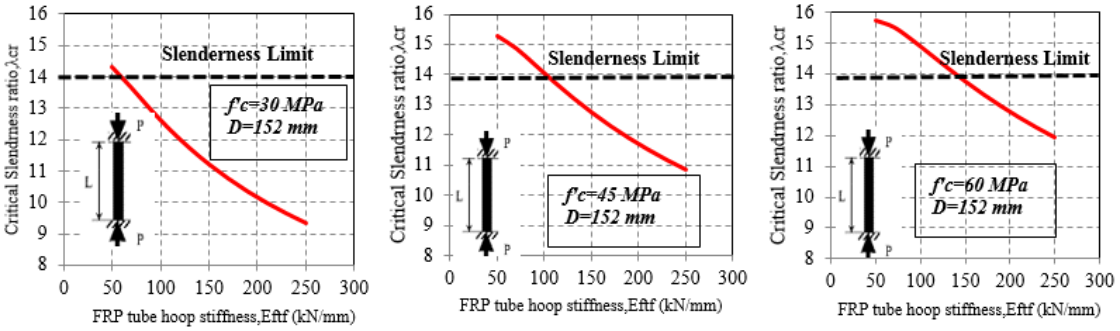


**Figure 5-6-** Effect of FRP hoop stiffness on critical slenderness ratio

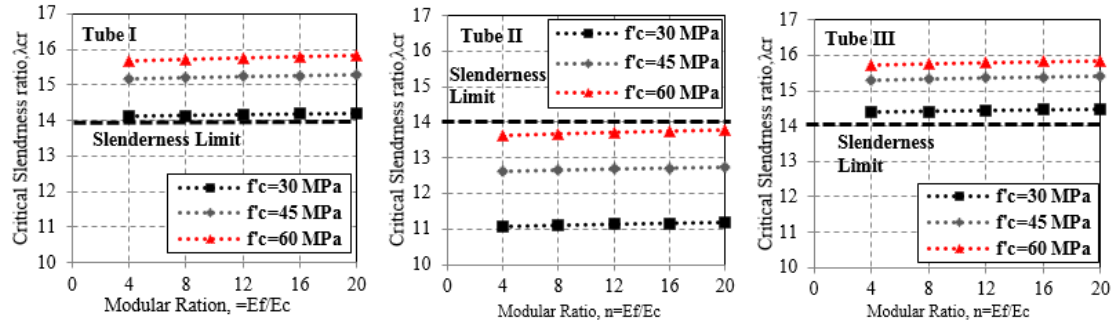


**Figure 5-7** -Effect of FRP bar modular ratio on critical slenderness ratio

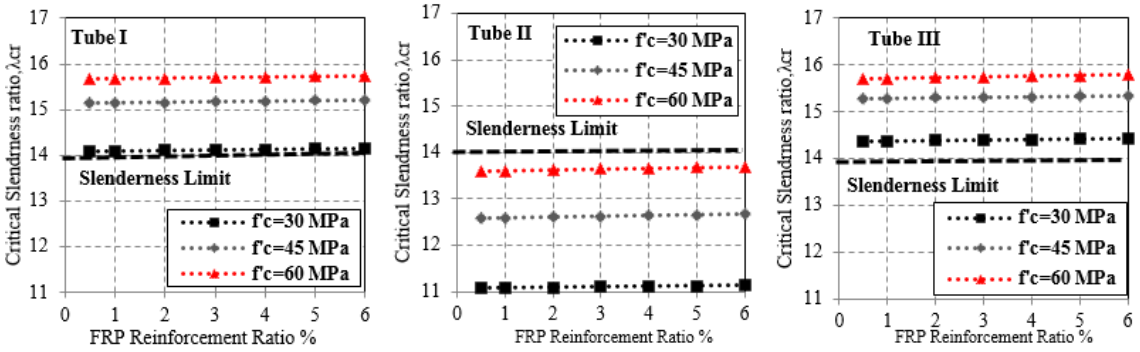


**Figure 5-8-** Effect of FRP bar reinforcement ratio on critical slenderness ratio

## 5.7 Conclusions

The main findings of this investigation can be summarized as follows:

1. Although, it is recommended by several researchers to use Euler tangent load to control the instability load of CFFT columns, this research showed that using the critical buckling load is more reliable for the instability analysis for FRP reinforced CFFT columns.
2. A design equation was introduced to calculate the slenderness limit for FRP CFFT columns, in addition, a slenderness limit of 14 was introduced as a safe value for design purpose.
3. The critical slenderness is affected by the properties of both concrete and tube, including the concrete compressive strength and the tube hoop stiffness.
4. The mechanical properties of FRP bars along with its reinforcement ratio have an insignificant effect on the buckling behavior of FRP reinforced CFFT tube.

# CHAPTER 6

# NONLINEAR FINITE ELEMENT ANALYSIS OF SHORT AND LONG REINFORCED CONCRETE COLUMNS CONFINED WITH GFRP TUBES

(Reference: **Reinforced Plastics and Composites,** V.13:pp.972 – 987, 2017)

## Abstract

Discrete three dimensional nonlinear finite element model is presented to understand the uniaxial behavior of concrete filled-Fibre Reinforced Polymer (FRP) tubes (CFFTs). A stress–strain relationship for confined concrete was used to model the concrete, Glass-FRP required Hashin's damage parameters and steel bars were modelled based on classic metal plasticity model. A comparison between experimental results found in the literature and the finite element model was conducted regarding the load deflection curves and the failure pattern of different test specimens. The model was found to be efficient in capturing the loads and deformations of slender CFFT columns. It was then used in a parametric study to understand the effect of different parameters including (Fibre orientation, number of layers of (GFRP) and steel reinforcement ratio) on the behavior of CFFT under axial compressive loading. It was observed that the behavior of the columns was greatly affected by the investigated analysis parameters.

**Keywords:** Finite Element Analysis; concrete; circular column; FRP Tube; Modelling.

## 6.1 Introduction

The use of confined concrete columns has increased widely in the last two decades especially in the structures designed to resist seismic loading due to the significant enhancement in ductility and strength of the confined concrete (Mohamed et al. 2012). Jackets and tubes made of fibre reinforced polymers (FRP) are among the most popular technique to achieve excellent lateral confinement to concrete in columns due to their distinct characteristics such as light weight, high strength, excellent corrosion resistance, good impact and fatigue properties, flexibility in design, and ease of fabrication. Several studies have been carried out to understand the compressive behavior of CFFT (Hong et al.2004, Fam et al.2005, Li G.2006, Ozbakkaloglu et al.2008,Mohamed et al.2010, Ozabkkaloglu et al. 2013.a, Vincent et al. 2014), these studies have demonstrated the ability of CFFTs to develop high inelastic deformation capacities which makes them an attractive choice in construction of high performed columns (Ozbakkaloglu et al.2006).It is well understood that the column parameters affect the axial compressive behavior of CFFTs columns , these include the amount and properties of FRP used to manufacture them size of CFFTs columns and concrete strength. Therefore, it is necessary to be able to model the effect of different column parameters on the behavior of CFFTs columns under concentric axial compression loads. A recent study carried out by Ozbakkaloglu (2013.b) demonstrated that for circular CFFTs, specimen size has only a slight influence on the compressive behavior of CFFTs with the ultimate axial strength and strain only slightly influenced by the size of CFFTs and in opposite it is significantly influenced by the amount and the characteristics of fibres used in their FRP tubes. As FRP confinement significantly affect the stress-strain behavior of concrete in CFFTs, an extensive comprehensive review was undertaken on large number of models to predict the stress–strain behavior of FRP-confined concrete under axial compression. (e.g., Mirmiran et al. 1997, Samman et al. 1998, De Lorenzis and Tepfers 2003; Lam and Teng 2003 , Bisby et al. 2005;Yu and Teng 2011 and Yazici and Hadi 2012). This review study revealed more than 100 stress strain models of FRP confined concrete which can classified into two main categories: (1) Design oriented models presented in closed-form expressions and (2) Analysis oriented models which predict stress-strain curves by an incremental procedure. The use of the design oriented models particularly advantageous in predicting the ultimate strength enhancement

and strain enhancement ratios (Ozbakkaloglu et al.2013.c). The proper use of the CFFT system requires the accurate prediction of the improved performance of the FRP-confined reinforced concrete (RC) columns based on the specific geometry, material properties, and amount of FRP utilized. In modern structural engineering research, finite element (FE) analyses are essential for interpretations to the experimental results and providing insights into structural behavior of FRP-confined RC columns. Despite the popularity of this research area, relatively few research studies on FE modelling of confined concrete have been reported to date (Mirmiran et al. 2000, Hu et al.2003, Montoya et al.2004, Chakrabarti et al. 2008, Son and Fam, 2008, Yu el al. 2010, Jiang and wu 2012, Hu et al. 2014, Talaeitaba et al. 2015, Lim et al. 2016) with very few focuses on the behavior of CFFTs (Hu et al.2003, Son and fam 2008). A recent study by (Ozbakkaloglu al. 2016) has employed the finite element modelling using ABAQUS for the prediction of (1) axial stress-axial strain, (2) lateral strain-axial strain, (3) axial stress volumetric strain, (4) plastic volumetric strain-axial plastic strain, and (5) plastic dilation angle-axial plastic strain relations. Comparisons with experimental results show that the predictions of the proposed model based on damage plasticity model of concrete are in close agreement with the test results of FRP-confined normal and high strength concrete .Nonlinear FE modelling can predict crack initiation and propagation, deflections, possible failure mechanisms and provide explanations to experimental observations, where the test measurements are impossible (Masmoudi et al. 2008). However, complexity of the non-linear FE models is inherent due to various theories used in material modelling. This complexity appears mainly in modelling RC members as constitutive models for steel bars and FRP jackets/tubes are well established. The key to the success of such FE models lies in the accuracy of the constitutive model for concrete (Teng et al. 2015).

The work described herein is on modelling the tested short and slender CFFT columns (Mohamed et al. 2010) using 3D finite element analysis using ABAQUS(R) version 6.11.1. Confined concrete columns are modelled under axial compressive loads and employs one of the most accurate design oriented models proposed by (Lam et al. 2003) which was originally modified from model adopted by (Richard et al. 1928).

The objectives of the present work are to numerically understand the failure mechanisms of concrete filled FRP tube columns under axial compressive load in light to the experimental results. It accounts for cracking and plasticity of concrete and include the effect of material and geometric nonlinearities. . It was then used in a parametric study to examine the effect of different key parameters on the ultimate capacity and failure mode of CFFTs, namely, number of FRP layers, fibre orientation and reinforcement ratio.

## 6.2 Numerical Modelling and Simulation

The numerical models adopted here are based on an experimental program carried out at the University of Sherbrooke, Canada (Mohamed et al. 2010). Four columns are selected for the verification of the finite element model. The details of these columns, test matrix and results are shown in Table 6-1. CFFT columns having lengths of 610, 914, 1,216, and 1,524 mm are tested under uniaxial compression loads to investigate the influence of the slenderness ratio (kl/r) on the critical buckling load and the ultimate load capacity ($P_u$) of such columns; where k is column effective length factor (equal 0.5 in our analysis: fixed-fixed columns); l is length of the specimen and r is the radius of gyration of cross section. Further details on test columns can be found in (Mohamed et al. 2010).

**Table 6-1-**Experimental Test Matrix and Results (Mohamed et al. 2010)

| ID | *Column Length* (mm) | *kl/r* | Concrete Compressive (MPa) | FRP Tube | | Internal Reinforcement | Yield Load, $P_y$ (kN) | Ultimate Load, $P_u$ (kN) |
|---|---|---|---|---|---|---|---|---|
| | | | | Materials | Layers | | | |
| 60IA | 610 | 8 | 30 | GFRP | 6 | 6-10M | 890 | 1652 |
| 90IA | 912 | 12 | 30 | GFRP | 6 | | 935 | 1454 |
| 120IA | 1216 | 16 | 30 | GFRP | 6 | | 996 | 1202 |
| 150IA | 1520 | 20 | 30 | GFRP | 6 | | 1086 | 1127 |

### 6.2.1 Modelling Approach

While the quasi-static implicit finite element solver can be used to model the present problem, difficulties with convergence and large number of iterations required had given the dynamic explicit solver the advantage. In such dynamic explicit solver, the equations of motion for the body are integrated using the explicit central-difference integration rule together with the use of lumped element mass matrices which is the key to the computational efficiency of the explicit procedure that allowed the inversion of the mass matrix that is used in the computation for the accelerations at the beginning of the increment. Moreover, the explicit procedure requires no iterations and no tangent stiffness matrix. The integration process is conducted using small time increments. The minimum time increment, i.e. stable time increment $\Delta t$, is determined based on the minimum element length, $L_e$, and the dilatation wave speed of the material, $C_d$, and is defined as $\Delta t = L_e/C_d$. The default time incrimination scheme in many commercial software, such as (ABAQUS/Explicit 2008) which is adopted here, is fully automatic and requires no user intervention. The explicit solver allows for solving high nonlinear problems involving both material and geometrical nonlinearities along with sophisticated contacts, damage and failure. However, inertia effects can be presented and will affect the obtained results. Several approaches can be used to minimize these inertia effects such as the use of smooth loading step and least one order of magnitude less than the strain energy as shown in Figure 6-1 for specimen 150IA.

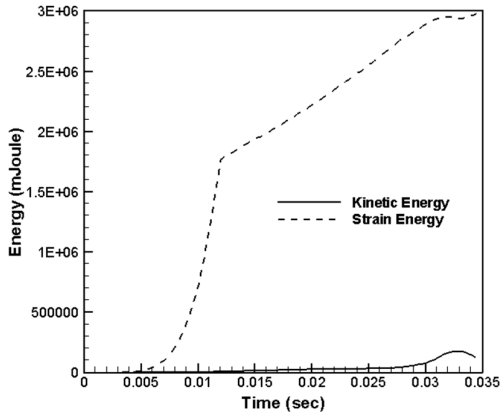


**Figure 6-1**-Kinematic vs. Strain energy for specimen 150IA

## 6.2.2 Materials Properties and Constitutive Models

### 6.2.2.1 Modelling of Confined Concrete

The model developed by (Lam and Teng 2003) model for the confined concrete is adopted in this study where they assumed that the stress–strain curve consists of two parts: the first is a parabolic section and the second is a straight line. The slope of the parabola at $\varepsilon_c$ =0 (initial slope) is the same as the elastic modulus of unconfined concrete $E_c$ and the nonlinear part of the first portion is affected to some extent by the presence of an FRP jacket. The parabolic first portion joins the linear second portion smoothly (i.e. there is no change in slope between the two portions where they join) and the linear second portion ends at a point where both the compressive strength and the ultimate axial strain of confined concrete are reached.

Figure 6-2 shows schematically the compressive stress–strain curves of confined concrete, where $f'_c$ is the unconfined concrete cylinder compressive strength, whose value is equal to 0.8 $f_{cu}$ and $f_{cu}$ is the unconfined concrete cube compressive strength. The corresponding unconfined strain ($\varepsilon_{co}$) is assumed as 0.002 as recommended by (ACI 318-14) and Euro code 2 (ENV-1992). The confined concrete compressive strength ($f'_{cc}$) and the corresponding confined strain ($\varepsilon_{cu}$) can be determined by Eqs. (1) and (2), respectively which were originally proposed by (Richart et al. 1928) and modified by (Lam et al.2003).

$$f'_{cc} = f'_c + 3.3 f_{l,a} \quad 6\text{-}1$$

$$\varepsilon_{cu} = \varepsilon_{co}\left(1.75 + 12\left(f_{l,a}/f'_c\right)\left(\varepsilon_{fe}/\varepsilon_{co}\right)^{0.45}\right) \quad 6\text{-}2$$

where $f_{l,a}$ is the lateral confining pressure of GFRP; $\frac{2 f_f t_f}{D}$; $f_f$ is the tensile strength of GFRP in the hoop direction which equals 345 MPa, $t_f$ is the total thickness of GFRP tube and equals 2.65 mm, $\varepsilon_{h,rup}$ is the hoop strain at FRP rupture and is taken as 0.02 (Mohamed et al.

2010). These values yield a maximum confinement pressure of 12.5 MPa. It should be noted here that the confinement pressure experienced by the concrete tube during the loading stage depends on the amount axial compressive loads applied and varies along the column length.

The full equivalent axial stress–strain curve for confined concrete shown in Figure 6-2 is defined by identifying the parabolic and straight line parts of the curve. Unlike the model proposed by (Lam and Teng 2003), the first part is assumed approximately linear range to the proportional limit stress, this assumption showed good results as compared to the experimental work. The value of the proportional limit stress is taken as $\varepsilon_{co}$. The Poisson's ratio $\upsilon_c$ of concrete under uni-axial compressive stress ranges from 0.15 to 0.22, with a representative value of 0.19 or 0.20 (American Society of Civil Engineers (ASCE) 1982). In this study, the Poisson's ratio of concrete is assumed to be 0.2 (Mohamed et al.2001; Yao et al.2009), while the initial slope of the stress-strain curve, Young's modulus, of confined concrete ($E_c$) is reasonably calculated using the empirical formula, Eq. (6-3), given by ACI318-14).

$$E_c = 4700\sqrt{f_c'} \quad 6\text{-}3$$

The second linear part of the stress strain curve joins the first part at a transition strain$\varepsilon_l$ which is given by:

$$\varepsilon_l = \frac{2f_{co}}{(E_c - E_2)} \quad 6\text{-}4$$

where $E_2$ is the slope of the linear second part of the stress-strain curve and is given by

$$E_2 = \frac{f'_{cc} - f_{co}}{\varepsilon_{cu}} \quad 6\text{-}5$$

where $f_o$ is the intercept of the stress axis by the linear second part. Samman et al (1998), proposed the following expression, Eq. (6), to define $f_o$which is adopted in this study:

$$f_{co} = 0.872f_c' + 0.371f_{l,a} + 6.258 \quad 6\text{-}6$$

Concrete cracking is phenomenologically modelled using Shear Damage initiation criterion used in conjunction with Mises plasticity. Damage initiation is assumed to occur at a strain of 0.028 while damage evolution (post failure behavior beyond $f'_{cc}$ in Figure 6-2) is assumed linear where complete degradation is assumed (trial and error) to take place at a maximum

displacement of 0.4mm. In addition element deletion criterion is activated to remove failed element from analysis to avoid analysis termination.

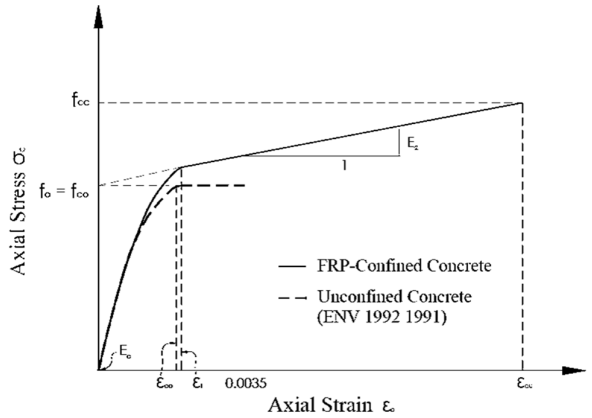


**Figure 6-2-**Stress-Strain Curve for FRP-Confined Concrete proposed by Lam and Teng

### 6.2.2.2 Modelling of GFRP Tube

In this study, glass-FRP (GFRP) tubes are used as the reinforcing jacket. The GFRP tubes are fabricated using filament winding technique with six layers (±60$^o$ relative to the column axis) E-glass fibre and Epoxy resin. The classical lamina theory is used to model GFRP tube with mechanical properties shown in Table 6-2. A damage criteria based on Hashin's failure model is used to model damage and failure of GFRP tubes. Model parameters for Hashin's damage criteria are shown in Table 6-3. The degradation of the material stiffness starts when Hashin's initiation criterion is reached for at least one of the failure modes. The damage variables, for the damage modes for which the initiation criteria are satisfied, evolve according to an energy-based evolution law with linear softening. Once the damage variable reaches the maximum degradation specified, no further damage takes place (ABAQUS 2008).

**Table 6-2-**Mechanical Properties of a GFRP Lamina

| $E_1$ (MPa) | $E_2$ (MPa) | $\upsilon_{12}$ | $G_{12}$ (MPa) | $G_{13}$(MPa) | $G_{23}$(MPa) |
|---|---|---|---|---|---|
| 28000 | 1040 | 0.31 | 5200 | 5200 | 3400 |

**Table 6-3-**Hashin's Damage Parameters

| Longitudinal Tensile Strength(MPa) | Longitudinal Compressive Strength(MPa) | Transverse Tensile Strength(MPa) | Transverse Compressive Strength(MPa) | Longitudinal Shear Strength(MPa) | Longitudinal Shear Strength(MPa) |
|---|---|---|---|---|---|
| 1200 | 140 | 40 | 40 | 20 | 20 |

#### 6.2.2.3 Modelling of Steel Bars

Steel reinforcement used in the experimental columns is a typical No. 10 steel reinforcing bars. Classical metal plasticity model based on von Mises yield criterion is used to define the behavior of the bar material. Mechanical properties for the bar, including an elastic modulus of 200 GPa, a yield stress of 462 MPa, a Poisson ratio of 0.3, an ultimate strain of 0.2, and an ultimate stress of 577 MPa were provided by the bar manufacturer.

### 6.2.3 Element type and mesh

The concrete core and the steel bars of the CFFT columns are modelled using linear tetrahedral 3-D solid elements having 8 nodes (C3D8R) while the GFRP tube is modelled with 8 nodes hexahedral in-plane general-purpose reduced integration continuum shell elements (SC8R). These elements have three and six degrees of freedom per node respectively and suit all column components. The element size is chosen adequately to eliminate errors due to meshing. The adopted mesh size must be smaller than any geometric feature in the FE model. A mesh size sensitivity analysis has been conducted to eliminate errors due mesh size dependency. Initial analysis started with uniform mesh, however, due to damage localisation close to columns' ends, finer mesh is considered close to the clamping location. The analysis shows that an average element size of 15mm will generate results that are independent on the mesh size. The total number of elements used for the concrete core, steel bars and GFRP tubes ranges from 46,084 to 92,400, 71, 40 to 17,780 and 10,248 to 18,228 respectively.

### 6.2.4 Modelling interactions between CFFT elements

The interaction between different elements within the CFFT must be properly defined to capture the underlying physics of the problem. Contact between steel bars and concrete and GFRP must be selected based on the objectives of the study. Usually cohesive surface interaction is used to model adhesion between concrete, steel bars and GFRP, however, in the present analysis such phenomenon is not considered. Moreover, the compressive loading mode assures continuous contact between concrete, steel rods and GFRP tube. Therefore, a general contact algorithm is used to define the interaction between all element and it includes all surface pairs and all with self. The contact properties assume only mechanical properties where tangential behavior is assumed frictionless and normal behavior is assumed hard. When surfaces are in contact they transfer shear forces as well as normal forces across their interface. A surface-based interaction with a contact pressure-over closure model in the normal direction and a nonlinear frictionless in the tangential directions between surfaces of tube and concrete core were assumed.

### 6.2.5 Boundary Conditions and Load Application

The CFFT columns are experimentally tested on a universal testing machine where upper and lower ends of the column fitted with end caps. These end caps are simulated using 3D rigid parts and covers 100 mm from the end of the specimen. The load and boundary conditions for rigid parts are defined at a reference point where all the degree of freedom are constrained except in the loading direction (axial direction) while the nodes at the bottom surface of the CFFT are restrained in all directions. An amplitude loading curve is used to define the rate of displacement prescribed at the reference point and to minimize the inertia effects, a smooth amplitude curve is used.

## 6.2.6 Model Verification

### 6.2.6.1 Load-displacement curves

In order to validate the assumed materials and geometrical models, the experimental setup is simulated and the results are compared. Figure 6-3 shows a comparison between numerical and experimental load-displacement curves of CFFT columns listed in Table 6-1. The load displacement curves of CFFT columns typically consist of three distinct stages. The first stage of these curves is linear up to approximately 80% of $f'_c$ representing the elastic response of the column. The second stage coincides with the initiation of lateral cracks as the confining pressure of the GFRP tube starts to operate. In this stage, the internal steel bars yield and the axial stiffness of the CFFT columns are gradually reduced. With the propagation of the lateral cracks and because of the confining pressure, the load deflection curve is distinguished by a hardening stage up to the failure point representing the third stage of the curve (refer to Figure 6-3). As shown in Figures 6-3-c and 6-3-d, increasing the slenderness ratio to 16 and 20 significantly changed the third stage of the load-deflection curve. The good agreements between the experimental and numerical results showed that the developed numerical model could effectively model such slender columns and capture damage occurring in different elements.

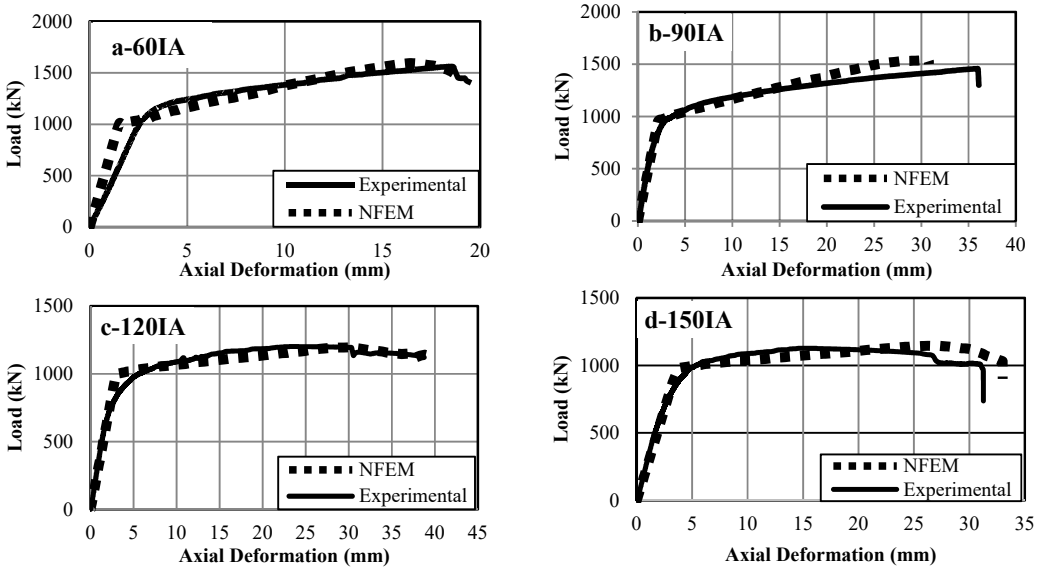

Figure 6-3-Experimental vs. Numerical Load-Displacement Curves for different columns listed in Table 6-1

#### 6.2.6.1 Failure pattern

In addition to load displacement curves, a good numerical model must be able to capture and predict different failure mechanisms and the associated deformed shape. Figure 6-4 shows comparisons between experimental and numerical failure modes for Hashin's damage parameter for short and slender columns. The failure mode varies from rapture of GFRP tubes for short specimens (60IA and 90IA) and buckling of long CFFT columns (120IA and 150IA). As can be seen from these figures, the failure location in the FE models coincides with the experimental ones as indicated by the red contours in the finite element figures for specimens (60IA and 90IA) which represent Hashin's damage greater than 1 in the GFRP tube and by the deformed configuration for specimens (120IA and 150IA).

**(a) Specimen 60IA (b) Specimen 90IA (c) Specimen 120IA (d) Specimen 150IA**

**Figure 6-4-**Comparison between the experimental failure mode and FE result for Hashin's damage parameter for short and slender columns

### 6.2.7 Effect of confinement pressure

The confinement pressure adopted in the developing the stress strain relation of the confined concrete is assumed constant during the loading process. However, the confinement pressure is expected to change based on the changes in the relative stiffness of the GFRP tube and the concrete itself. Figure 6-5(a) shows the load history for sample 60IA plotted against relative crosshead displacement. The contact pressure along the tube axis is shown in Figure 6-5(b) at different percentages of the crosshead displacement. The length under the rigid cap and the other fixed end are omitted in these plots due to the high constraints set at these locations leading to extreme contact pressures. Figure 6-5(b) shows that the contact pressure increases with increasing the axial displacement. At around 20% of the maximum crosshead displacement, i.e. close to the yield point in Figure 6-5(a), the contact pressure starts to build up and increases subsequently until it reaches its peak value at 70% of the maximum crosshead displacement which corresponds to the peak load attained before failure. Subsequent crosshead displacement causes the region of the effective contact to drop by approximately 20% at crosshead displacement 10% higher than that corresponding to the peak load and significantly drop to 20% of the initial contact length at approximately 20% crosshead displacement higher than that corresponding to the peak load. The time average contact pressure "FE Average" shown in Figure 6-5(b) indicates that the confinement pressure experienced by the concrete is similar to the constant pressure, "CE Average", used in developing the stress strain relation of the confined concrete adopted in the finite element model. It should be noted that in calculating "FE Average", contact pressures after failure are not included in the average calculation.

Similarly, Figure 6-6 shows the loading history and confinement pressure distribution along the tube axis for relatively long sample 150IA. The confinement pressure again increases with increasing the axial deflection where at the end of the linear part of the load deflection, i.e. at 24% of the machine crosshead displacement, the confinement pressure reaches approximately

110 kPa. At 62% of the machine crosshead displacement, i.e. peak load at the onset of buckling, the maximum confinement pressure attained is approximately 4 MPa which is almost one third of the confinement pressure used in developing the stress-strain values of the confined concrete. However, the good agreement between the experimental and finite element simulations presented in Figures 6-3-d and 6-4-d show that the developed concrete model is also capable of predicting other failure modes such as buckling although the maximum calculated confinement pressure is not achieved during the loading process.

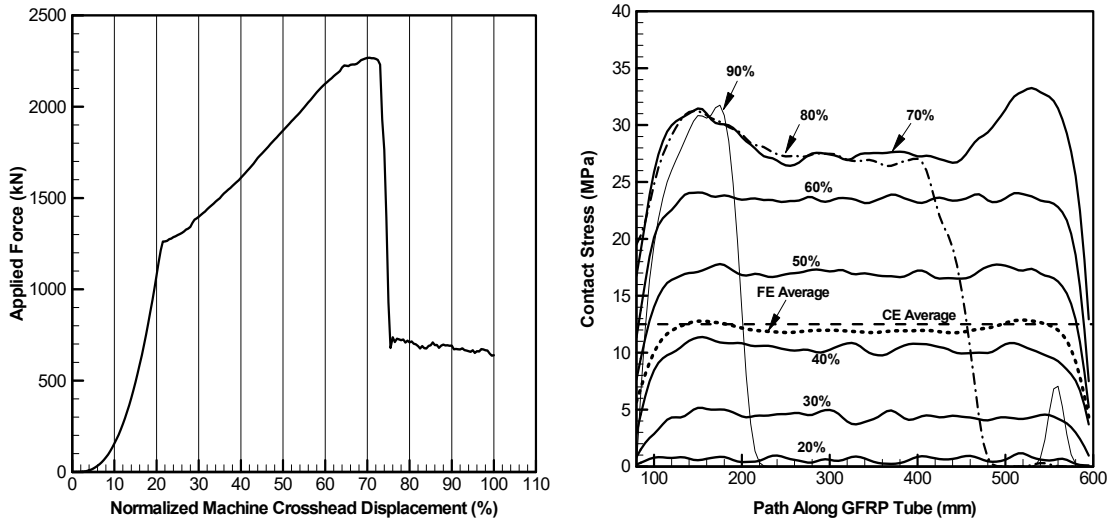


Figure 6-5-(a) Load history and (b) contact pressure along tube axis, for sample 60IA

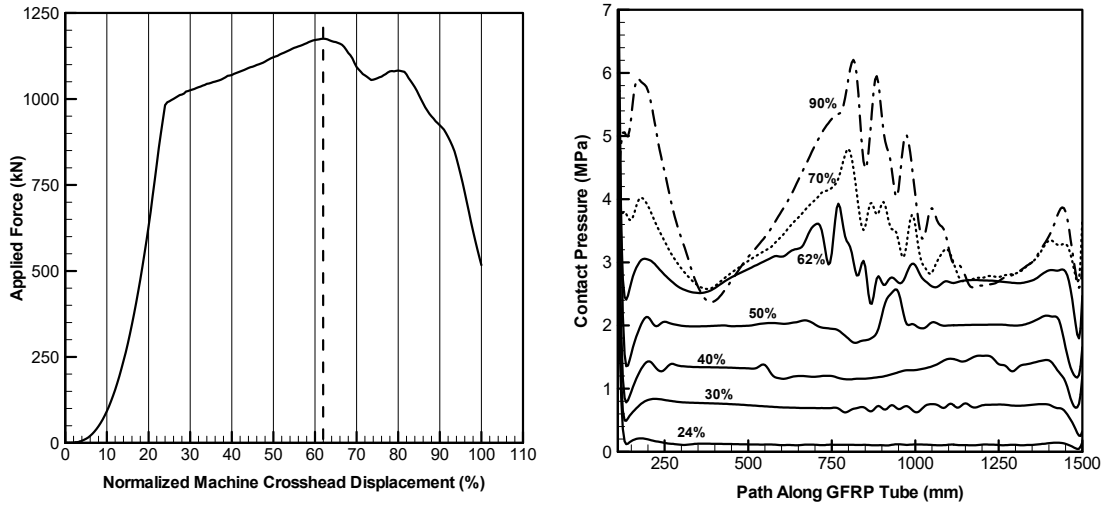

**(a)** **(b)**

Figure 6-6-(a) Load history and (b) contact pressure along tube axis, for sample 150IA

### 6.2.8 Failure mechanism of axially loaded CFFT

The mode of failure differs according to the slenderness ratio of specimens as it varies between rupture of confining FRP to overall buckling of CFFT (Mohamed et al. 2010). A comparison between different parts of the load displacement curves and the specimen behavior during the loading process till failure assisted in defining the failure mechanism of each specimen and the effect of loading on different parts of the specimen (steel, concrete, and GFRP). For a column with slenderness ratio of 8 (60IA -length =610 mm), the results of the load deflection curve and failure of different element are shown in Figure 6-7. In the load deflection curve (Figure 6-7.a), point A indicates yielding of the steel bars at a load ($P_y$) approximately equals 60% of the ultimate peak load (Figure 6-7.b). Point B on the curve represents the load after reaching its peak value where the limit stresses exceeded the critical failure stresses, the column fails at ($P_u$) nearly equals 1,600 kN and the failure mode is a combination of local buckling of internal steel bars at the column mid height (Figure 6-7.c), and rupture of the confining FRP tubes (Figure 6-7.d) and then cracking of the concrete appeared where the concrete core reached its limit stress as shown in Figure 6-8.

For a column with a slenderness ratio of 12 (90IA), the failure mechanism is almost the same as column 60IA where point A in the load deflection curve shown in Figure 6-9.a indicates the yielding of steel bars at a load ($P_y$) approximately equals 60% of the ultimate peak load (Figure 5-9.b) and the column fails when the limit stresses exceed the critical load Pu which is approximately 1,500 kN. Point B in the load deflection curve indicates the failure mode which is a combination of local buckling of internal steel bars at the column mid height (Figure 6-9.c) and rupture of the confining FRP tubes (Figure 6-9.d). Crushing of concrete appeared after the CFFT reached the peak load and rupture of GFRP occurred as shown in Figure 6-10.

For columns with slenderness ratio 16 and 20 (120IA, l = 1,216 mm and 150IA, l = 1,520 mm) the mode of failure changes to instability of the CFFT columns. For column 120IA, point A in the load deflection curve (Figure 6-11.a) indicates the starting of the buckling mode as the stress distribution along the column is nearly uniform until the buckling mode starts where the

stress distribution (S33) is no longer uniform but the column continues to stiffen as shown in Figure 6-11.b. As the loading process continues, the stresses along the column become non-uniform until tensile cracks appears on one side of the middle section and degradation in load carrying capacity occurs (point B in Figure 6-11.a) resulting in failure and instability of the CFFT as shown in Figure 6-11.c. Figure 6-12.a shows the location of the cracks in the concrete column after removing the GFRP tube which is confirmed by the finite element modelling.

The behavior of column 150IA is similar to that of 120IA where stress distribution under compressive loading along the column is nearly uniform until the starting of the buckling mode (Point A in load deflection curve Figure 6-13.a) where the stress distribution (S33) is no longer uniform but the column continues to stiffen as shown in Figure 6-13.b. As the loading process continues, the stresses along the column become more non-uniform until tensile cracks appears on one side and degradation in load carrying capacity occurs (Point B in Figure 6-13.a) resulting in failure and instability of the CFFT as shown in Figure 6-13.c. When the GFRP tube is removed, it is found that the concrete failure pattern in the FE model resembles that in the experimental model for specimen 150IA as shown in Figure 6-12.b. The failure modes of different specimens show that the greater the slenderness ratio, the more significant the buckling of the specimen.

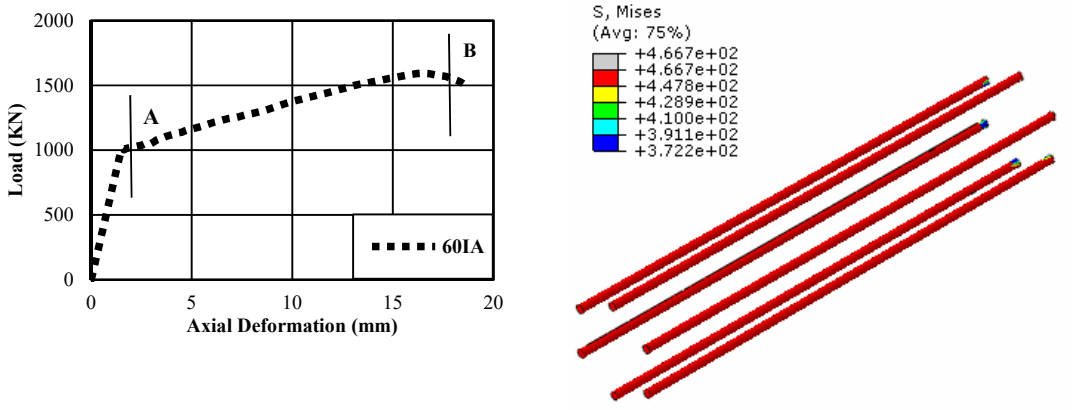


**(a)** **(b)**

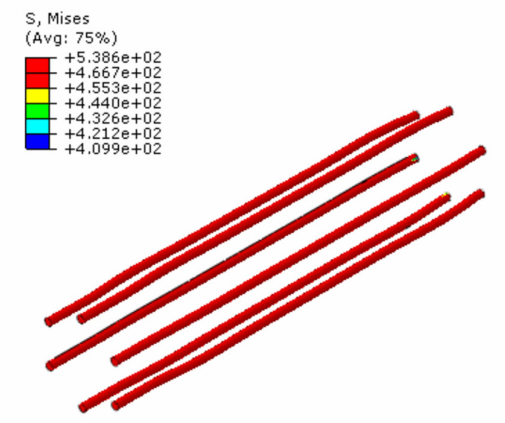


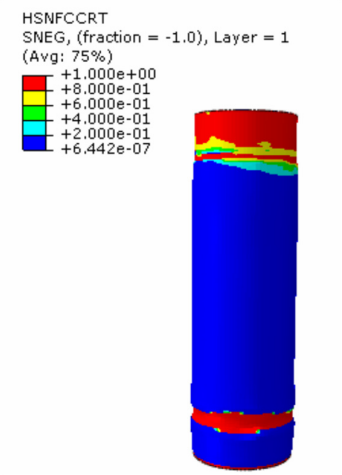


**(c)** **(d)**

**Figure 6-7-**Results of the load deflection curve and elements of Specimen 60IA: (a) Load-Deflection curve, (b) Yielding of steel bars, (c) Local buckling of steel bars at failure, and (d) Rupture of FRP at failure indicated by Hashin's damage parameter

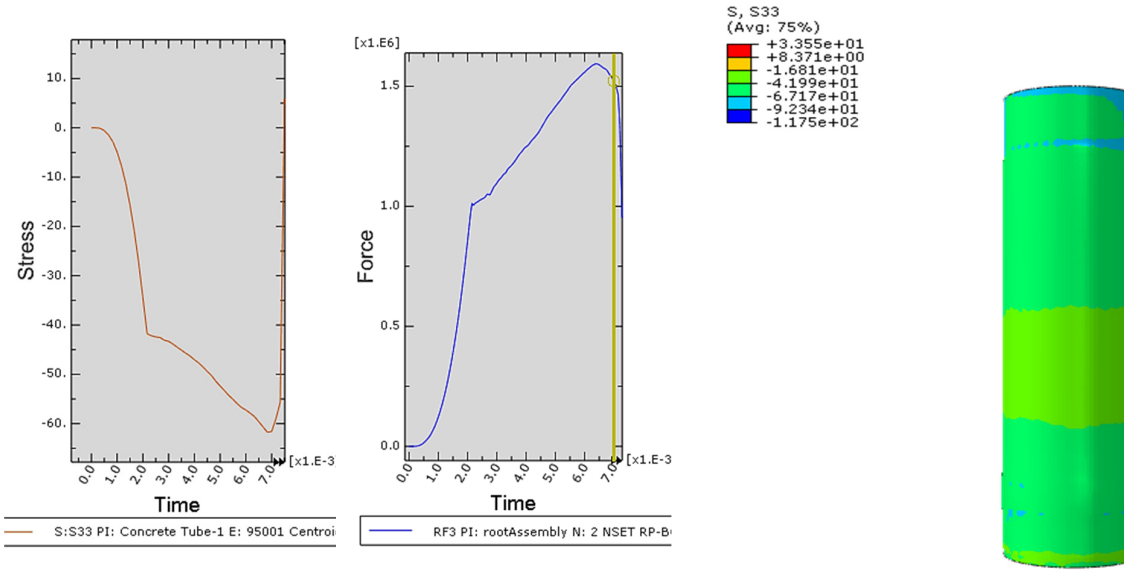


**Figure 6-8-**Point of crushing of concrete at an element in the mid-section for specimen 60IA

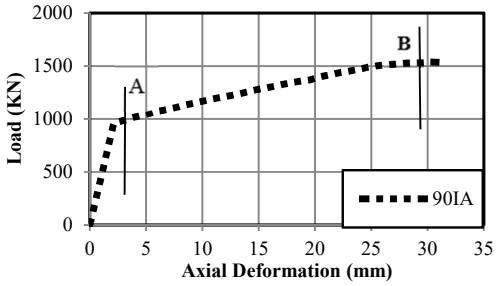


**(a)**

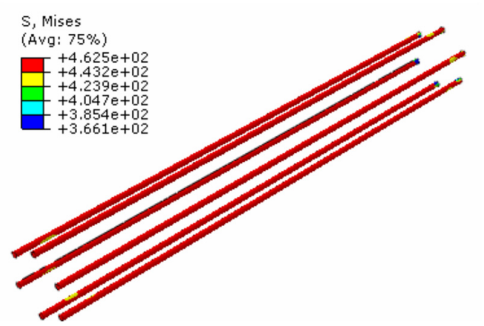


**(b)**

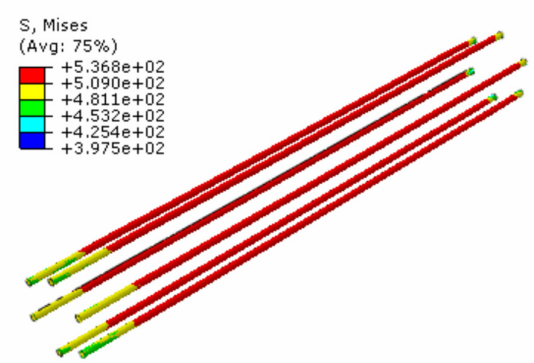


**(c)**

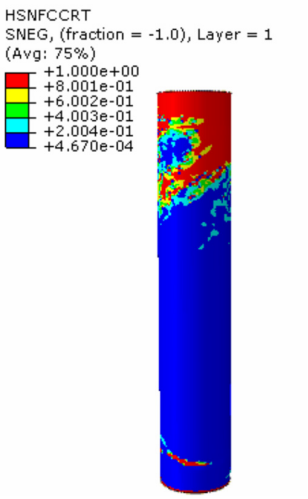


**(d)**

**Figure 6-9-**Results of the load deflection curve and behavior of Specimen 90IA: (a) Load-Deflection curve, (b) Yielding of steel bars, (c) Local buckling of steel bars at failure, and (d) Rupture of FRP at failure indicated by Hashin's damage parameter

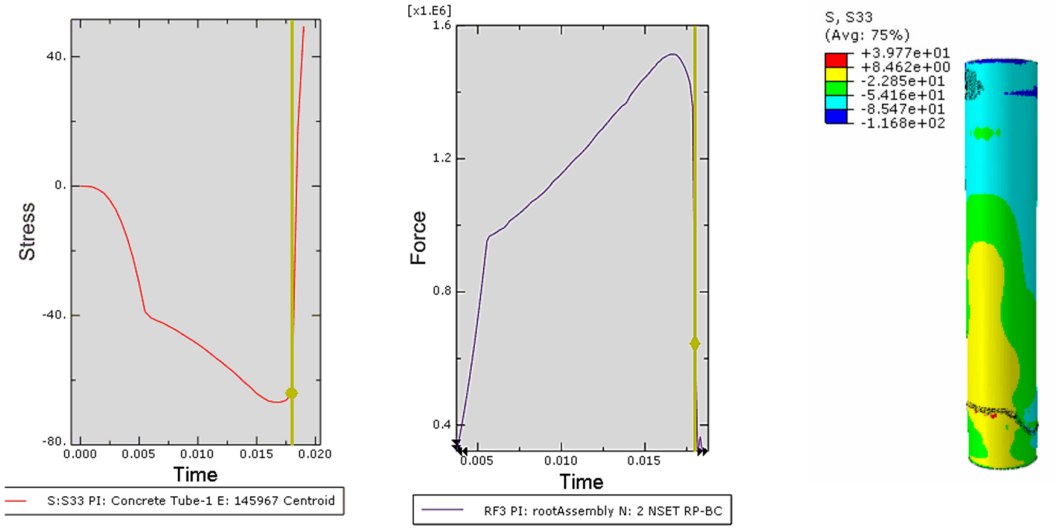


**Figure 6-10**-Point of concrete crushing in specimen 90IA

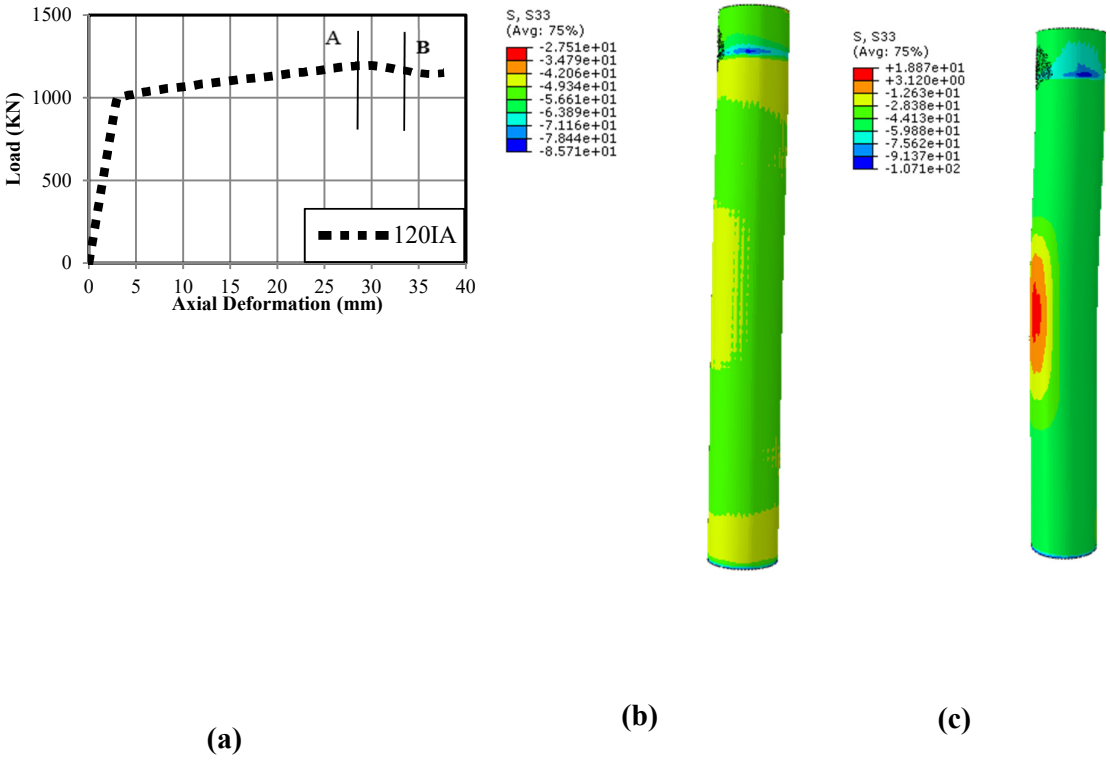


**(a)** **(b)** **(c)**

**Figure 6-11-**Results of the load deflection curve and behavior of Specimen 120IA: (a) Load-deflection curve, (b) Start of the buckling mode, and (c) Failure and instability of CFFT

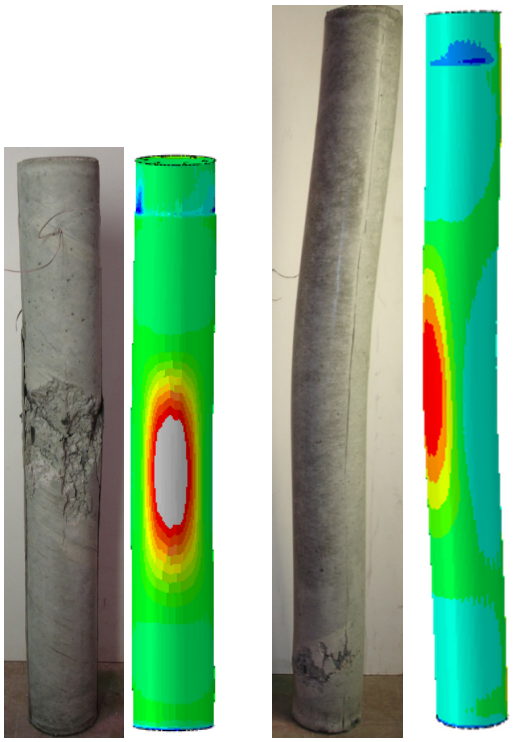

**(a) Specimen 120IA (b) Specimen 150IA**

Figure 6-12-FE Model Vs Experimental for concrete core

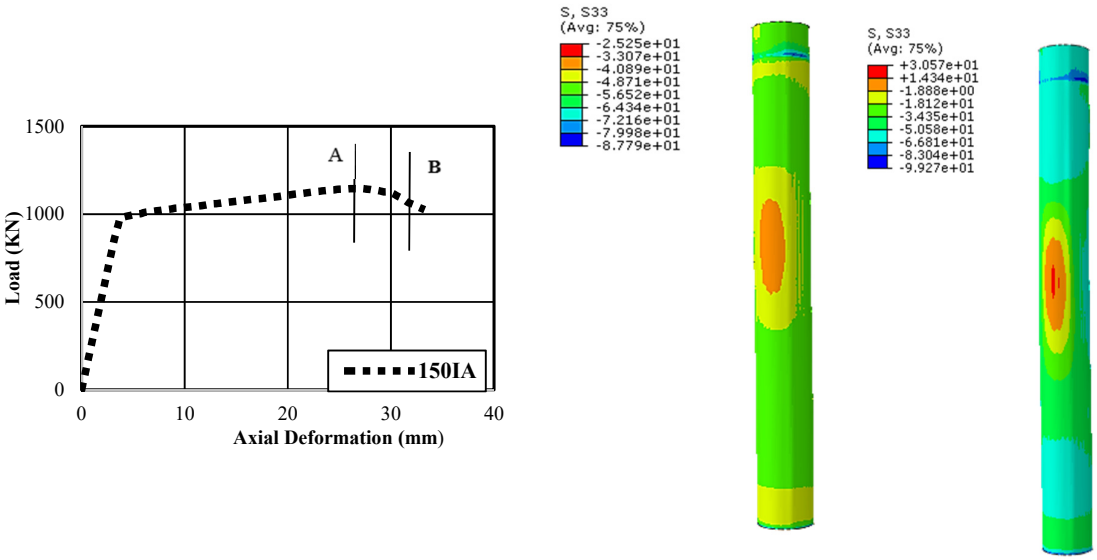


**(a)** **(b)** **(c)**

**Figure 6-13-** Results of the load deflection curve and behavior of Specimen 150 IA: (a) Load- deflection curve, (b) Start of the buckling mode, and (c) Failure and instability of CFFT.

## 6.3 Effect of design variables on load carrying capacity and failure modes (Parametric Study)

The results of the developed FE models showed a good agreement with the experimental results for the tested CFFT columns under axial compressive load. This verified finite element model can be extended to investigate the effect of different design parameters on the behavior of CFFT columns. These design parameters are divided into three groups which include the number of GFRP layers, fibre orientations, and reinforcement ratio of steel bars ($\rho_s$). Details of these design parameters and design of experimental simulations for this study are presented in Table

6-4, the comparison of the load displacement curves for different parameters are represented in Figure 6-14 and discussed in details in the following sections.

### 6.3.1 Effect of number of FRP layers on CFFT behavior

Columns of Group number 1 are modelled to study the effect of number of FRP layers on CFFT behavior. As expected, the ultimate load carrying capacity increases as the number of layers increases regardless the change in the slenderness ratio as shown in Fig. 6-14.a and Fig. 6-14.b respectively. For columns with slenderness ratio (*kl/r=8),* increasing the number of layers 300% (i.e., from 2 layers to 8 layers) increases the ultimate load carrying capacity by 25% (i.e., from 1480 KN to 1980KN), all the specimens in this set fails by to combination of rupture of FRP and crushing of the concrete, while for columns with slenderness ratio (*kl/r=20)* increasing the number of layers 300% (i.e., from 2 layers to 8 layers) increases the ultimate load carrying capacity by 8% (i.e., from 1085 KN to 1174KN) ,all the specimens in this set fails due to instability of CFFT column. Increasing the number of FRP layers increases the confined concrete strength and stiffness, which increases the concrete contribution to the axial load resistance mechanisms and delaying the onset of the tube failure. For the column with low number of FRP layers (i.e. number of layers =2), once local buckling of steel bars occurs, concrete begins to dilate more rapidly and lose the confinement effect. This is understandable as the confinement depends on the radial pressure provided to the concrete core by FRP tube and as the confinement pressure of two FRP layers is considered very small they cannot provide the desired confinement and cannot increase the compressive strength considerably. In case of specimens with 6 and 8 FRP layers, beyond the initiation of the local buckling of steel bars, the concrete is still well-confined and sustained the high compressive stresses. Therefore, it is noted that the compressive strength of the FRP confined concrete depends on the thickness of FRP tube, it is suggested that the CFFT designed FRP must have sufficient thickness otherwise the structure is not meet its design objectives and the strengthening effect cannot be fully realized, also it is noted that the effect of increasing the number of layers decreases as the slenderness ratio increases as the buckling mode failure occurred in the long column is controlled by the column's stiffness which is not affected by the fibre thickness.

### 6.3.2 Effect of fibre orientation

The behavior of FRP-confined concrete is significantly influenced by the orientation of the confining fibres and it is important to understand and be able to model the influence of fibre angle on the behavior of FRP-confined concrete (Li et al 2006). To study the effect of the fibre orientation, columns of Group 2 are modelled. Figures 6-14.c and 6-14.d show the effect of fibre angle on the load carrying capacity and failure of CCFT. From both figures, it is observed that as the angle (θ) in angle ply laminates increases with longitudinal direction (i.e.: angle ± 75) the failure load of the specimen increases, therefore it is concluded that the fibre efficiency reducing significantly with an increase in the fibre alignment with respect to the hoop direction and that's agreed well with what have been mentioned in previous studies on the influence of fibre orientation on the behavior of confined concrete (Vincent and Ozbakkaloglu, 2013).

### 6.3.3 Effect of reinforcement ratio

Figure 6-14.e and Figure 6-14.f show that the ultimate load will significantly increase with increasing the steel reinforcement ratio ($\rho_s$) where $\rho_s$ can be expressed as:

$$\rho_s = \frac{A_s}{A_c}$$

Where $A_s$ is the total area of steel bars and $A_c$ is the area of the concrete section = $\pi r^2$

Specimens of Group 3 with different reinforcement ratios (2.5%, 4.3% and 5.8%) are modelled. The higher the value of $\rho_s$, a higher ultimate load can be obtained. For columns with slenderness ratio (*kl/r*=8) the ultimate load for column with $\rho_s$= 2.5% is 1594 kN which is smaller than the ultimate loads for columns with $\rho_s = 4.3\%$ & $5.5\%$ which are 2134 kN and 2269 kN, respectively, while columns with slenderness ratio (*kl/r*=20) the ultimate load for column with $\rho_s$= 2.5% is 1145kN which is smaller than the ultimate loads for columns with $\rho_s = 4.3\%$ & $5.5\%$ which are1448 kN and 1565 kN, respectively. Also it can be observed that the curves become more linear for both slenderness ratios in the axial stiffness at the hardening region as the steel reinforcement ratios become higher.

**Table 6-4-** list of materials and dimensions parameters for the study

| *Group* | *Column Length(mm)* | *Slenderness Ratio (kl/r)* | *Concrete Compressive Strength (MPa)* | *GFRP Tube No. of Layers* | *Steel Reinforcement Ratio (%)* | *Fiber orientation* |
|---|---|---|---|---|---|---|
| *1* | *610* | *8* | *30* | *2* | *2.5%* | *±60* |
| | | | | *6* | | |
| | *1520* | *20* | | | | |
| | | | | *8* | | |
| *2* | *610* | *8* | *30* | *6* | *2.5%* | *±30* |
| | | | | | | *±45* |
| | *1520* | *20* | | | | *±60* |
| | | | | | | *±75* |
| *3* | *610* | *8* | *30* | *6* | *2.5%* | *±60* |
| | | | | | *4.3%* | |
| | *1520* | *20* | | | *5.8%* | |

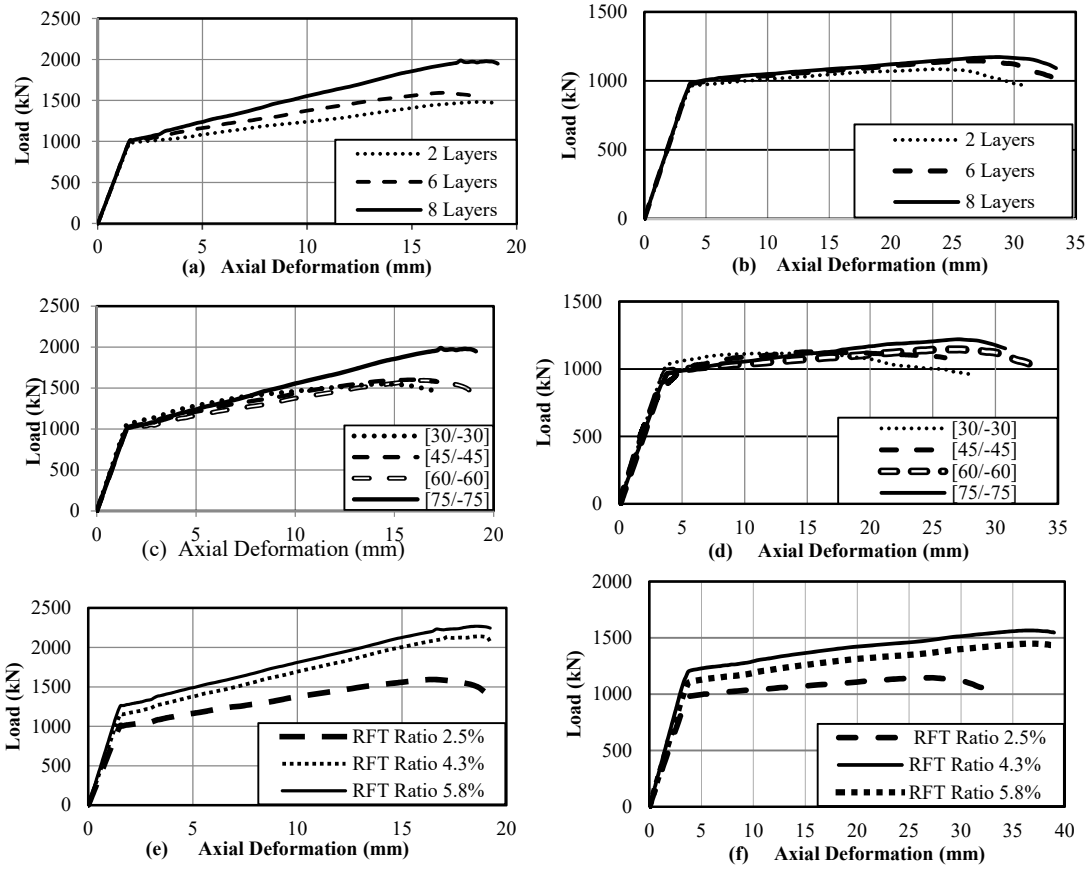


**Figure 6-14-** Load-displacement curves (a) specimens with (kl/r=8) with different FRP Layers, (b) specimens with (kl/r=20) with different FRP Layers, (c) specimens with (kl/r=8) with different fiber orientation, (d) specimens with (kl/r=20) with different fiber orie

## 6.4 Summary and Conclusions

A finite element (FE) model is developed to predict the axial behavior of CFFT columns. The model is verified against the experimental results of full scale CFFT columns with different slenderness ratio (*kl/r*). The model is then used in a parametric study to address the effect of the fibre orientations as well as the fibre tube thickness and the reinforcement ratios for the internal steel bars. The following conclusions can be drawn:

1. A nonlinear finite element model is developed using ABAQUS software, the model accounts for material and geometric nonlinearities. Very good agreement with the experimental results is observed for the load-deflection responses and failure patterns.
2. The model can accurately detect the material failure of FRP tube in the short columns through the hashin's damage failure criteria and capturing the buckling failure mode of long slender columns. In addition, the cracking of the concrete tube is accurately detected through shear damage initiation criterion used in conjunction with Mises plasticity.
3. The concrete model adopted here is linear in the elastic part unlike the model proposed by (Lam and Teng 2003) where the first part is parabolic, however the proposed linear behavior model showed good results as compared to the experimental work which calls for the need to develop more accurate constitutive models to represent the actual behavior of confined concrete which is currently undergoing.
4. Fibre orientation and FRP thickness have considerable effects on the behavior and axial load carrying capacity of CFFTs. The FRP tube confinement effect cannot be fully realized without proper fibre orientation and sufficient number of FRP layers.
5. The ultimate load capacity of the CFFT increased as the angle (θ) in angle ply laminates, relative to longitudinal axis is increased and as the number of FRP layers increased, the rate of increase is more pronounced for the short columns than the long slender ones.
6. For the long slender tube columns (*kl/r=20*) the ultimate load capacity seems to be nearly constant and independent on the increase in the angle (θ) with the longitudinal direction and the increase of the number of FRP layers, this may be attributed to the buckling failure behavior of these columns.

7. While increasing the reinforcement ratio ($\rho_s$) in the CFFTs, a higher ultimate load can be obtained and a more linear curve is observed in the axial stiffness at the hardening region.

# CHAPTER 7

# CONCLUSIONS AND RECOMMENDATIONS

## 7.1 Conclusions

The current study aims to understand the behavior of concrete-filled FRP tube (CFFT) columns. The study included experimental and theoretical investigations and finite element modeling. In the experimental program, 5 steel reinforced CFFT and 5 CFRP reinforced CFFT columns, were tested under axial and eccentric loads. All the specimens were 152mm in diameter and 912 mm in height and of this study were constructed using normal concrete strength with 28-day average concrete compressive strength equal to 30 ±1 MPa. Glass-fibre reinforced polymer (GFRP) tubes were used as structural formwork for the CFFT specimens with total thickness of 2.65 mm (6 layers). For eccentrically loaded CFFT columns, four eccentricity distances were used (10, 20, 30 and 40 mm) with eccentricity to diameter ratio (e/D) 0.1, 0.2, 0.3 and 0.4, respectively. The experimental results including axial- moment interaction diagrams and moment-curvature curves were compared to analytical results from section analysis models. Stresses were integrated over the section either by using strain compatibility and force equilibrium method by adopting the layer-by-layer approach considering proper constitutive models for materials. Moreover, the effective flexural stiffness was investigated and discussed considering the presence of the tube as an external confinement and the presence of the internally reinforcement bars either steel or FRP bars. Proposed expressions were, therefore, developed to reflect the results obtained from the experimental database and the analysis of this research work. Finally, a non-linear finite element modeling using ABAQUS software was presented to understand the failure mechanism of the CFFT columns including the cracks initiation, and propagation, deflections, possible failure mode. This was attributed by considering an elastoplastic model for confined concrete stress-strain

curve. The results of this study were presented by three articles and the following conclusions were drawn:

### 7.1.1 Specimens Structural Performance (Experimental Results)

***Strength, behavior and failure mode***

1. The behavior of steel and CFRP reinforced CFFT columns under eccentric loads is completely different as compared to those tested under concentric loads in terms of ultimate load capacities and failure modes, where the load carrying capacities of CFFT columns under load eccentricities, *e/D* ratios ranged from 0.10 to 0.4 were reduced by 42 to 75%, respectively, as compared to that of the same CFFT columns under concentric load.
2. The behavior of CFRP reinforced CFFT columns under eccentric loads behaved similarly to that the counterpart reinforced with steel bars, in terms of load carrying capacities and deformations. However, the load carrying capacities of steel and CFRP reinforced CFFT columns were reduced due to the presence of the moment resulting from the applied load with eccentricity.
3. Rupture of the FRP tube in the hoop direction and local buckling of internal bars are the dominant in case of concentric loading. While overall instability of the columns along with the combination of tensile rupture of the FRP tubes and CFRP bars or steel yielding in the tension side with excessive axial and lateral deformations are the dominant in case of eccentric loading.
4. For concentrically loaded columns, no lateral deformation was recorded up to 85% of the ultimate load due to axial loading, however for eccentrically loaded columns; the lateral displacement of the columns was significant indicating instability of the columns. The lateral deformation of the eccentrically columns increased gradually with the load increase up to the peak load. After that the deformation increased progressively with a significant decrease in the load carrying capacities up to the complete instability of the column.

5. CFRP reinforced specimen exhibits a more significant reduction of stiffness after initiation of cracks in comparison with steel reinforced specimen. This returned to the higher young's modulus of steel than that of CFRP.

***Efficiency of CFRP bars***

6. The experimental investigation conducted in this study indicated that the CFRP bars could be used as a longitudinal internal reinforcement for CFFT columns under eccentric loads, provided that the maximum compression strength is limited to 35% of the ultimate tensile bar strength.
7. The recorded bar strain at peak can reach up to 0.65% ultimate tensile strain (55% of the ultimate tensile bar strain) and 0.45% ultimate compressive strain (36% of the ultimate tensile bar strain). These values proved the effective contribution of the CFRP bars in resisting tensile and compressive stresses.

***Interaction Diagram***

8. The failure envelope of the FRP reinforced CFFT columns was unlike the steel reinforced CFFT columns where no balance point was indicated. This was due to the variation of the linearly elastic stress strain response of CFRP bars until failure while for the steel bars a well-defined yield plateau behavior occurred.

### 7.1.2 Theoretical Analysis

***Interaction Diagram***

9. Constructing a theoretical *P-M* diagrams based on strain compatibility -force resultant and layer-by-layer methods predict quiet well the axial load bending moment for both steel and FRP reinforced CFFT columns and pertained reasonably close values to the experimental results.

***Moment-Curvature Diagram***

10. The developed analytical model for computing the moment-curvature diagram based on the layer by layer numerical integration provided accurate predictions compared to

the experimental results. It also shows that regardless the type of reinforcement and the eccentric ratio all specimens exhibit nonlinear moment-curvature (M-φ) responses.

***Parametric Study***

11. The parametric investigation showed that the increase in the unconfined concrete strength, longitudinal reinforcement ratio and number of layer of FRP tube increase the moment capacity of the columns. Increasing ($\frac{A_{bar}}{A_g}$) and $f'_c$ has a significant influence on the moment capacity of the columns which increased by 68% on changing ($\frac{A_{bar}}{A_g}$) from 1% to 8% and increased by average 15 % on increasing $f'_c$ from 25 MPa to 40 MPa. Yet increasing the number of FRP tube layers shows insignificant increase in the moment capacity of the columns which increased on average 6% when increasing the number of layers from 3 to 8 layers.

## 7.1.3 Effective Flexural Stiffness

12. The proposed design equations were developed using a simplified format to include all the parameters affecting the flexure stiffness of steel and FRP CFFT columns, respectively as follow;

$$EI_{e-s} = \alpha_c E_c I_g + \alpha_s E_s I_s + \alpha_t E_t I_t$$

$$EI_{e-FRP} = \alpha_c E_c I_g + \alpha_f E_f I_f + \alpha_t E_t I_t$$

where a multiple linear regression analysis was used to predict the coefficients of different variables included in the equations format. This type of analysis produced accurate estimation of the CFFT column stiffness equation.

13. Increasing the eccentricity and axial load ratios result in a reduction in the effective flexure stiffness ($EI_e$) of the slender CFFT column. Thus, a new stiffness reduction factor for concrete $\alpha_c$ was suggested, where $\alpha_c = 0.2\left(\frac{l}{D}\right) - \frac{e}{D}\left(\frac{0.5}{1+e/D}\right) - 0.4\left(\frac{P_u}{P_o}\right)$.

14. Stiffness reduction factors for reinforcing bars $\alpha_s = 0.8$ and $\alpha_f$=0.7 were proposed for steel and FRP reinforced CFFT columns, respectively.
15. The effectiveness of the confinement induced by the external FRP tube was taken into consideration in the formulation of the design equation where a new stiffness reduction factor for FRP tube $\alpha_t$ was proposed. $\alpha_t$ depends mainly on the strength-reinforcement ratio of FRP tube and concrete ( $\beta$ ) and was formulated as ( $\alpha_t = 0.6\beta + 0.9$ ).
16. The design equations were compared with the present experimental results and those available in the literature and proved to be reasonably accurate for practical engineering design applications.

### 7.1.4 Buckling Instability and Slenderness Limit

17. A simplified equation was suggested to calculate the slenderness limit for FRP CFFT columns, in addition, a slenderness limit of 14 was introduced as a safe value for design purpose.
18. The critical slenderness limit is significantly affected by the concrete compressive strength and tube hoop stiffness, while the mechanical properties of FRP bars along with its reinforcement ratio induce an insignificant effect on the slenderness limit.

### 7.1.5 Finite Element Modeling

19. The finite element model using ABAQUS software can accurately detect the material failure of FRP tube in the short columns through the Hashin's damage failure criteria and capturing the buckling failure mode of long slender columns. In addition, the cracking of the concrete tube is accurately detected through shear damage initiation criterion used in conjunction with Mises plasticity. The concrete model adopted here is linear in the elastic part unlike the model proposed by (Lam and teng 2003) where the first part is parabolic, however the proposed linear behavior model showed good results as compared to the experimental work.

20. Fibre orientation and FRP thickness have considerable effects on the behavior and axial load carrying capacity of CFFTs. The FRP tube confinement effect cannot be fully realized without proper fibre orientation and sufficient number of FRP layers (6-8 layers).
21. For the long slender tube columns (*kl/r=20*) the ultimate load capacity seems to be nearly constant and independent on the increase in the angle (θ) with the longitudinal direction and the increase of the number of FRP layers, this may be attributed to the buckling failure behavior of these columns.

## 7.2 Recommendations for Future Work

Based on the findings and conclusions of the current study, some limitations of this work still require additional research on CFFT columns design to cover the following points:

1. Using high strength concrete has been well known in research nowadays. Integrating such type of concrete with FRP tube and FRP bars could be promising for both materials.
2. The current study is concerned with circular CFFT columns. Similar methodologies are believed to be equally applicable and can be extended to include CFFT columns with rectangular and other irregular shapes.
3. Experimental and theoretical investigations are required to investigate the performance of CFFT columns under seismic loads.
4. Studying the effect of concrete shrinkage inside the FRP tube.
5. Punching behavior of CFFT-flat slab connections.
6. Behavior of rigid CFFT-concrete roof (B.M transfer).

## 7.3 Conclusions

Cette thèse vise à bien comprendre le comportement des colonnes faites avec des tubes en polymère renforcé de fibres (PRF) remplis de béton armé (CFFT). L'étude comporte des travaux expérimentaux et théoriques ainsi qu'une modélisation par des éléments finis. La partie expérimentale consiste en cinq colonnes CFFT renforcées avec des barres d'acier et cinq autres colonnes CFFT renforcées avec des barres de fibres de carbone (PRFC). Ces colonnes ont été testées sous des charges axiales et excentriques.

Les échantillons utilisés dans ce programme expérimental sont confectionnés avec un béton ordinaire ayant une résistance à la compression à 28 jours de 30 MPa ± 1 MPa.

Le diamètre et la hauteur des colonnes testées sont égales à 152, et 912 mm, respectivement. Les tubes en PRFV ont été utilisés comme un coffrage structural pour les échantillons des colonnes CFFT avec une épaisseur totale de 2,65 mm (6 couches). Pour les colonnes CFFT testées sous une charge excentrique, quatre distances d'excentricité ont été utilisées (10, 20, 30 et 40 mm) avec des rapports d'excentricité :(e/D) de 0,1, 0,2, 0,3 et 0,4 respectivement.

Les résultats expérimentaux y compris les diagrammes d'interaction charge axiale versus moment ainsi que les courbes moments versus courbure ont était comparés avec les résultats obtenus par les modèles théoriques.

Les contraintes sont intégrées dans la section étudiée soit par l'utilisation de la méthode de comptabilité des déformations et l'équilibre de forces ou par l'utilisation de la méthode de couche par couche en considérant les différents modèles constitutifs des matériaux.

L'effet de la rigidité en flexion a été étudiée et analysée en considérant le rôle des tubes en PRF au confinement extérieur des colonnes ainsi que la présence des barres d'armature soit en acier ou en polymère renforcé par de fibres de carbone à l'intérieur des colonnes. Des modèles proposés ont été développés et comparés aux résultats expérimentaux. Finalement, une modélisation non-linéaire par éléments finis a été effectuée en utilisant le logiciel ABAQUS pour comprendre le mécanisme de rupture des colonnes CFFT. Ce mécanisme contient

l'initiation des fissures, la propagation des fissures, la déflection des colonnes ainsi que l'estimation de la manière de rupture.

### 7.3.1 Performance Structurale des échantillons CFFT (Résultats expérimentaux)

**Résistance, Comportement et mode de rupture**

1- Le comportement des colonnes CFFT renforcées en acier et les colonnes CFFT renforcées en polymère des fibres en carbone (PRFC) sous charge excentrique est complètement différent de celui sous charge axiale en termes de résistance et mode de rupture. Les résistances des colonnes CFFT sous charge excentrique, sont réduites de de 42 à 75%, lorsque le rapport d'excentricité est augmenté de 0,1 à 0,4, respectivement, par rapport à celle des mêmes colonnes CFFT sous charge axiale.

2- Le comportement des colonnes CFFT renforcées de barres en PRFC est similaire à ceux renforcées de barres en acier en termes de résistances et déformations.

3- Sous un chargement axial, la rupture des tubes en polymère renforcé de fibres (PRF) dans la direction circonférentielle des tubes et le flambement des barres internes sont les modes de rupture dominants. Par contre, dans le cas d'un chargement excentrique, la combinaison de rupture de traction des tubes en PRF, des barres en PRFC et les barres d'acier ainsi que l'excès des déformations axiales et latérales engendrent une instabilité globale des colonnes CFFT.

4- Pour les colonnes CFFT testées sous une charge axiale, aucune déformation latérale (hors de l'axe de la colonne) n'a été observée jusqu'à une valeur de 85% de la charge ultime dû aux conditions de chargement axiale. Par contre, pour les colonnes testées sous une charge excentrique, un déplacement latéral significatif a été enregistré indiquant une instabilité globale des colonnes CFFT. Le taux de la déformation latérale des colonnes CFFT sous charges excentriques augmente graduellement avec l'augmentation du taux de chargement jusqu'à l'application de la charge maximale de rupture.

5- Les échantillons renforcés avec des barres en PRFC montrent une réduction importante des valeurs de rigidité après l'initiation des fissures par rapport aux échantillons renforcées avec des barres en acier. Ceci est probablement dû à la faible valeur du module d'Young des barres en PRFC par rapport à celle des barres en acier.

**Efficacité des barres PRFC**

6- Les résultats expérimentaux de ce programme de recherche montrent que les barres en PRFC peuvent être utilisées comme armature longitudinale interne dans les colonnes CFFT sous charges excentriques à condition que la résistance en compression maximale soit limitée à 35% de la résistance en traction ultime de barre.

7- Les déformations maximales enregistrées dans les barres en PRFC peuvent atteindre jusqu'à 65% de déformation ultime de traction (55% de déformation ultime de traction) et 45% de déformation ultime de compression (36% de déformation ultime de traction). Ces valeurs ont prouvé la contribution effective des barres en PRFC en résistant aux contraintes de traction et de compression.

**Diagramme d'interaction**

8- L'enveloppe de la rupture des colonnes CFFT armées de barres en PRFC était différente par rapport à celle des colonnes CFFT armées de barres en acier. Ceci est probablement dû à la variation de la réponse de contrainte élastique linéaire des barres en PRFC jusqu'à la rupture tandis que le comportement de plateau ductile pour les barres en acier peut être une cause de cette différence dans les enveloppes de rupture entre les deux séries de colonnes CFFT (CFRP versus acier)

### 7.3.2 L'analyse Théorique

**Diagramme d'interaction**

9- Un modèle théorique représentant les diagrammes P-M basé sur la méthode de comptabilité des déformations versus Force-résultante, ainsi que la méthode de couche-

par-couche prédit de manière efficace les valeurs des charges axiales ainsi que les moments fléchissant pour les colonnes CFFT renforcées de barres en PRFC ou en acier.

**Diagramme de Moment-courbure**

10- Le modèle analytique développé pour prédire les valeurs du diagramme de moment-courbure montre des résultats théoriques très proches des résultats expérimentaux. La méthode de calcul utilisée pour développer ce modèle est l'intégration numérique couche par couche. Il montre aussi que les réponses obtenues sont toutes non-linéaires pour diagramme de moment-Courbure (M-φ). Le type de renforcement utilisé et le rapport d'excentricité n'ont pas d'effet significatif sur la non-linéarité des échantillons testés.

**Étude paramétrique**

11- Cette recherche montre que les paramètres clés qui influencent l'augmentation de la capacité en flexion des colonnes sont : l'augmentation de la résistance non-confinée du béton, l'augmentation du taux d'armature longitudinale et l'augmentation de l'épaisseurdu tube en PRF. Augmenter le rapport $(\frac{A_{bar}}{A_g})$ et la résistance en compression du béton $f'_c$ possède un effet significatif sur l'augmentation de la capacité des moments de colonnes. Augmenter le rapport $(\frac{A_{bar}}{A_g})$ de 1% à 8% engendre une augmentation de 68% de la capacité de moment des colonnes tandis que l'augmentation de $f'_c$ de 25 MPa à 40 MPa provoque une augmentation de celle-ci de 15%. L'augmentation de l'épaisseur du tube en PRF de X à Y mm dans les colonnes n'a pas montré un effet significatif sur l'augmentation de la capacité des colonnes (6%).

### 7.3.3 La rigidité en flexion effective

12- Les équations de conception proposées ont été développées pour inclure tous les paramètres qui influencent la rigidité en flexion des colonnes armées de barres en acier ou de barres en PRFC respectivement comme suit;

$$EI_{e-s} = \alpha_c E_c I_g + \alpha_s E_s I_s + \alpha_t E_t I_t$$

$$EI_{e-FRP} = \alpha_c E_c I_g + \alpha_f E_f I_f + \alpha_t E_t I_t$$

Ou une analyse multiple de régression linéaire a été utilisée pour inclure tous les paramètres existants dans ces formules. Ce type d'analyse prédit avec une bonne précision la valeur de la rigidité en flexion des colonnes CFFT.

13- L'augmentation des rapports d'excentricité et des charges axiales provoque une diminution des valeurs de rigidité effective ($EI_e$) des colonnes élancées. Un nouveau facteur de réduction de la rigidité du béton $\alpha_c$ est proposé ou

$$\alpha_c = 0.2\left(\frac{l}{D}\right) - \frac{e}{D}\left(\frac{0.5}{1+e/D}\right) - 0.4\left(\frac{P_u}{P_o}\right)$$

14- Les valeurs des facteurs de réduction des rigidités pour les barres en acier et en PRFC sont; $\alpha_s = 0.8$ et $\alpha_f$=0.7, respectivement.

15- L'efficacité de confinement des tubes PRF extérieurs est considérée dans la formulation de l'équation de conception ou un nouveau facteur de réduction de rigidité des tubes PRF $\alpha_t$ est proposé. Il dépend principalement sur le rapport des sections $A_f/A_g$ (pourcentage de renforcement des tubes PRF) et du béton (β). Ce facteur est formulé comme suit; ($\alpha_t = 0.6\beta + 0.9$)

16- Les équations de conception développées dans cette étude montrent une très bonne corrélation lorsqu'elles sont comparées avec les résultats expérimentaux et aussi avec ceux tirés des recherches antérieures.

### 7.3.4 L'instabilité de flambage et de l'élancement limité

17- Une équation simplifiée pour trouver l'élancement critique est proposée pour les colonnes confinées par des tubes en PRF. Une limite d'élancement de 14 est présentée comme une valeur sûre pour éviter une rupture par flambage.

18- l'élancement critique est légèrement affecté par l'épaisseur du tube et la résistance à la compression du béton, tandis que les propriétés mécaniques des barres PRF et le pourcentage d'armature ont un effet non significatif sur la limite d'élancement.

### 7.3.5 Modélisation par éléments finis

19- Un modèle par éléments finis a été développé et a permis de prédire avec une bonne précision le mode de rupture dans les colonnes CFFT courtes. Le critère de rupture pour le tube en PRF utilisé dans le modèle par éléments finis est celui de Hashin. Cependant, le mode de rupture des colonnes CFFT élancées est le flambage. Le modèle du béton proposé dans cette étude est linéaire dans la partie élastique contrairement à celui proposé par (Lam et al. 2003) ou la première partie est parabolique. Ce modèle montre une bonne corrélation avec les résultats expérimentaux obtenus dans cette étude.

20- L'orientation des fibres et l'épaisseur du tube en PRF ont des effets considérables sur le comportement et la capacité de charge portante des colonnes CFFT. L'effet de confinement des tubes PRF est optimum avec une orientation des fibres optimales et une épaisseur suffisante (6-8 épaisseurs).

21- Pour les colonnes élancées (*kl/r=20*), l'augmentation de la capacité ultime est constante et indépendante de l'augmentation de l'angle (θ) de l'orientation des fibres.. Ce phénomène est attribué au comportement de rupture provoqué par le flambement des colonnes.

## 7.4 Recommandations pour les travaux futurs

Basé sur les découvertes et les conclusions de l'étude actuelle, des recherches supplémentaires sur les conceptions des colonnes CFFT peuvent couvrir les points suivants;

1. Le béton haut résistance est bien connu dans les domaines de la recherche. L'intégration de ce type de béton avec des colonnes CFFT et des armatures de de PRF pourrait être prometteuse.
2. La recherche actuelle est réalisée sur des formes cylindriques. Il sera intéressant d'évaluer le comportement sous charges axiales et excentriques de colonnes carrées et rectangulaires
3. Des études expérimentales et théoriques seront nécessaires pour évaluer la performance des colonnes CFFT sous charges sismiques.

# REFERENCES

AASHTO, LRFD. (2009). "Bridge Design Guide Specifications for GFRP—Reinforced Concrete Bridge Decks and Traffic Railings." Washington (DC): American Association of State Highway and Transportation Officials.

ABAQUS standard user's manual. (2008). ''Hibbitt. Karlsson andSorensen." Inc. ,USA

Abdallah , M., Shazly,M., Mohamed, ,H., Masmoudi,R., and Mousa, A.(2017)" Nonlinear finite element analysis of short and long reinforced concrete columns confined with GFRP tubes ." J. Reinf. Plast. Comp., 13:972 – 987.

ACI committee 318 (1995). "Building code requirements for structural concrete." ACI 318-95, Farmington Hills, MI.

ACI committee 318 (2014). "Building code requirements for structural concrete." ACI 318-14, Farmington Hills, MI.

ACI committee 440 (2015). "Guide for the Design and Construction of Concrete Reinforced with FRP Bars." ACI 440.1R-15, Farmington Hills, MI.

Afifi, M. Z., Mohamed, H. M., and Benmokrane, B. (2013). "Axial capacity of circular concrete columns reinforced with GFRP bars and spirals." J. Compos. Constr., ASCE, 18(1), 04013017.

AISC. Specifications for structural steel buildings. ANSI/AISC 360-16. Chicago.

Al-Sayed, S.H., Al-Salloum, Y.A. & Almusallam, T.H., (2000). "Performance of glass fiber reinforced plastic bars as a reinforcing material for concrete structures." Journal Composites Part B: Engineering, 31(6–7), pp.555–567.

ASCE (1982). ''Task Committee on Concrete and Masonry Structure. State of the art report on finite element analysis of reinforced concrete." New York.

Bažant, Z. P., and Cedolin, L., (1991) “Stability of Structures: Elastic, Inelastic, Fracture and Damage Theories,” New York: Oxford University Press, 1011

Bisby, L., Ranger, M. (2010) “Axial-flexural interaction in circular FRP-confined reinforced concrete columns” Constr. Build. Mater. 24 (9) 1672–1681.

Bisby, A.J.S. Dent, and M.F Green (2004) "A comparison of models for FRP-confined concrete", Journal of Composites for Construction, American Society of Civil Engineers, New York, USA, (9).

Bonet JL, Miguel PF, Fernandez MA, Romero ML. (2004)” Biaxial bending moment magnifier method.” Eng Struct; 26(13):2007–19.

Collins, M. P., Mitchell, D., and MacGregor, J. G. (1993). “Structural design considerations for high-strength concrete.” ACI Concrete international, 15(5), 27-34.

CSA A23.3 (1994). “Design of concrete structures, Technical Committee on Reinforced Concrete Design.” CSA A23.3-94. Rexdale, Ontario, Canada.

CSA A23.3 (2014a). “Design of concrete structures, Technical Committee on Reinforced Concrete Design.” CSA A23.3-14. Rexdale, Ontario, Canada.

CSA S6 (2014b). “Canadian highway bridge design code.” CSA S6-14. Rexdale, Ontario, Canada.

CSA S806 (2012). “Design and construction of building components with fiber reinforced polymers,” CSA S806-12. Rexdale, ON, Canada.

Chan, W.W.L., (1955). “The Ultimate Strength and Deformation of Plastic Hinges in Reinforced Concrete Frameworks.” Magazine of Concrete Research (London), 7(21), pp.121–132.

Chakrabarti, A., Chandra, A., and Bharagava, P. (2008). “Finite element analysis of concrete columns confined with FRP sheets.” J. Reinf. Plast. Compos., 27(12), 1349–1373

Chen, W. F. and Atsuta, T., (1976) "Theory of Beam-Columns: In-Plane Behavior and Design, "McGraw Hill, Inc., 513.

Chen, H.L., Sami Z., and GangaRao, H.V.S. (1992) "Vibro-Acoustic Characterization of Materials and Structures." NCA-Vol. 14,ASME.

Choo, C. C., Harik, I. E., and Gesund, H. (2006). "Minimum reinforcement ratio for fiber reinforced polymer reinforced concrete rectangular columns." ACI Struct. J., 103(3), 460–466.

De Lorenzis, L., and Tepfers, R. (2003). "Comparative study of models on confinement of concrete cylinders with fiber reinforced polymer composites." J. Compos. Constr., 10.1061/(ASCE)1090-0268(2003) 7:3(219), 219–237.

De Luca, A., Matta, F., and Nanni, A. (2010). "Behavior of full-scale glass fiber-reinforced polymer reinforced concrete columns under axial load." ACI Struct. J., 107(5), 589–596.

EC2 (2004). "Design of concrete structures. Part 1–1. General rules and rules for buildings." EN 1992-1, Brussels, Belgium.

Fam, A.Z. & Rizkalla, S.H., (2001)." Confinement model for axially loaded concrete confined by circular fiber-reinforced polymer tubes." ACI Struc J, 98(4), pp.451–461.

Fam, A.Z. & Rizkalla, S.H., (2002). "Flexural Behavior of Concrete-Filled Fiber-Reinforced Polymer Circular Tubes."J. Compos. Constr., ASCE, 6(2), pp.123–132.

Fam, A., Greene, R. and Rizkalla, S.H., (2003a). "Field Applications of Concrete-Filled FRP Tubes for Marine Piles." ACI SP, (SP-215-9), pp.161–180.

Fam, A., Flisak, B. and Rizkalla, S. (2003b)"Experimental and analytical modeling of concrete-filled fiber-reinforced polymer tubes subjected to combined bending and axial loads." ACI Struc. J., 100(4), pp.499–509.

Fam, A.Z. and Rizkalla, S., (2005). "Rectangular Filament-Wound GFRP Tubes Filled with Concrete under Flexural and Axial Loading : Experimental Investigation." J. Compos. Constr., ASCE, 9(2), pp.25–33

Fan X. and Zhang M. (2016)" Behavior of inorganic polymer concrete columns reinforced with basalt FRP bars under eccentric compression: An experimental study." Composites Part B, 104: 44-56

Fardis, M. and Khalili, H., (1981). "Concrete encased in fiber glass reinforced plastic." ACI, (78(6)), pp.440–6.

Hadhood, A., Mohamed, H. M., and Benmokrane, B. (2016). ". Circular High-Strength Concrete Columns Reinforced with GFRP Bars and Spirals under Concentric and Eccentric Loading: Experimental Study." J. Comp. constr., 10.1061/ (ASCE) CC.1943-5614.0000734.

Hadi, M. N. S., Karim, H., and Sheikh, M. N. (2016a). "Experimental Investigations on Circular Concrete Columns Reinforced with GFRP Bars and Helices under Different Loading Conditions." J. Compos. Constr., ASCE; 20(4). 10.1061.

Hadi, M.N.S., Khan, Q.S. & Sheikh, M.N. (2016b)"Axial and flexural behavior of unreinforced and FRP bar reinforced circular concrete filled FRP tube columns." Constr. Build. Mater, 122, pp.43–53.

Harik, I. E. Gesund, H. (1986) "Reinforced concrete column in biaxial bending." Concr. Frame Struct. Stab. Streng., 111-132.

Hognestad, E. (1952). "A study of combined bending and axial force in reinforced concrete specimens." Ph.D. dissertation, University of Illinois.

Hognestad, E., Hanson, N. W., and McHenry, D. (1955). "Concrete stress distribution in ultimate strength design." ACI J. Proc., 52(6), 455-480.

Hong, W.-K. & Kim, H.-C. (2004) "Behavior of concrete columns confined by carbon composite tubes." Canadian J. of Civ. Engin., 31(2), pp.178–188.

Hu HT, Huang CS, Wu MH, and Wu YM. (2003) ''Nonlinear analysis of axially loaded concrete-filled tube columns with confinement effect." J Struct Eng ASCE; 129:1322–9.

Issa, M.S., Metwally, I.M. and Elzeiny, S.M., (2012). “Performance of eccentrically loaded GFRP reinforced concrete columns.” World Journal of Engineering, 9(1), pp.71–78.

Karbhari VM, Gao Y. (1997) ‘‘Composite jacketed concrete under uniaxial compression verification of simple design equations.’’ J Mater Civ Eng, ASCE; 9(4):185 –93.

King, J.W.H., (1946). “The Effect of Lateral Reinforcement in Reinforced Concrete Columns.” The Structural Engineer (London), 24(7), pp.355–388.

Khan QS, Sheikh MN and Hadi M. (2016) “Axial-Flexural interactions of GFRP-CFFT columns with and without reinforcing GFRP bars.” J Compos Constr; 21(3).

Khan QS, Sheikh MN, Hadi M. (2017) “Concrete Filled Carbon FRP Tube (CFRP-CFFT) columns with and without CFRP reinforcing bars: Axial-flexural interactions.” Compos Part B, 09.025.

Khuntia, M., and Ghosh, S. K. (2004a). “Flexural Stiffness of Reinforced Concrete Columns and Beams: Analytical Approach,” ACI Struct. J., V. 101, No. 3, May-June, pp. 351-363.

Khuntia, M., and Ghosh, S. K. (2004b). “Flexural Stiffness of Reinforced Concrete Columns and Beams: Experimental Verification,” ACI Struct. J., V. 101, No. 3, May-June, pp. 364-374.

Kobayashi, K., and Fujisaki, T. (1995). “Compressive behavior of FRP reinforcement in non-prestressed concrete members.” Proc. 2nd Int. RILEM Symp. On Non-Metallic (FRP) Reinforcement for Concrete Structures, E & FN Spon, London, 267–274.

Jiang, J. F., and Wu, Y. F. (2012). “Identification of material parameters for Drucker-Prager plasticity model for FRP confined circular concrete columns.” Int. J. Solids Struct., 49(3–4), 445–456.

Jiang, T., and Teng, J. G. (2012)” Theoretical model for slender FRP-confined circular RC columns.” Constr. Build. Mater., 32, 66–76.

Jiang, T., and Teng, J. G. (2013) “Behavior and design of slender FRP confined circular RC columns.” J. Compos. Constr., 443–453.

Teng, JG., Xiao, QG., Yu, T., and Lam, L. (2015) ‘‘Three-dimensional finite element analysis of reinforced concrete columns with FRP and/or steel confinement.” Eng Stru, Elsevier. (97), pp.15-28

Tikka Timo K., Mirza SA.(2005) “Nonlinear EI equation for slender reinforced concrete columns.” ACI Struct J; 102(6):839–48.

Tikka Timo K., Mirza SA. (2008) “Effective flexural stiffness of slender structural concrete columns.” Canad J Civil Eng; 35: 384–99.

Lam, L. and Teng, J.G., (2003). “Design-oriented stress–strain model for FRP-confined concrete.” Constr. Build. Mater. 17(6–7), pp.471–489.

Lotfy, E.M., (2010). “Behavior of reinforced concrete short columns with Fiber Reinforced polymers bars.”J. Civ. Struc. Eng., 1(3), pp.545–557.

Lee, J. H., and Son, H. S. (2000). “Failure and strength of high-strength concrete columns subjected to eccentric loads.” ACI Struct. J., 97(1), 75-85.

Li G, Maricherla D, Singh K., and Pang SS, John M. (2006) ‘‘Effect of fiber orientation on the structural behavior of FRP wrapped concrete cylinders. ’’ J Compos Struct; 74(4):475–83.

Lillistone D, Jolly CK.(1997) “Concrete filled fibre reinforced plastic circular columns.” In;Proceedings of Composite construction-conventional and innovative conference, composite construction-Conventional and innovative;759-764.

Lloyd, N. A., and Rangan, B. V. (1996). “Studies on High-Strength Concrete Columns under Eccentric Compression,” ACI Struct. J., V. 93, No. 6, Nov.-Dec., pp. 631-638.

Lim J., Ozbakkaloglu, T., Gholampour,A., Bennett,T., Sadeghi, R., (2016) “Finite-Element Modeling of Actively Confined Normal-Strength and High-Strength Concrete under Uniaxial, Biaxial, and Triaxial Compression. ’’ J.Stru.Eng. DOI: 10.1061/(ASCE)ST.1943.

Mander, J. B., Priestley, J. N., and Park, R. (1988). “Theoretical Stress-Strain Model for Confined Concrete,” J. Struct. Eng., ASCE, 114(8), 1804-1826.

Mavichak V, Furlong RW. (1976) “Strength and stiffness of reinforced concrete columns under biaxial bending.” Research report 7-2F. Center for Highway Research. November 1976.

Mehanny S. S. F. KuramotoH. Deierlein G. G.(2001)“Stiffness modeling of RC beam-columns for frame analysis.” ACI Struct J; 98; 215-225.

Mirmiran A, Shahawy M. (1996) “A new concrete-filled hollow FRP composite column. “Compos Part B ;27 B:263–8.

Mirmiran, A., and Shahawy, M., (1997) “Dilation Characteristics of Confined Concrete,” Mechanics of Cohesive-Frictional Materials, V. 2, pp. 237-249.

Mirmiran, A. (1998). “Length Effects on FRP-Reinforced Concrete Columns,” Proceedings of the 2nd International Conference on Composites in Infrastructure, Tucson, Ariz., pp. 518-532.

Mirmiran, A., Zagers, K., and Yuan, W. Q. (2000). “Nonlinear finite element modeling of concrete confined by fiber composites.” Finite Elem. Anal. Des., 35(1), 79–96.

Mirmiran, A., Yuan, W., and Chen, X. (2001a). “Design for Slenderness in Concrete Columns Internally Reinforced with Fiber-Reinforced Polymer Bars,” ACI Struct. J., V. 98, No. 1, Jan.-Feb., pp. 116-125.

Mirmiran, A., Shahawy, M., and Beitleman, T., (2001b), “Slenderness limit for hybrid FRP concrete columns,” Journal of Composites for Construction, ASCE, Vol. 5, No.1, pp. 26-34.

Mirza, S. A. (1990). "Flexural Stiffness of Rectangular RC Columns," ACI Struct. J., V. 87, No. 4, July-Aug., pp. 425-435.

Mirza S. A. MacGregor J. G. (1982) "Probabilistic study of strength of reinforced concrete members." Canad J Civil Engi. 2. 9(3), 431-448.

Miyauchi K, Inoue S, Kuroda T, Kobayashi A. (1999) "Strengthening effects of concrete columns with carbon fiber sheet.'' Trans Jpn Concr Institute; 21:143 –50.

Mohamed, H. M., Afifi, M. Z. and Benmokrane, B. (2014). "Performance evaluation of concrete columns reinforced longitudinally with FRP bars and confined with FRP hoops and spirals under axial load." J. Bridge Eng., DOI: 10.1061/(ASCE)BE.1943-5592.0000590, 04014020.

Mohamed, H., and Masmoudi, R. (2008) "Compressive Behaviour of Reinforced Concrete Filled FRP Tubes." ACI Spec Publi (SP), SP-257-6, pp. 91-109.

Mohamed, H.M. and Masmoudi, R., (2010)." Axial Load Capacity of Concrete-Filled FRP Tube Columns: Experimental versus Theoretical Predictions." J. Compos. Constr., ASCE, 14(2), pp.231–243.

Mohamed H, Abdel-Baky H, Masmoudi R. (2010) "Nonlinear stability analysis of concrete-filled fiber-reinforced polymer-tube columns: experimental and theoretical investigation." ACI struct J; 107, 699-708.

Mohamed, H.M., Masmoudi, R. (2011) " Deflection prediction of steel and FRP-reinforced concrete-filled FRP tube beams." J Compos Constr., (ASCE), 15(3): 462-472

Mohamed S. (2001) "Infrastructure M. Development and Behavior of a New Hybrid Column in Systems'' Doctoral thesis. The University of Alabama in Huntsville.

Montoya, E., Vecchio, F. J., and Sheikh, S. A. (2004). "Numerical evaluation of the behavior of steel- and FRP-confined concrete columns using compression field modelling." Eng. Struct., 26(11),1535–1545.

Moussa, A. (1993).” Finite element modelling of shotcrete in tunneling” Ph. D. Dissertation, University of Innsbruck, Austria

Nanni, A. & Bradford, N.M., (1995). “FRP Jacketed Concrete under Uniaxial Compression.” Constr. Build. Mater., 9(2), pp.115–124.

Ozbakkaloglu, T., and Saatcioglu, M. (2006). “Seismic behavior of high-strength concrete columns confined by fiber reinforced polymer tubes.” J. Compos. Constr., (ASCE) 10: 6(538), 538–549.

Ozbakkaloglu T, Oehlers DJ.( 2008) “Concrete-filled square and rectangular FRP tubes under axial compression. ” ASCE J Compos Constr;12(4):469–77.

Ozbakkaloglu, T. & Lim, J.C., (2013a). “Axial compressive behavior of FRP-confined concrete: Experimental test database and a new design-oriented model”. Compos Part B: Eng, 55(1), pp.607–634.

Ozbakkaloglu T. (2013b)”Compressive behavior of concrete-filled FRP tube columns: assessment of critical column parameters.” Eng Struct; 2013, 51: 188–199.

Ozbakkaloglu, T.,and Vincent, T., (2014). “Axial Compressive Behavior of High Strenght Concrete Filled FRP Tubes”. J. Compos. Constr., ASCE ,16 (1), pp.10–20.

Ozbakkaloglu T, Gholampour A., Jian C. Lim (2016) “Damage-Plasticity Model for FRP-Confined Normal-Strength and High-Strength Concrete’’ J. Compos. Constr., ASCE.1943-5614.0000712.

Parvathaneni, H.K., Iyer, S. & Greenwood, M. (1996)” Design and construction of test mooring pile using super prestressing.” Proc., Advanced Compo. Mater. Bridg. Struc.t (ACMBS), , p.313–324.

Prabhu G. Sundarraja M. Kim Y. (2015) “Compressive behavior of circular CFST columns externally reinforced using CFRP composites.” Thin Walled Struct. 87 ,139–148.

Richart, F., Brandtzaeg, A. and Brown, R.L., (1928). “A Study of the Failure of Concrete under Combined Compressive Stresses.” University of Illinois Bulletin, 26, Bullet(12), pp.1–104.

Richart, F., Brandtzaeg, A. and Brown, R.L., (1929). "The Failure of Plain and Spirally Reinforced Concrete in Compression," Bulletin No. 190, Engineering Experimental Station, University of Illinois, Urbana, IL, 74 pp.

Roy, H.E.H. and Sozen, M.A., (1965). "Ductility of Concrete. Flexural Mechanics of Reinforced Concrete" SP-12, ASCE, Detroit, pp.213–224.

Saafi, M., Toutanji, H.A. and Li, Z., (1999). "Behavior of concrete col- umns confined with fiber reinforced polymer tubes." ACI Struct. J., 96(5),, p.96(5), 500–509.

Saadatmanesh, H., Ehsani, M. & Li, M., (1994). "Strength and ductility of concrete columns externally reinforced with fiber composite straps." ACI Struct J, (91(4)), pp.434–47.

Sadeghian P. Fam A. (2014) "Slender reinforced concrete columns strengthened with longitudinal FRP reinforcements." The 7th International Conference on FRP Composites in Civil Engineering. CICE 2014; Vancouver, Canada.

Samaan, M., Mirmiran, A. & Shahawy, M., 1998. "Model of Concrete Confined by Fiber Composites." J. Compos. Constr., ASCE , 124(9), pp.1025–1031.

Son, J.-K., and Fam, A. (2008). "Finite element modeling of hollow and concrete-filled fiber composite tubes in flexure: Model development, verification and investigation of tube parameters." Eng. Structures, 30, 2656–2666.

Spoelstra MR, Monti G. (1999) "FRP-confined concrete model.'' J Compos Constr, ASCE;3(3):143 –50.

Talaeitabaa,S., Halabiana,M., Torkib, M., (2015) "Nonlinear behavior of FRP-reinforced concrete-filled double-skin tubular columns using finite element analysis" ThinWalled Struct., 95, 389-407

Teng J, Chen J, Smith S, Lam L. (2002) "FRP strengthened RC structures. '' John Wiley & Sons Inc.

Tikka, T., Francis, M. & Teng, B., 2010. Strength of Concrete Beam-Columns Reinforced with GFRP Bars. 2nd International Structures Specialty Conference, Winnipeg, Manitoba.

Timoshenko, S. P., and Gere, J. M. (1961) "Theory of Elastic Stability", 2nd Edition, McGraw-Hill Book Co., New York, 541.

Tobbi, H., Farghaly, A. S., and Benmokrane, B. (2012). "Concrete columns reinforced longitudinally and transversally with glass fiber-reinforced polymers bars." ACI Struct. J., 109(4), 1–8.

Toutanji H, Saafi M (2002) "Stress-strain behavior of concrete columns confined with hybrid composite materials." Mater Struct 35:338–347.

Vincent T, Ozbakkaloglu T (2013) "Influence of fiber orientation and specimen end condition on axial compressive behavior of FRP-confined concrete." Constr Build Mater, 47 (2013) 814–826.

Vincent T, Ozbakkaloglu T (2014) "Influence of shrinkage on compressive behavior of concrete-filled FRP tubes: an experimental study on interface gap effect. Constr Build Mater 75:144–156.

Wei, Y.Y. & Wu, Y.F., (2012). "Unified stress-strain model of concrete for FRP-confined columns." Constr Build Mater, 26(1), pp.381–392.

Westerberg B. (2002) "Slender column with uniaxial bending. International Fedaration for Structural Concrete (fib). Technical report, bulletin 16. Design examples for 1996 FIP recommendations practical design of structural concrete."January 2002. p. 121–42.

Whitney, C. S. (1942). "Design of Reinforced Concrete Specimens Under Flexure and Combined Flexure and Direct Compression." ACI J. Proc., 33, 483-498.

Wu, W. P. (1990). "Thermomechanical Properties of Fiber Reinforced Plastic (FRP) Bars." Ph.D. dissertation, West Virginia Univ., Morgantown, WV, 292.

Xiao Y, Wu H. (2000) "Compressive behavior of concrete confined by carbon fiber composite jackets.'' J Mater Civ Eng, ASCE; 12(2):139 –46.

Xue, W., Hu, X., and Fang, Z. (2014). "Experimental studies of GFRP reinforced concrete columns under static eccentric loading." 7th international Conference on Fiber Reinforced Polymer (FRP) Composites in Civil Engineering (CICE 2014), Vancouver, Canada.

Yao GH, Huang YJ, Song BD, and Tan W., (2009) "Analysis for static behavior of steel and concrete composite members with plastic-damage model.'' Prog Steel Build Struct; 11:12–8.

Yazici, V., and Hadi, M. N. (2012). "Normalized confinement stiffness approach for modeling FRP-confined concrete." J. Compos. Constr., 10.1061/(ASCE)CC.1943-5614.0000283, 520–528.

Yu T, and Teng JG.(2011) "Design of concrete-filled FRP tubular columns: provisions in the Chinese technical code for infrastructure application of FRP composites. " J Compos Constr;15(3):451–61.

Yu, T., Teng, J. G., Wong, Y. L., and Dong, S. L. (2010). "Finite element modeling of confined concrete—I: Drucker–Prager type plasticity model." Eng. Struct., 32(3), 665–679.

Zadeh, H. J., and Nanni, A. (2012). "Design of RC columns using glass FRP reinforcement." J. Compos. Constr., ASCE, 17(3), 294-304.

Zadeh, H. J., and Nanni, A. (2017). "Flexural Stiffness and Second-Order Effects in Fiber-Reinforced Polymer-Reinforced Concrete Frames." ACI Struct. J., 114(2), 533